

University of Trento
University of Brescia
University of Padova
University of Trieste
University of Udine
University IUAV of Venezia

Riccardo Morbin (Ph. D. Student)

**STRATEGIES FOR SEISMIC ASSESSMENT OF
COMMON EXISTING REINFORCED CONCRETE
BRIDGES TYPOLOGIES**

Prof. Carlo Pellegrino (Tutor)

2013 / 02

UNIVERSITY OF TRENTO

Engineering of Civil and Mechanical Structural Systems

Ph. D. Head's Prof. Davide Bigoni

Final Examination 15 / 04 / 2013

Board of Examiners:

Prof.ssa Maria Paola Gatti (Università degli Studi di Trento)

Prof. Giovanni Scudo (Politecnico di Milano)

Prof. Alessandro De Stefano (Politecnico di Torino)

Prof. Fabio Biondini (Politecnico di Milano)

SUMMARY

This study concerns a new probabilistic framework to evaluate road/railway bridges after an earthquake by means of analytical fragility curves and inspections on the structure. In particular, the assessment is performed on existing reinforced concrete (RC) bridges with a common structural scheme in Italy (multi-span simply supported girder bridges). The framework is set up of 6 steps and each step is investigated. Steps 1 and 2 are a sort of preliminary work before the seismic event occurs: the creation of a database to collect all information about bridges in specific road/railway networks (step 1) and the generation of fragility curves for each bridge (step 2): fragility curves are instruments describing the probability of a structure being damaged beyond a specific damage state for various levels of ground shaking. Since step 2 is a crucial step for the outcomes of the framework, a wide investigation on the generation of fragility curves is presented, considering bridges located in strategic road network points in Veneto region (North-Eastern Italy) and different numerical modellings, in order to evaluate the best seismic vulnerability assessment. Moreover, particular attention is given to retrofit interventions by means of Fiber Reinforced Polymer (FRP) and their effect on bridge seismic vulnerability reduction. The other steps concern activities to carry out after a seismic event, useful for emergency and post-emergency phases. Step 3 regards a method to decide if inspections on bridge are needed in relation to the occurred earthquake seismic intensity; if the seismic intensity measure reaches a specific threshold, step 4 suggests how to perform visual inspections on bridges, under a probabilistic point of view, and to generate the damaged bridge fragility curves. After that, the last two steps try to give useful information to Institution and owners of bridges in order to reach an optimal road/railway network management in post-earthquake phases. Step 5 concerns a quick procedure to decide whether or not allowing traffic over damaged bridges, whereas step 6 gives information about economical benefits coming from a comparison between replace costs and retrofitting costs (considering FRP retrofitting interventions) of damaged bridges. In order to clarify the framework procedure, an example for each step is developed.

SOMMARIO

Questo studio riguarda una nuova procedura probabilistica per valutare ponti esistenti stradali/ferroviari dopo un evento sismico per mezzo di curve di fragilità analitiche e ispezioni sulla struttura. In particolare, la valutazione riguarda ponti esistenti in calcestruzzo armato aventi uno schema strutturale comune in Italia (ponti multicampata in semplice appoggio). La procedura è composta di 6 fasi e ciascuna fase è stata approfondita. Le fasi 1 e 2 sono una sorta di lavoro preliminare da eseguire prima che l'evento sismico accada: l'impostazione di un database per raccogliere tutte le informazioni riguardo i ponti di una specifica rete stradale/ferroviaria (fase 1) e la costruzione delle curve di fragilità per ciascun ponte (fase 2): le curve di fragilità sono grafici che esprimono la probabilità condizionata di un manufatto di eguagliare o eccedere un certo livello di danno per diverse intensità dell'azione sismica. Poiché la fase 2 è una fase importante per i risultati finali dell'intera procedura probabilistica, è presentato un ampio studio sulla costruzione delle curve di fragilità, considerando alcuni ponti localizzati in posizioni strategiche della rete stradale della regione Veneto (Italia nord orientale) e differenti modellazioni numeriche, al fine di valutare la modellazione più conveniente per la stima della vulnerabilità sismica. Inoltre, particolare attenzione è posta sugli interventi di adeguamento con materiali FRP e il loro effetto sulla riduzione della vulnerabilità sismica del manufatto. Le altre fasi riguardano le attività da svolgere dopo un evento sismico, utili per le fasi di emergenza e post-emergenza. La fase 3 riguarda un metodo per decidere se iniziare o meno le ispezioni su un ponte in relazione all'intensità sismica del terremoto accaduto; se l'intensità sismica raggiunge o supera una certa soglia, la fase 4 indica come effettuare le ispezioni visive sui manufatti, a livello probabilistico, e come generare le curve di fragilità dei ponti eventualmente danneggiati. Infine, le ultime due fasi cercano di fornire informazioni utili agli enti che gestiscono la rete stradale per ottenere un'organizzazione ottimale della rete stradale/ferroviaria nelle fasi dopo il terremoto. La fase 5 riguarda una veloce procedura per decidere se permettere o meno il traffico sui ponti che hanno subito l'evento sismico, mentre la fase 6 fornisce informazioni riguardo possibili vantaggi economici, che derivano da un confronto tra costi di ricostruzione e costi di riparazione (considerando interventi con materiali FRP) dei ponti danneggiati. Per chiarire la procedura qui descritta, si è svolto un esempio esplicativo per ogni fase.

DEDICATION

“Ho capito che spesso tutti sono convinti che una cosa sia impossibile, finché arriva uno sprovveduto che non lo sa e la realizza.”

Albert Einstein

A tutti gli “sprovveduti”.

ACKNOWLEDGEMENTS

My PhD years have been one of the most valuable experiences of my life, in particular for the people with whom I had the privilege to work.

First, I wish to thank my supervisor prof. Carlo Pellegrino for his guidance, support and encouragement during this study and in many other facets of my Research.

I also would like to extend my gratitude to prof. Claudio Modena for the possibilities he gave me to improve as researcher and engineer.

I am grateful to Dr. Hao Zhang for his suggestions and help on this study, the research period under his supervision at The University of Sydney was great for me.

Thanks also due to graduate students for helping me to carry out some analysis of this study.

Moreover, I like to thank wonderful fellow of my research group and wonderful guys of "room 101" at the University of Sydney, for their help and for all coffees and biscuits pleasantly got together...because smiling is the smell of the life!

A thank to my friends, the ones indeed, because they encouraged me in many circumstances.

My special thank to my parents and my relatives to have supported me in all my choices.

The last, but not the least at all, a great and special thank to Lisa, the most important person of my life, because her suggestions and simply her nearness give me essential support to reach my goals.

CONTENTS

1 INTRODUCTION	11
1.1 Background.....	11
1.2 Objectives and scope of research	13
1.3 Thesis organization.....	14
2 STATE OF THE ART	17
2.1 Earthquake risk assessment.....	17
2.2 Seismic hazard	21
2.3 Seismic vulnerability	22
2.3.1 Empirical fragility curves	25
2.3.2 Analytical fragility curves.....	27
2.3.2.1 <i>Damage states</i>	27
2.3.2.2 <i>Methods</i>	28
2.3.2.3 <i>Accelerograms for non-linear dynamic analysis (NLDA)</i>	32
2.4 Flexural and shear behavior of RC columns.....	33
2.5 Defect detectability function.....	40
2.6 Fiber-reinforced polymer (FRP) retrofitting interventions.....	43
2.6.1 Effective confining pressure	44
2.6.2 Stress-strain curve	46
3 PROBABILISTIC FRAMEWORK FOR SEISMIC ASSESSMENT OF MAINSHOCK-DAMAGED BRIDGES	49
3.1 Step 1: collecting bridges information for a database.....	50
3.2 Step 2: generation of fragility curves	52

3.2.1	Investigation on the generation of fragility curves	52
3.2.1.1	<i>The case study bridge from Fener bridge</i>	53
3.2.1.2	<i>The A27 overpass bridge</i>	71
3.2.1.3	<i>Conclusions</i>	79
3.3	Step 3: inspections beginning.....	80
3.3.1	Step 3 example	81
3.4	Step 4: inspections progress	83
3.4.1	Updating fragility curves.....	85
3.4.2	Step 4 example	86
3.5	Step 5: allowing traffic.....	87
3.5.1	Step 5 example	89
3.6	Step 6: costs probability evaluation	90
3.6.1	Step 6 example	92
4	CONCLUSIONS AND RECOMMENDATIONS.....	95
4.1	Recommendation for further studies.....	99
	NOTATIONS.....	101
	LIST OF FIGURES	105
	LIST OF TABLES.....	109
	BIBLIOGRAPHY	111

1 INTRODUCTION

1.1 Background

Human life, building stocks and lifelines can be subjected to many natural hazards such as earthquake, floods, windstorms, icing, tsunamis, debris flows, which can cause significant casualties and economic losses. For stocks of buildings or lifelines such as transport networks, gas, water, telecommunication facilities these natural hazards represent a serious treat, since they can cause severe disruptions and a long recovery time to regain complete operability. Emergency and post-emergency responses play an important role in life rescue and reduction of economic losses in such events.

The fast socio-economic development of many urban areas has often been characterized by the construction of new infrastructures to meet the increasing demands of mobility. Transport networks are indeed essential for carrying out various economic and strategic activities immediately following a catastrophic event mainly to allow initially rescue operations.

In transport lifelines, bridges are the most vulnerable elements and they can experience structural problems like due to environmental conditions and natural disasters: concrete cover damage that exposes bars to atmosphere, steel corrosion, concrete damage by icing cycles, ageing of structural materials leading to the degradation of their mechanical properties, etc. The allocation of limited budget resources for the retrofitting is a key issue in stock management. The optimal allocation of a limited budget is a challenge connected to the prioritization to maximize the service level.

In this context some crucial questions arise. How can we forecast the seismic response (and, in general, the response to natural disasters) of complex systems, like transport lifelines? How can we retrofit systems and rely on them for emergency? How can we retrofit stocks to minimize economic losses due to natural events? Is it possible to have, in real-time, post-event information on the conditions and operability of bridges? Can we have an effective tool for evaluation of best budget allocation for decision makers? How can we take advantage of the modal shift (inter-modality exchange) between different transport networks?

Concerning earthquake as a major disaster, a procedure for the estimation of risk in multi-modal transport networks and best budget allocation for retrofitting and monitoring structures should be considered. An optimum research procedure can be used to obtain these results in order to prioritize retrofitting interventions and monitoring strategies for significant bridges as most vulnerable element of the surface transport network. The emergency and post-emergency phases can be treated as one of the objectives for this optimum research procedure.

Very few procedures for this type of complex problems have been developed in the literature for particular contexts. In the USA, FEMA (Federal Emergency Management Agency) prepared a methodology for the estimation of the losses caused by different natural hazards. These procedures, called HAZUS (FEMA, 2004), is coded into software running on a GIS system that allows performing risk analyses. The key feature of this computer program is the ease of retrieval of data, for seismic action, transport networks, soils, etc.

Shiraki et al. (2007) presents a general method for the calculation of risk in transport networks, starting from seismic scenarios built for California. They computed the network travel time delay and then correlated the annual occurrence rate for earthquake scenarios to produce the system risk curve. Kiremidjan et al. (2007) runs a simulation for the transport network degradation, including effects like liquefaction, ground motion, landslides, etc., Werner et al. (2006) proposes a procedure called Redars, used by Caltrans for the seismic risk analysis. In that paper there is also an application to California transport system. Shinozuka et al. (2006) and Sgaravato et al. (2008) study the socio-economic effect of the seismic retrofit implemented on bridges in Los Angeles Area Freeway Network, Seville & Metcalfe (2005) studies on similar topics in New Zealand. In Italy, one of the Mediterranean countries with a high seismic risk where previous earthquakes had relevant social and economic effects, Codermatz et al. (2003) performs a risk analysis by mean of GIS software in the Friuli Venezia Giulia in North-Eastern Italy: they accounted for bridge fragility, but there is no information about the effects on the transport system. A first attempt about some partial aspects of such a procedure applied in Italy is shown in (Carturan et al., 2010a; Carturan et al., 2010b; Carturan et al., 2013).

Within this context, seismic vulnerability assessment of bridges in the road/railway networks is essential to obtain accurate results from the above-mentioned procedures. Fragility curves can be considered as one of the most performing tools to assess existing bridge seismic vulnerability (Shinozuka et

al., 2000b; Monti & Nisticò, 2002; Franchin et al., 2006; Lupoi et al., 2006; Padgett & DesRoches, 2008; Carturan et al., 2012; Zanini et al., 2013): they are instruments describing the probability of a structure being damaged beyond a specific damage state for various levels of ground shaking. Probabilistic approach is necessary because a number of uncertain variables are considered, for example the intensity of expected ground motion and the characteristics of the structural elements.

Since it is well known the importance of the topic, this study is focused on seismic vulnerability assessment of reinforced concrete (RC) existing bridges with a common structural scheme in Italy (multi-span simply supported girder bridges) by means of fragility curves. The bridges are located in strategic road network points in Veneto region. In particular, seismic vulnerability evaluation concerns damaged bridges after a seismic event by means of a new probabilistic framework based on inspections on the structure: fragility curves construction is investigated in depth within this framework. The aim is to provide useful information to owners or Institutions to decide whether or not allowing traffic over the bridge and repairing immediately mainshock-damaged bridges. The outcomes of this framework can be used to improve and complement the above-mentioned procedures regarding the seismic assessment of the whole road and railway networks in order to better plan emergency, post-emergency responses and a priority for an optimal budget allocation.

1.2 Objectives and scope of research

The main goal of this study is to define a new framework to evaluate bridges after a seismic event. A challenge of the evaluation of bridges after a seismic event is to define a correlation between observable damages on bridges and their residual traffic capacity: this is primarily due to the difficulty to model analytically mechanisms occurring on old RC bridges when subject to a seismic event (e.g. previous damage on structural elements) and to decide the closure of the bridge only by means of rapid visual inspections and previous analyses, both affected by uncertainties. These two reasons can hardly be solve altogether and they point out that there is a lack of literature on this topic. Taking into account these aspects and some relevant study that concerns

evaluation of bridges after an earthquake, e.g. (Mackie & Stojadinović, 2006; Franchin & Pinto, 2009; Zhou et al., 2010), the procedure here presented is based on visual inspections taking into account uncertainties by analogy with a defect detectability function (Mori & Ellingwood, 1994). Within this framework, more focus is given to the construction of seismic analytical fragility curves for existing RC bridges: a comparison between results coming from different bridges analytical modellings with an increasing level of complexity is presented in order to highlight different approximations. It is emphasized that considering simplified analytical models of the bridge (Karim & Yamazaki, 2001, 2003) can overestimate or underestimate the vulnerability of the structure. Moreover, a number of existing RC bridges needs strengthening because of improper design for seismic loads. Some examples of retrofitting/strengthening methods for bridges are: steel or FRP confinement of piers, increase of the cross-section, increase the amount of steel reinforcements, modification of the static loading path, base isolation, use of seismic damping devices, interventions on masonry arches etc. Regarding retrofit techniques for bridges with the aim of reducing their vulnerability, particular interests is dedicated to the confinement of piers with traditional and innovative materials such as Fiber Reinforced Polymer (FRP) composites (Teng et al., 2002; Tastani et al., 2006; Pellegrino & Modena, 2010). The effect of this innovative FRP retrofitting is evaluated in terms of influence on the fragility curves.

1.3 Thesis organization

Recent developments in the field of Performance Based Engineering (PBE) are reviewed in the first part of this work, with particular reference to seismic performance of structures. Probabilistic aspects of earthquake risk assessment, seismic hazard and structural seismic vulnerability are examined and, in this context, reinforced concrete (RC) existing structures behavior under seismic loads is analyzed. Other relevant topics, important for the development of this study, are presented: damage inspections, considering a detectability function, and structural retrofitting interventions by means of Fiber-Reinforced Polymers (FRP).

Then, the main topic of this study is developed: a probabilistic framework for mainshock-damaged bridges. The framework is set up of 6 steps and each step is investigated in depth. The first two steps are a sort of preliminary work before the seismic event occurs: the creation of a database to collect all information about bridges in specific road/railway networks (step 1) and the generation of fragility curves for each bridge (step 2). Since step 2 is a crucial step for the outcomes of the framework, a wide investigation on the generation of fragility curves, considering different numerical modellings, is presented in order to evaluate the best seismic vulnerability assessment. The other steps concern activities to carry out after a seismic event, useful for emergency and post-emergency phases. Step 3 regards a method to decide if inspections on bridge are needed in relation to the occurred earthquake seismic intensity; if the seismic intensity measure reaches a specific threshold, step 4 suggests how to perform visual inspections on bridges, under a probabilistic point of view, and to generate the damaged bridge fragility curves. After that, the last two steps try to give useful information to Institution and owners of bridges in order to reach an optimal road/railway network management in post-earthquake phases. Step 5 concerns a quick procedure to decide whether or not allowing traffic over mainshock-damaged bridges, whereas step 6 gives information about economical benefits coming from a comparison between replace costs and retrofitting costs (considering FRP retrofitting interventions) of damaged bridges. In order to clarify the framework procedure, an example for each step is developed.

Finally, main conclusions are summarized and recommendations for further studies are suggested.

2 STATE OF THE ART

The Performance Based Engineering (PBE) is the basis of the new structural design codes and specifications for civil infrastructures all over the world. The use of probabilistic concepts in this field comes from awareness that loads arising from usage and external events (demand), man-made and natural hazards and strengths of material constructions (capacity) are uncertain in nature. These aspects cause risk, which is managed by the provisions in standards and codes. Structural reliability methods provide tools to determine the safety levels and set the characteristic loads, load factors, load combinations and resistance or material factors in codes. The management of risk due to earthquakes can be brought into this context and considered one of the main hazards among the ones impacting civil infrastructures, in particular because of its social and economical effects.

In this context, emergency (e.g. immediately after the seismic event) and post-emergency phases become particularly important: consequences of earthquakes on bridges have to be known (e.g. by means of visual inspections) in order to plan aids in emergency phase and decide strengthening/retrofitting interventions during post-emergency phase.

2.1 Earthquake risk assessment

Injured and dead people and economical losses due to earthquakes in recent times have been the stimulus to improve engineering practices for earthquake-resistance design and retrofit of civil infrastructures, in particular bridges and buildings. Seismic load has some peculiarity in comparison with other kind of loads: it is a base excitation rather than a clearly defined load (as live, wind or snow), the structural response is dynamic and it needs to be related to damage that occurs under repeated (usually inelastic) cycling and the structural actions induced by a seismic event are system-wide, whereas the effects of many other loads are more or less localized. Moreover the philosophy of earthquake-resistance design is to limit the occurrence of life-threatening damage under the design earthquake rather than to prevent its occurrence entirely; however, the

structure has to retain a substantial margin of safety against overall collapse so that occupants and users can get to safety.

In order to achieve these ambitious objectives, the performance assessment and design process has been divided into simpler elements in terms of the description, definition and quantification of earthquake intensity measures (IMs), engineering demand parameters (EDPs), damage measures (DMs) and decision variables (DVs). Commonly used examples of the above parameters are peak ground acceleration and first-mode spectral acceleration (IMs), interstory drift ratios and inelastic component deformations (EDPs), damage states of structural and nonstructural elements (DMs) and dead (fatalities), direct financial losses and downtimes (DVs). A consistent probabilistic framework is used to explicitly and rigorously quantify the inherent uncertainties and randomness in all the above-mentioned variables. The mean annual frequency of DV is obtained by applying the theorem of the total probability (Cornell & Krawinkler, 2000; Yeo & Cornell, 2005):

$$P(DV) = \iiint P(DV|DM) \cdot |dP(DM|EDP)| \cdot |dP(EDP|IM)| \cdot |dH(IM)| \quad (2.1)$$

where:

- $P(DV|DM)$ is the probability that DV exceeds a specific value, conditioned by the structural damage DM. Estimation of DV comes from probabilistic analysis of economic losses, which is difficult to perform;
- $P(DM|EDP)$ is the probability that DM exceeds a specific value, when a certain value is given to parameter EDP. Considering different IMs, this term is denoted as seismic fragility;
- $P(EDP|IM)$ is the probability that EDP exceeds a certain value given a particular value of IM;
- $H(IM)$ is the seismic hazard of the site, obtained by a Probabilistic Seismic Hazard Analysis (PSHA).

Eq. (2.1) is commonly referred to as the “PEER Equation” because it comes from the Pacific Earthquake Engineering Research Center. The most important universities of the U.S. West Coast, like Berkley and Stanford, are among its members.

Each of the components in the above equation is designed to require inputs from a specific discipline, for instance $H(IM)$ from seismologist and geotechnical engineers, $P(EDP|IM)$ from structural engineers and $P(DV|DM)$ from cost

estimator. Probabilistic information of DV can be used by building owners and stakeholders to make better seismic-risk related decision. The PEER Performance-Based methodology is schematically shown in Fig. 2.1.

The PEER Equation involves pair-wise sequences of four random variables: it assumes one-step memory in the individual component such that we don't need to condition on all previous components, but only on the last one. For example, it assumes that $P[DM > x | EDP = y \text{ and } IM = z]$ is equal to $P[DM > x | EDP = y]$, that is a function of only y . This presumes that EDP is "sufficient" with respect to DM and thus IM doesn't need to be included in the equation (Cornell, 2004).

The PEER Equation has been developed for mainshocks, which are commonly modeled as homogeneous Poisson processes with time-independent mean rate of occurrences or intensity functions. Moreover, since PSHA is usually performed using the mean annual rates of mainshock occurrences, the resulting probabilistic description of DV is usually also defined on an annual basis. This mean annual basis is also consistent with current safety criteria, which are commonly expressed in terms of mean annual fatality frequencies. Consequently, because of the duration of one year, which is implicit in the PEER Equation, and because of the rarity of mainshocks, the likelihood of multiple mainshock events is small. If the duration of interest is chosen to be other than one year (e.g. T), then the mean number of events exceeding $DV = x$ in T becomes $P(DV) \cdot T$. If T is much longer than one year (e.g. the nominal life of the considered structure), the multiple mainshocks are more likely. In this case, PEER Equation assumes that the damage structure is repaired to its pre-mainshock state (usually intact) before another earthquake occurs. However, if the DV is financial losses, the PEER Equation contains no explicit consideration of the time-value of money, because future financial losses are not discounted back to the present-day value.

Considering all these aspects, seismic risk can be viewed as the probability of observing a certain economic loss at a specific site during a defined time period: it depends on seismic hazard, vulnerability and exposure values. Exposure value is the economic estimates of the considered structure, population, economic activities and public services subjected to risk in a specific site.

In the light of what above-mentioned, application of seismic risk is very complex and difficult to quantify, particularly for the estimate of exposure value. Consequently it is often replaced by the probability of observing a certain damage level in a time period, so it's computed taking into account only seismic hazard and vulnerability: this risk is usually called specific risk (in this study

specific seismic risk is considered, so it's simply called seismic risk in the following). Eq. (2.1) becomes:

$$P(DV) = \int P(DV|IM) \cdot dH(IM) \quad (2.2)$$

where, in this case, DV coincides with DM. Assessment of expected damage for a set of Performance Levels (PLs) is obtained by convolution of the hazard probability density function, so it is obtained by seismic hazard and seismic fragility curves (Cordermatz et al., 2003; Grendene, 2006):

$$P_{PL} = \int_{IM} P(D > d_{PL} | IM) \cdot \left| \frac{dH(IM)}{dIM} \right| dIM \quad (2.3)$$

where $P(D > d_{PL} | IM)$ is the fragility curve associated to the damage level d_{PL} and $H(IM)$ is the seismic hazard function. The integral in Eq. (2.2) is known as convolution integral. If IM is a discrete variable with a finite set of values, Eq. (2.3) results as the following by means of the theorem of total probability (Ellingwood & Kinali, 2009):

$$P_{PL} = \sum_{IM} P(D > d_{PL} | IM) \cdot |\Delta H(IM)| \quad (2.4)$$

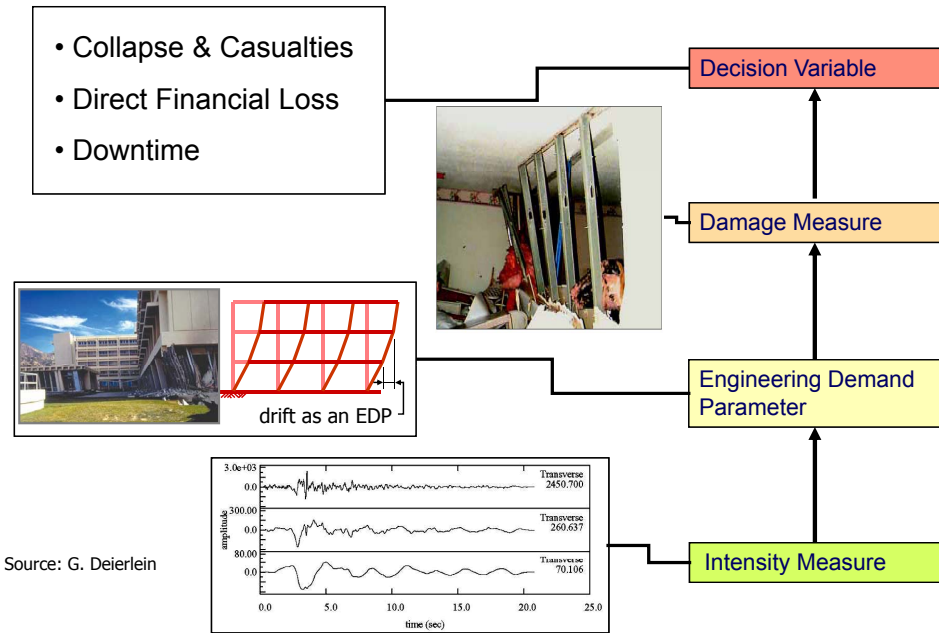


Fig. 2.1 PEER Performance-Based methodology (source by Deierlein, G.).

2.2 Seismic hazard

Seismic hazard is the probability of observing a certain level of ground shaking, Peak Ground Acceleration PGA or Spectral acceleration at 1s $S_a(1s)$, in a defined time period at a studied site. A distinction must generally be made between standard and local seismic hazards. Standard seismic hazard refers to standard ground conditions, and local hazard identifies the local effects produced by geomorphologic conditions of the site and their contribution to seismic hazard.

Seismic hazard is measured by the seismic hazard curve that usually represents the mean annual frequency by which a certain value of seismic action intensity is exceeded (Fig. 2.2). It can be obtained by a conventional Probabilistic Seismic Hazard Analysis – PSHA and it is assumed as a lognormal cumulative probability function (Cornell, 1968). Today, this is still the most

commonly used method worldwide to calculate hazards and draw up regional-scale zonation maps.

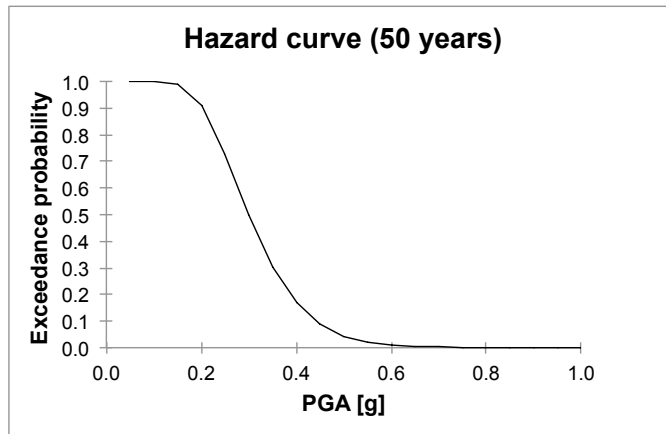


Fig. 2.2 Example of seismic hazard curve (50 years).

2.3 Seismic vulnerability

Seismic structural damage is important to assess during an earthquake risk evaluation. For a given structure, for instance a bridge, it is possible to predict, deterministically, the level of ground shaking necessary to achieve a target level of response or a damage state. Moreover assuming material properties and other structural characteristics which influence the overall capacity of the structure requires that certain assumption be made about the ground motion and the site condition, aspects which affect seismic demand. Both structural and site condition parameters aren't exact and they invariably have a measure of both randomness and uncertainty associated with them. Fig. 2.3 shows how these uncertainties can be considered. In a deterministic point of view the intersection of the two curves gives only one level of performance (or performance point), instead, considering a probabilistic distribution both for demand and capacity, a set of performance points can be possible.

Fragility curves can be considered as one of the most performing tools in order to characterize the probabilistic aspects of the phenomena, in particular to assess existing bridge seismic vulnerability (Shinozuka et al., 2000b; Monti & Nisticò, 2002; Franchin et al., 2006; Padgett & DesRoches, 2008; Zanini et al., 2013). They are instruments describing the probability of a structure being damaged beyond a specific damage state (or performance level) for various levels of ground shaking IM (Fig. 2.4), typically peak ground acceleration (PGA) or spectral acceleration (S_a). There are several methods to construct fragility curves and, mostly, these methods can be subdivided in two typologies: empirical fragility curves and analytical fragility curves, which are described in the followings, in particular for bridges.

The main assumption for all this methods is that fragility curve is a log-normal cumulative probability function (VV.AA., 1999; Cornell et al., 2002; Monti & Nisticò, 2002; Choi et al., 2003; Nielson & DesRoches, 2007): if structural capacity and seismic demand are random variables that approximately fit either a normal or log-normal distribution then, by means of the central limit theorem, it can be shown that the composite probability is log-normally distributed. Only two parameters are needed to define such a curves: a median (the 50th percentile) and a normalized logarithmic standard deviation. The cumulative probability functions is given by:

$$P(D > d_{PL} | IM) = P(S_d > S_c | IM) = \Phi \left[\frac{\ln(S_d / S_c)}{\beta} \right] \quad (2.5)$$

where S_d is the structural demand (damage on the structure) which changes for each IM, S_c is the structural capacity related to a specific performance level (median or expected value), β is the normalized composite log-normal standard deviation which takes into account uncertainty and randomness for both demand and capacity, it can also be computed as $\beta = \sqrt{\beta_d^2 + \beta_c^2}$ considering demand and capacity contributions respectively, and $\Phi[\bullet]$ is the standard normal distribution function.

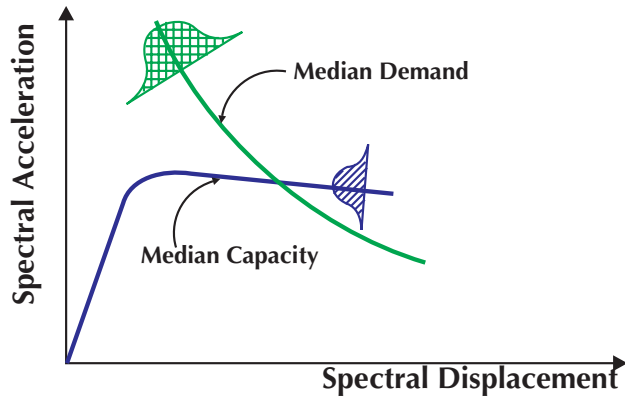


Fig. 2.3 Capacity-Demand Acceleration-Displacement spectra showing uncertainty in structural behavior and ground motion [source by VV.AA. (1999), in particular Mander, J.B.].

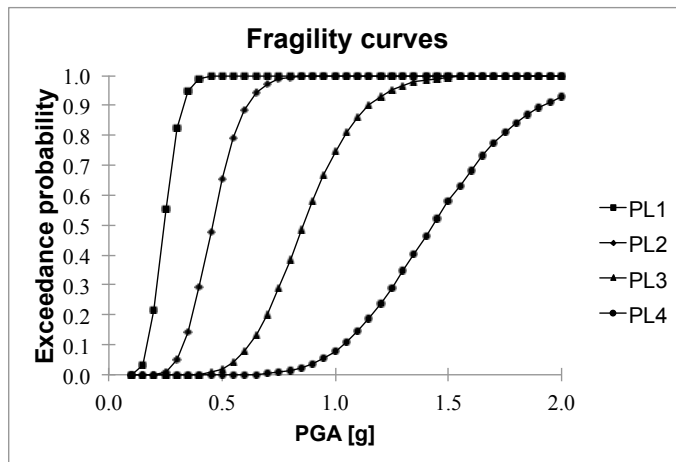


Fig. 2.4 Example of fragility curves for existing bridges considering four Performance Levels (PLs).

2.3.1 Empirical fragility curves

Empirical fragility curves are based on bridge damage data from past earthquakes, without considering any analytical analysis of bridge. Various methods were developed to generate empirical fragility curves: for example Shinozuka et al. (2000b) uses the maximum likelihood method to generate the curves from the observations of bridge damage in the 1995 Kobe earthquake. Another method is the RISK-UE method (Mongeo et al., 2003) based on the procedure described in HAZUS'99 (Federal Emergency Management Agency, 2001). As shown in Table 2.1, it classifies bridges in 15 typologies taking into account materials, column bent, type, span continuity and design (conventional or seismic). The considered damages states are shown in Table 2.2 and mainly they are descriptive damages states in according to HAZUS'99.

The fragility curves (median and dispersion of lognormal distribution) are mainly provided according to typology (Table 2.1), possible damages (Table 2.2), skew angle, length of the bridge, number and width of spans, spectral acceleration at 0.3s and 1.0s. The median is calculated by a specific empirical formula for each match of typology and damage state, whereas the dispersion is fixed at 0.6 for each match, as suggested in HAZUS'99.

Although these methods are express, they have some limitation and drawback. For instance ground motion intensity and its effects on the bridge may be different depending on the site where the structure was built. Another limitation is that damages on bridges due to lifetime or past earthquakes are not taken into account and they are different for each structure.

Analytical fragility curves can solve some of these limitations.

Material	Column Bent Type	Span Continuity	Design	Category
All	Single Span	-	Conventional	1
			Seismic	2
Concrete Bridges	Single	Simple Support	Conventional	3
			Seismic	4
		Continuous	Conventional	5
			Seismic	6
	Multiple	Simple Support	Conventional	7
			Seismic	8

		Continuous	Conventional	9
			Seismic	10
Steel Bridges	Multiple	Simple Support	Conventional	11
			Seismic	12
	All	Continuous	Conventional	13
			Seismic	14
Other			15	

Table 2.1 Typologies of bridges (RISK-UE).

Damage State Description	
None	/
Minor	Minor cracking and spalling to the abutment, cracks in shear keys at abutments, minor spalling and cracks at hinges, minor spalling at the column (damage requires no more than cosmetic repair) or minor cracking to the deck.
Moderate	Any column experiencing moderate (shear cracks) cracking and spalling (column structurally still sound), moderate movement of the abutment (<5cm), extensive cracking and spalling of shear keys, any connection having cracked shear keys or bent bolts, keeper bar failure without unseating, rocker bearing failure or moderate settlement of the approach.
Extensive	Any column degrading without collapse – shear failure - (column structurally unsafe), significant residual movement at connections, or major settlement approach, vertical offset of the abutment, differential settlement at connections, shear key failure at abutments.
Complete	Any column collapsing and connection losing all bearing support, which may lead to imminent deck collapse, tilting of substructure due to foundation failure.

Table 2.2 Possible consequences of earthquake on bridges (HAZUS'99 and RISK-UE).

2.3.2 Analytical fragility curves

Analytical fragility curves are developed through seismic analyses of the structure. Most of the analytical methods in the literature consist of three steps: simulation of ground motions, modelling of bridges taking into account the uncertainties and generation of fragility curves from the seismic response data of the bridges. The seismic response can be obtained from different types of analysis: non-linear time history analysis (Choi et al., 2003; Morbin et al., 2010), elastic spectral analysis (Hwang et al., 2000) and non-linear static analysis (Shinozuka et al., 2000a).

Some theoretical aspects regarding the construction of analytical fragility curves are in the followings.

2.3.2.1 Damage states

The generation of fragility curves requires definition of damage levels. Damage measures in earthquake engineering proposed in scientific literature are numerous and various and they can be defined for each structural element and sub-elements (local indexes) or related to the entire global structure (global indexes). An excellent review can be found in Cosenza & Manfredi (2000). The most commonly used parameters for the evaluation of structural damage are the ductility (rotation, curvature or displacement) and the plastic energy dissipation.

Considering kinematic or cyclic ductility as damage measure means to assume that the collapse of the structural model is expected for maximum plastic displacement, not taking into account the number of plastic cycles and the amount of dissipated energy. Structural collapse can be determined by a monotonic test.

When energy is taken as damage measure, the structure is considered to have a certain amount of energy, which can plastically dissipate. Collapse occurs when this amount of energy is reached during cyclic loads. Usually the assessment of the structural energy is hard to obtain.

Other damage indexes are based on the combination of ductility and energy, but the difficulty related to the evaluation of structural energy holds over.

As a result of that, the ductility is the parameter mainly used in literature to define a damage index. A comparison is usually made between the maximum plastic range reaches during cyclic loads and a value that expresses whether or

not the structure is in safe conditions. Assessment of intermediate damage levels can be determined. For example, considering reinforced concrete (RC) bridge piers, Choi (2002) proposed ductility damage indexes for each one of the descriptive damage states reported in HAZUS'99 (Table 2.2). These indexes (Table 2.3) are referred to the seismic demand on the base section of piers and they are calculated by the following formula:

$$d_{PL} = \frac{x_{max}}{x_y} \quad (2.6)$$

where x_{max} is the maximum horizontal displacement of a target point (e.g. the point at the top of the pier) during the time history of an earthquake and x_y is the horizontal displacement at the same point in relation to steel yielding in the base cross-section of the pier.

Damage states	Minor (PL1)	Moderate (PL2)	Extensive (PL3)	Complete (PL4)
Piers (d_{PL})	$1 \leq d_{PL} < 2$	$2 \leq d_{PL} < 4$	$4 \leq d_{PL} < 7$	$d_{PL} \geq 7$

Table 2.3 Definition of damage states based on ductility base pier section (Choi, 2002) in accordance to HAZUS'99 (RISK-UE) damage states.

Also a shear failure PL can be defined, e.g. piers shear failure. This PL is unique because shear failure is considered a brittle failure: it could be defined as in Eq. (2.6) where x_y is replaced by x_s , the horizontal displacement of the target point in relation to the pier shear failure, corresponding to the base cross-section of the pier, if the pier is considered as a cantilever.

The choice to consider flexural PLs, based on kinematic ductility, and/or shear failure PL depends on the pier behavior subjected to horizontal forces: in terms of displacements and strength, it is influenced by sectional behavior, geometrical characteristics, rotations at foundation level, presence of isolation device, etc. This topic is reviewed in detail in §2.4.

2.3.2.2 *Methods*

Different methods to generate fragility curves are in literature. All these methods agree that the damage function is well fitted by a lognormal distribution, e.g. Song & Ellingwood (1999); Monti & Nisticò (2002), but other probability density

functions (pdfs) could be considered. Here below two procedures, which will be considered in the following, are presented.

PROCEDURE A

According to Monti & Nisticò (2002), the damage function D in Eq. (2.5) can be defined as:

$$D = D(G(p), S_a | IM) \quad (2.7)$$

where G is the mechanical model of the structure (entire model or only the elements more vulnerable), p are statistical parameters which take into account uncertainties about mechanical characteristics of materials, S_a is the spectral acceleration at 1.0s, but it could be also considered the PGA.

Replacing Eq. (2.7) in Eq. (2.5), we obtain:

$$P(D > d_{PL} | IM) = P[D(G(p), S_a | IM) > d_{PL}] = \int_{D(IM) > d_{PL}} f_D(D | IM) dD \quad (2.8)$$

where f_D is the pdf that represents the damage.

A point of the fragility curve referred to a value of IM for a considered d_{PL} is calculated as follows:

- mean and variance values for n statistical parameters p are estimated and they are described by pdfs f_{pi} ;
- each pdf is subdivided in m intervals Δp_i^k and the central value p_i^k has an occurrence probability $f_{pi}(p_i^k) \cdot \Delta p_i^k$;
- the occurrence probability of the k .th combination Δp_i^k of $i = 1, \dots, n$ parameters is calculated (statistically independent):

$$\prod_{i=1}^n f_{pi}(p_i^k) \Delta p_i^k \quad (2.9)$$

- In this case, all the possible combinations among the m values of the considered n parameters are $k = 1, \dots, m^n$;
- seismic analyses of the structural model G are performed for every k -th combination and damage D_k is recorded as above mentioned;

- a damage pdf $f_D(D|IM)$ is defined by calculating mean $E[D]$ and variance $Var[D]$ values as follows:

$$E[D] = \sum_{k=1}^{m^n} D_k \left[\prod_{i=1}^n f_{p_i}(p_i^k) \Delta p_i^k \right] \quad (2.10)$$

$$Var[D] = \sum_{k=1}^{m^n} (D_k - E[D])^2 \left[\prod_{i=1}^n f_{p_i}(p_i^k) \Delta p_i^k \right] \quad (2.11)$$

- the integral in Eq. (2.8) is solved numerically and the integration lower bound is the damage value (e.g. pier ductility) for each considered Performance Level (PL).

PROCEDURE B

Given the seismic Intensity Measure IM (e.g. PGA or S_a), the average seismic structural demand S_d (strongly related to the damage by Eq. 2.6) can be defined by means of the following formula (Nielson & DesRoches, 2007):

$$S_d = e^A IM^B \quad (2.12)$$

This law can be represented by a straight line having the following equation:

$$\ln(S_d) = \lambda = A + B \ln(IM) \quad (2.13)$$

where A and B coefficients are calculated by linear regression of the entire set of the data, which depends on the probabilistic characterization of materials strengths (Cornell et al., 2002), and λ the average value related to a specific IM. An example of this linear regression is presented in Fig. 2.5.

After finding A and B coefficients and the dispersion, the fragility curve becomes a cumulative lognormal distribution as shown in Eq. (2.8). The lognormal distribution f_D , in this case expressed by d_{PL} , is defined in the following equation:

$$f_D(d_{PL}|IM) = \frac{1}{\sqrt{2\pi\epsilon}d_{PL}} \exp \left[-\frac{1}{2} \left(\frac{\ln d_{PL} - \lambda}{\epsilon} \right)^2 \right] \quad (2.14)$$

where ε is the dispersion and the other terms are above-defined. It should be pointed out that this probabilistic seismic demand model is performed for a specific IM range, but extrapolation beyond this range within reason is allowed by assuming a lognormal fit.

Both the procedures are referred to a single pier ($P_{f,PL, \text{pier}}$). Considering a bridge set up by N piers, the probability of the entire structure ($P_{f,PL, \text{system}}$) to get a certain PL for each IM is:

$$\max_{\text{pier}=1}^N [P_{f,PL, \text{pier}}(\text{IM})] \leq P_{f,PL, \text{system}}(\text{IM}) \leq 1 - \prod_{\text{pier}=1}^N [1 - P_{f,PL, \text{pier}}(\text{IM})] \quad (2.15)$$

where the lower bound is the probability of failure for a systems whose components are fully stochastically dependent, e.g. piers of multi-span continuous girder bridges, whereas the upper bound is the probability of failure for systems whose components are stochastically independent, e.g. piers of multi-span simply supported girder bridges (Choi et al., 2003).

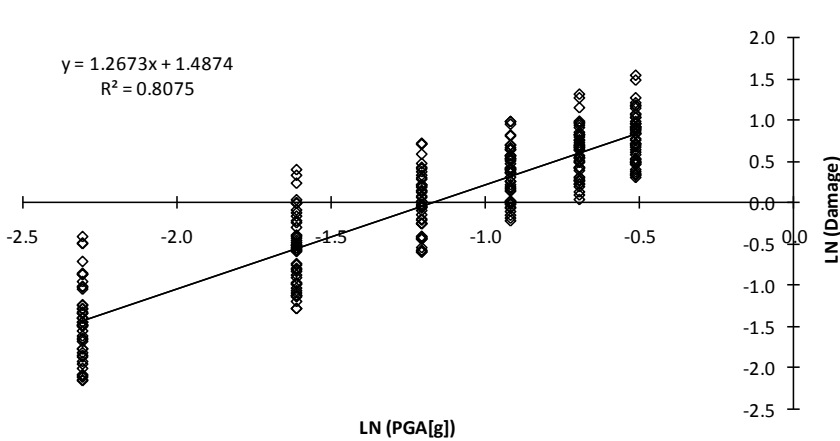


Fig. 2.5 Example of linear regression in a $\ln(\text{PGA}/g)$ vs. $\ln(\text{Damage})$ diagram.

2.3.2.3 *Accelerograms for non-linear dynamic analysis (NLDA)*

Once defined the response parameters to be recorded, the above-described procedures are suitable for any seismic analysis. In particular for non-linear dynamic analysis (NLDA), a set of accelerograms has to be chosen.

Accelerograms can be natural (i.e. coming from real seismic events) or artificial (i.e. coming from any analytical method) and both of them must have content in frequency which fits that of the target spectrum for the specific site where the structure was built.

Concerning artificial accelerograms, the stochastic vibration method (Vanmarcke, 1976) is considered in this study. This method is implemented in SIMQKE code (Gasparini & Vanmarcke, 1976), which calculates power spectral density function from a defined response spectrum (Eurocode 8, Italian Building Code (2008) or user-defined) and uses this function to derive the amplitudes of sinusoidal signals having random phase angles uniformly distributed between 0 and 2π . The sinusoidal motions are summed to generate independent accelerograms (compatible with the response spectrum). In this work the target spectra are horizontal and vertical elastic response spectra with 5% damping coefficient and 4s largest period. Artificial accelerograms total duration is 20s: the stationary part of the accelerograms starts after 2s and its duration is 10s, according to Italian Ministry of Infrastructures (2008). The response spectra ordinates of these accelerograms are in the range of 90% (lower bound) and 130% (upper bound) with respect to the ordinates of the above-mentioned target spectra (Fig. 2.6).

Whereas, concerning natural accelerograms, REXEL code (Iervolino et al., 2010) allows to search for sets of 7 records compatible, in the average, with design spectra coming from Eurocode 8, Italian Building Code or user-defined. Records may also reflect the seismogenetic feature of the sources (magnitude and epicentral distance), ground motion intensity and soil conditions. The databases contained in REXEL are the European Strong-motion Database (ESD), the Italian Accelerometric Archive (ITACA) and the Selected Input Motions for displacement-Based Assessment and Design (SIMBAD).

In order to carry out NLDA for different IMs (e.g. PGA), each accelerogram (natural or artificial) is scaled by a numerical factor to obtain various values of IM and perform the fragility analysis, e.g. Franchin & Pinto (2009).

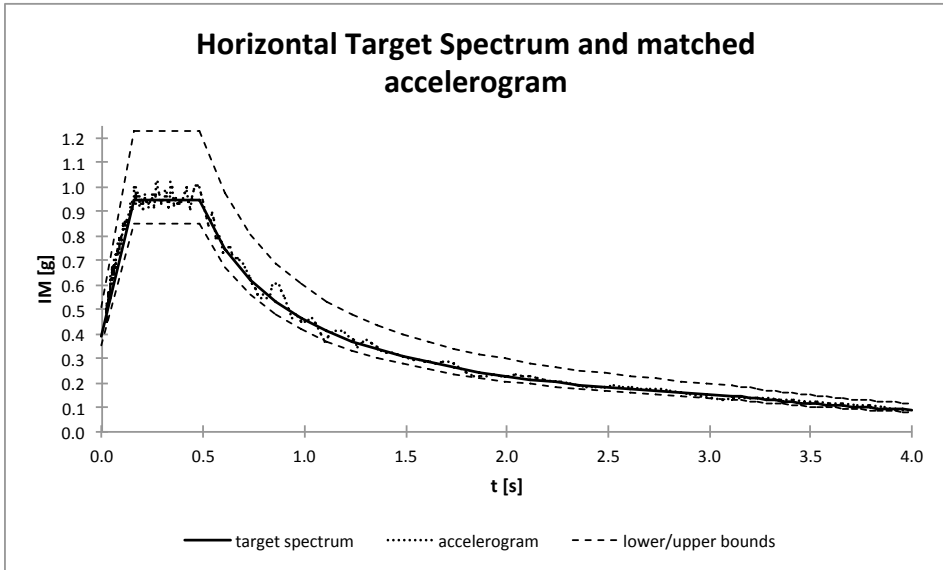


Fig. 2.6 Example of a horizontal target spectrum with a matched accelerogram by Vanmarcke (1976) method.

2.4 Flexural and shear behavior of RC columns

Piers and columns are mainly used to transfer deck or floor gravity loads to foundations by means of axial compression. However, when subjected to a seismic load, these vertical structural members result essential components of the lateral force resisting system. Damage caused by horizontal actions (flexural and shear) can compromise the axial load capacity of the vertical members and lead to collapse. The importance of this topic was highlighted by the development of seismic design in the early Seventies.

A shear critical column (column vulnerable to shear failure) is assumed to have a linear elastic force-deformation law up to flexural yield. If the induced shear force in the column reaches the shear strength at a value lower than nominal yield strength, then the assessment usually implies failure at very low displacements. This can make the procedure too conservative. Therefore, Miranda et al. (2005) suggest that a particular source of flexibility occurs in

those columns in which shear capacity is reached prior to development of full flexural strength: the force-deformation response shows a loss of stiffness before the actual failure occurs. The formation of stable diagonal shear cracks in the columns has been identified as the source of flexibility that allows additional member displacements.

It has been recognized that shear strength of RC columns is reduced with increasing ductility. As lateral drift increases, the flexural-shear cracks widen and the concrete mechanism of shear transfer degrades due to loss of aggregate interlock. The Applied Technology Council (1981) proposed a conceptual model that described the relationship between shear strength and displacement ductility. Idealizing flexural response, three possible failure modes of columns subjected to lateral displacements are considered (Fig. 2.7). Flexural failure occurs if the shear force corresponding to the nominal flexural strength is less than the shear capacity for any value of ductility (Fig. 2.7a). A flexural shear failure takes place when the column reaches its flexural capacity first, but if the ductility increases the corresponding shear force exceeds the shear strength envelope and a shear failure happens (Fig. 2.7b). A brittle shear failure occurs when column capacity is reached before developing its flexural strength (Fig. 2.7c). This conceptual model is considered in several ductility dependent shear capacity models, e.g. (Priestley et al., 1994; Kowalsky & Priestley, 2000; Sezen, 2002).

Ductility can be related to lateral drift, so the ductility dependent shear models can be used to determine the drift corresponding to shear failure. In general, when the drift at shear failure is reached, a rapid degradation of strength occurs and application of other lateral loads can compromise its vertical load bearing capacity. Priestley et al. (1996b) agrees that the drift at shear failure can be considered that point which correspond to the ductility level where the flexural strength response curve intersects the shear strength envelope (Fig. 2.7b,c). Sezen (2002) suggests not to use shear capacity models to calculate the shear failure of columns that fail in flexural-shear, because he finds high uncertainties when drift at shear failure is evaluated. Elwood (2002) compares the available drift capacity models with external database results and he finds no satisfactory comparisons, therefore he proposes an empirical drift capacity model that provides better results.

Since a drift capacity model exclusively design to predict the failure drift of columns in which shear failure occurs before flexural yielding is not yet proposed, assessment of this type of columns has to be carry out by means of

shear capacity model approach. However, a bilinear flexural response curve is normally used and no allowance is made for the loss of stiffness that results from shear cracking.

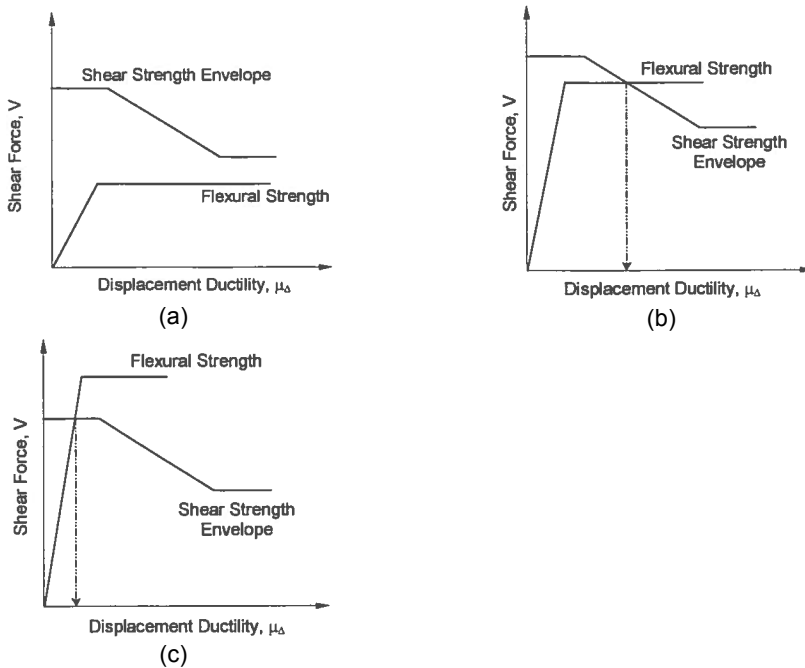


Fig. 2.7 RC column failure modes classification according to (Applied Technology Council, 1981): flexural failure (a), flexural-shear failure (b) and brittle shear failure (c). Source by Miranda et al. (2005).

Fig. 2.8 shows the force-deformation law of two rectangular reinforced concrete columns. Bilinear flexural response curve is usually obtained from a bilinear approximation of the moment-curvature diagram associated to the column critical section. By definition, shear deformations are neglected in its construction. Shear deformations tend to be small in column dominated by flexure, so the bilinear approximation is good in these cases (Fig. 2.8a). On the contrary, shear deformations usually account for a large portion of the total displacements in shear dominated columns, moreover significant additional displacement occur after shear cracks open in the column. These shear related effects cause a rather conservative prediction of lateral drift provided by bilinear flexural curve (Fig. 2.8b). This (experimental) force-deformation response shows a loss of stiffness before the actual failure occurs and, because of

localized softening, the column starts to fail at much higher displacements than predicted by the approach in Applied Technology Council (1981).

Considering shear capacity model approach, Calvi et al. (2005) aims to reduce the conservatism associated to the assessment of RC column by means of a curve constructed by independently calculating the flexural stiffness and shear stiffness of the column (Fig. 2.9). These stiffnesses are evaluated in three phases of the column response: elastic behavior, flexurally cracked behavior and behavior after shear cracking. In this stiffness-based approach, the accuracy of the calculated displacement depends on the certainty of the considered force level.

The presented aspects on this topic show that further studies need to be conducted in order to model correctly flexural-shear behavior of RC columns.

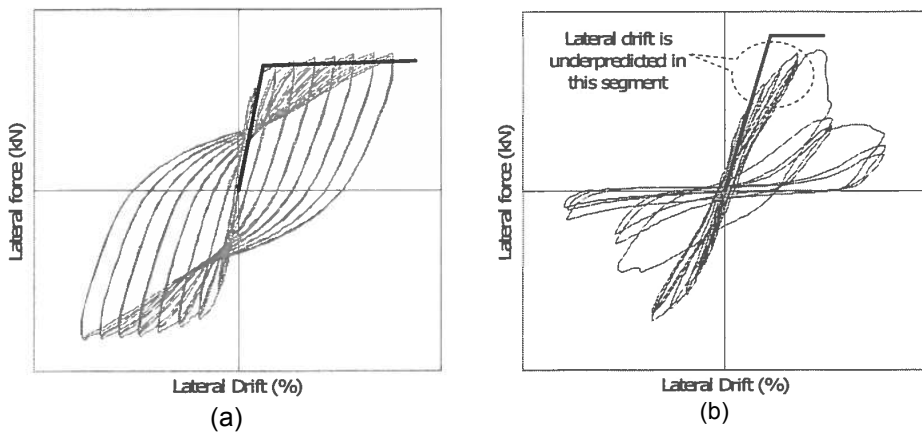


Fig. 2.8 Reinforced concrete column failure modes: flexural failure (a) and brittle shear failure (b). Source by Miranda et al. (2005).

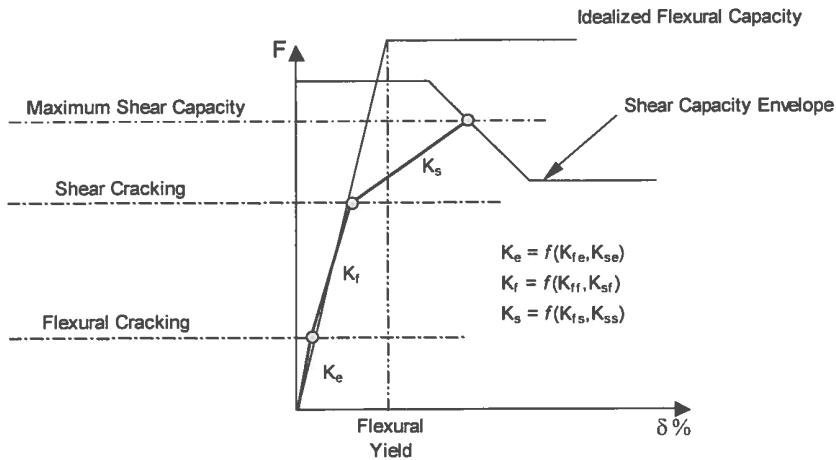


Fig. 2.9 Total force-deformation response according to Calvi et al. (2005).
Source by Miranda et al. (2005).

Construction of the shear-capacity envelope is carried out considering the above-presented shear models. In particular, Miranda et al. (2005) suggests that shear model proposed by Kowalsky & Priestley (2000) provides a much better correlation with experimental results for the “bridge-type” columns, i.e. columns with a relative large cross section with many longitudinal bars closely spaced around the perimeter. Whereas Sezen (2002) shear model seems to achieve better results for “building-type” columns, i.e. vertical elements characterized by a smaller cross section and few longitudinal bars around the perimeter. Since this study mostly concerns bridges, shear capacity envelope by the former is presented.

Kowalsky & Priestley (2000) predicts shear strength V_A of a particular member as the sum of three components:

$$V_A = V_c + V_s + V_p \quad (2.16)$$

where V_c is the concrete mechanism, V_s the steel truss mechanism and V_p the axial load contribution. The contribution of shear strength of the concrete mechanism is based on the product the effective shear area and shear strength of concrete according to the following formula:

$$V_c = \alpha\beta\gamma\sqrt{f_{c0}}(A_e) \quad (2.17)$$

where A_e is the effective shear area, taken as $0.8A_g$ (A_g is the gross area of a concrete section) and f_{c0} the unconfined concrete maximum stress. The shear strength of concrete is represented by the term $\gamma\sqrt{f_{c0}}$ which degrades with increasing ductility (Fig. 2.10a).

The factors α and β are used as multipliers to take into account the effect of column aspect ratio and longitudinal steel ratio (Fig. 2.10b,c).

The contribution of the transverse reinforcement to shear resistance is represented by the following formula:

$$V_s = \frac{A_{st} f_{y,st} d'}{s} \cot \theta \quad (2.18)$$

where θ is the inclination of diagonal cracks with respect to the column axis, 30° recommended by Priestley et al. (1994), A_{st} is the transverse steel area, d' considers the reduced column width across which the shear strength of steel truss mechanism is mobilized and it's calculated as:

$$d' = d - c - c_m \quad (2.19)$$

where d is the column depth, c is the depth of compression zone and c_m is the cover to main bars.

The axial load component of the model reflects the contribution to shear strength that comes from the formation of an inclined compression strut along the height H of the column. It is calculated as (Priestley et al., 1994):

$$V_p = P \tan \alpha = \frac{d - c}{2L} P \quad (2.20)$$

where P is the axial load in the inclined strut, c is the depth in the compression zone and L is the column shear span ($L = H$ for cantilever columns and $L = H/2$ for columns in reverse bending), as shown in Fig. 2.11.

More details about flexural-shear behavior of RC structural vertical members can be found in Miranda et al. (2005).

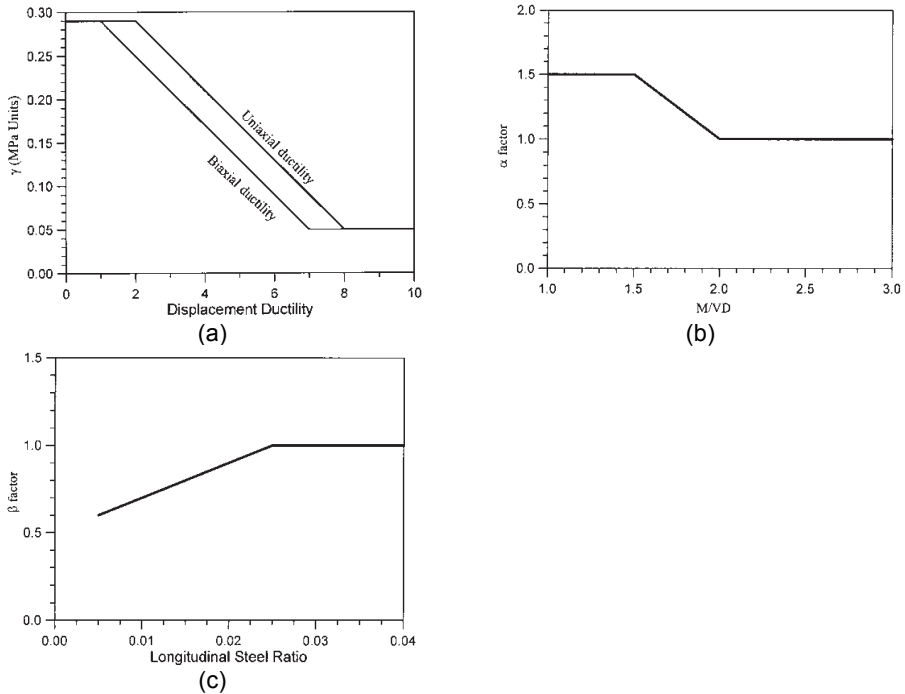


Fig. 2.10 Factors for calculating shear strength: γ factor for shear strength of concrete (a), α factor for column aspect ratio (b) and β factor for longitudinal steel ratio (c). Source by Kowalsky & Priestley (2000).

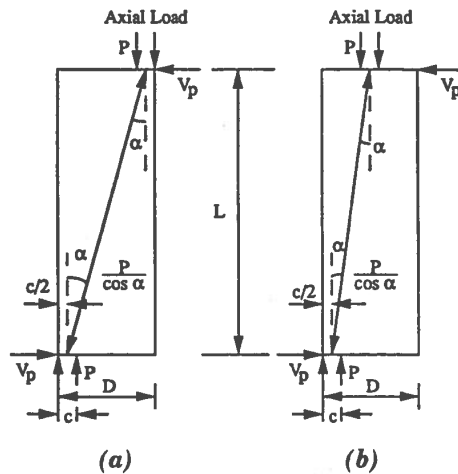


Fig. 2.11 Axial load contribution in columns with double bending (a) and single bending (b). Source by Priestley et al. (1994).

2.5 Defect detectability function

Durability can be defined as the conservation of the physical and mechanical characteristics of the structure and the materials with which the structures are built, this conservation must have duration equal to the design life of the building. Indeed, a structure has a sufficient durability if, with ordinary maintenance, it maintains strength and stability characteristics during all its life, preserving its attitude to be used: some recent improvements about maintenance and rehabilitation of civil engineering systems can be found in Biondini & Frangopol (2011). Durability is fundamental to ensure safety levels established in the design Codes.

Environmental factors can reduce the integrity of existing structures. Some damages caused by environmental conditions, regarding existing reinforced concrete (RC) structures, are the following: concrete cover damage that exposes reinforcing steel bars to atmosphere and, so, to corrosion, concrete carbonatation that induces steel corrosion, concrete damaged by icing cycles, concrete damaged by deicing salts that induce volume increment causing concrete spalling and steel corrosion, ageing of structural materials leading to the degradation of their mechanical properties, etc.

In particular, steel reinforcement corrosion protection depends on density, quality and thickness of concrete cover and cracking. The basic environment created by concrete application over steel reinforcement helps to limit corrosion, which increases with low pH conditions. The higher concrete cover and the lower concrete porosity and cracking, the higher the protection ensured to the structure. Cover density and quality is achieved by controlling the maximum water/cement ratio and the minimum cement content. It may also be related to concrete strength class. Two phases can be individuated in the life of a reinforced concrete structures: the beginning of corrosion, in which the protective film of the bars is destroyed, and then corrosion propagation, which starts after the destruction of the protective film, until reaching the serviceability limit state. There are several environmental causes that could induce corrosion: we start analyzing carbonation action.

As above-mentioned, another environmental cause that could induce corrosion is the carbonatation. Carbonation is a chemical reaction that leads to calcium carbonate (CaCO_3) formation. This process requires three elements: carbon dioxide (CO_2), present in surrounding air, calcium phases (Ca), present in concrete, water (H_2O), present in the pores. The presence of water and air in

concrete matrix increases when the porosity and cracking are high, creating an intense fluids exchange flux. When the reactions take place, pH value of concrete is above 13, whereas pH value of fully carbonated concrete is below 9. Once the carbonation process reaches steel reinforcement, rebar will deteriorate due to passive film destruction, and corrosion will start. As we expect, carbonation process speed mainly depend on two parameters: concrete porosity and moisture content. In particular, when the relative humidity (RH) in the pores is higher than 90% carbon dioxide is not able to enter the pore, and when RH is lower than 40% carbon dioxide cannot dissolve in water. To evaluate corrosion induced by carbonation, the most used test is the Phenolphthalein test. This compound is used as an acid or base indicator: where in contact or presence of acid, it will turn colorless, whereas with a base it will turn into a pinkish violet color.

Another environmental cause that can induce corrosion is due to chlorides presence, and for this reason it is a phenomenon mainly localized for marine structures or for structures located in tropical climates. Chlorides corrosion time of beginning depends on several factors, such as the quantity of chlorides on the R.C. external surface, the cementitious matrix characteristics, concrete cover thickness and critical content of chlorides. In general it is a quick process, which induce severe rebar localized erosion, known as pitting phenomenon. For structures exposed to the atmosphere, when the localized attack begins, the corrosion velocity can vary from some tenths of $\mu\text{m}/\text{year}$ to one 1 mm/year: this last value is reached when the humidity increases from 70 to 95%, and the quantity of chlorides from 1 to 3% (in weight with respect to the cement). Moreover, passing from temperate to tropic climate, corrosion velocity increases faster, due to the higher quantity of chlorides deriving from marine breeze and the higher relative humidity of the air, which helps their penetration in the matrix. Also the compacting degree of concrete can influence the corrosion levels due to chlorides, because of the porosity dependence of the process. In practice, corrosion due to chlorides, when started, can rapidly cause unacceptable reduction of bar cross-section. Marine structures which have both air and water contact (partial submerged) are the ones subjected to the highest damage due to chloride corrosion: the zone of the tides is the structure part in contact with tides, which varies from the maximum to the minimum level, and the zone of sprinkles is the one where sprinkles arrived due to crest tides break.

However, periodic inspection of degrading structure followed by suitable maintenance may restore it to near-original condition. In particular, a component

may not even be replaced or repaired during maintenance unless damage is detected and larger than a certain threshold. In this case the effect of the damage overlooked at an inspection or detected but not repaired also should be considered. To reach this goal, it's necessary to consider the probability of detecting damages of a given size or extent and to introduce models which take into account damage initiation and intensity.

Different methods can be considered to perform inspections: usually non-destructive evaluation (NDE) methods are preferred because most of them maintain the structure in service during tests. Some of NDE methods are the followings: visual inspections, Schmidt hammer, pachometer, dynamic tests, ultrasonic pulse velocity tests, etc.

None of these NDE methods can detect a given defect with certainty. Their imperfect nature needs to be described in statistical terms. Fig. 2.12 illustrates the probability $d(x)$ of detecting a defect of size x . Such a relation is called defect detectability function (DDF) and it conceptually exists for each inspection technology (Mori & Ellingwood, 1994).

The maintenance of structures is strongly related to the effect of inspection, which depends on the DDF associated with a specific NDE method. The inspection with higher $d(x)$ makes repair more likely: for instance, if an inspection is perfect, i.e. $d(x)=1$ for $x>0$, the inspected component will be restored to its original condition by the repair.

The simplest DDF which can be considered is a step DDF with one threshold x_{th} , where x_{th} is the minimum detectable value of damage. In other words, damage with intensity greater than x_{th} is detected with probability one, $d(x)=1$, while damage with intensity less than x_{th} is overlooked with probability one, $d(x)=0$.

In general DDF is not a step DDF, but rather a non-decreasing function of damage intensity (Fig. 2.12). We can notice that a DDF has the same property as a cumulative density function (cdf), i.e. non-decreasing and taking a value within $[0,1]$: $d(x)$ can be taken into account as a step DDF in which threshold value, x_{th} , is a random variable with the cdf.

More details about DDF and its application on maintaining reliability of structures can be found in Mori & Ellingwood (1994).

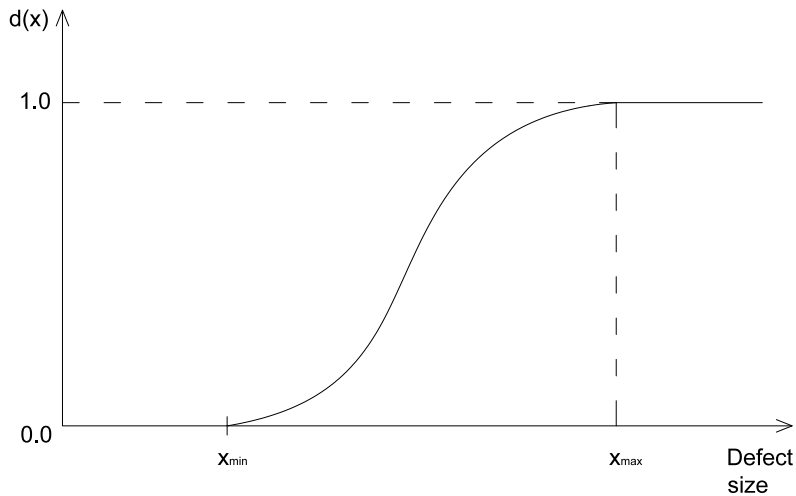


Fig. 2.12 Example of defect detectability function (DDF).

2.6 Fiber-reinforced polymer (FRP) retrofitting interventions

A number of existing RC bridges need retrofitting because of improper design or construction, change of the design loads, damage caused by environmental factors or seismic events (Priestley et al., 1996a; Kim & Shinozuka, 2004; Pan et al., 2010; Zhou et al., 2010). FRP technique has become a common and competitive technique for retrofitting RC elements: in particular, FRP jacketing is commonly used to increase compressive strength and ductility of RC elements subjected to prevalent compressive actions (e.g. circular and rectangular columns and bridge piers).

Structural behavior of FRP strengthened RC elements has been studied during last years and the first generation of design guidelines for strengthened concrete was made: some examples of such guidelines are European fib bulletin 14 (fédération internationale du béton, 2001) and Italian Recommendations CNR-DT 200 2004 (National Research Council, 2004). Analytical models proposed by these guidelines and other studies (e.g. Harajli et al. (2006); Tastani et al. (2006); Wang & Wu (2008)) seem not to sufficiently investigate interaction mechanisms between internal existing steel

reinforcement and external FRP, important aspect for RC elements mostly in compression. In this study the model developed in Pellegrino & Modena (2010) is considered: it takes into account that the steel reinforcement can reduce the efficiency of the FRP retrofit modifying the structural behavior of the columns at the ultimate limit state (Tinazzi et al., 2003; Pellegrino & Modena, 2010).

2.6.1 Effective confining pressure

Regarding the case of circular columns with internal steel stirrups or spirals, as in the bridge taken as an example, the confinement pressure f_{ls} due to transverse reinforcement is usually calculated as:

$$f_{ls} = \frac{1}{2} k_s \rho_{st} f_{y,st} \quad (2.21)$$

where ρ_{st} is the transverse steel ratio, $f_{y,st}$ the yield stress of the transverse steel reinforcement and k_s the coefficient of efficiency for the confining transverse steel.

The confinement pressure f_{lf} due to FRP composite is computed as:

$$f_{lf} = \frac{1}{2} k_f \rho_f E_f \epsilon_f^{eff} \quad (2.22)$$

where k_f is a coefficient of efficiency equal to 1 for continuous wrapping with fibers perpendicular to the longitudinal axis of the pier (National Research Council, 2004), E_f is the elastic modulus of the FRP retrofit and ρ_f is the FRP retrofit ratio, equal to:

$$\rho_f = \frac{4n_f t_f}{d} \quad (\text{circular columns}) \quad (2.23a)$$

$$\rho_f = \frac{2n_f t_f (b+h)}{bh} \quad (\text{rectangular columns}) \quad (2.23b)$$

being n_f and t_f the number of FRP layers and the thickness of the single FRP layer respectively, d the diameter of the circular cross-sections, b and h the width and the height, respectively, for the rectangular cross-sections.

The main features proposed in the model of Pellegrino and Modena are described in the following. More details on this analytical model can be found in Pellegrino & Modena (2010).

The term $\varepsilon_f^{\text{eff}}$ in Eq. (2.22) is the effective hoop FRP strain: according to the experimental results available in literature this strain is less than the ultimate FRP strain ε_{fu} . On this basis, most of the analytical models reduce the ultimate FRP strain ε_{fu} for the calculation of the confinement pressure at failure with a coefficient of efficiency of the FRP retrofit k_ε :

$$\varepsilon_f^{\text{eff}} = k_\varepsilon \varepsilon_{fu} \quad (2.24)$$

For concrete columns with steel reinforcement, the coefficient of efficiency of the FRP k_ε shows a significant dependence on the parameter C defined as follows:

$$C = \frac{E_{y,\text{long}} \cdot \rho_{y,\text{long}}}{E_f \cdot \rho_f} \quad (2.25)$$

where $E_{y,\text{long}}$ and $\rho_{y,\text{long}}$ are the elastic modulus of the longitudinal steel reinforcement and the longitudinal steel ratio respectively, whereas E_f and ρ_f are the elastic modulus of the FRP and the FRP retrofit ratio. The reason why k_ε shows a significant dependence on the parameter C, which represents the ratio between longitudinal steel and FRP rigidities, is that external FRP confinement in columns provides additional restraining for vertical steel rods, postponing buckling especially when steel stirrups are poorly stepped. Due to the interaction between the two materials, if the rigidity of the external FRP jacketing is not enough to contrast buckling of vertical bars, stress concentrations in the FRP can occur and cause its premature failure. Hence the coefficient of efficiency of the FRP k_ε for concrete columns with steel reinforcement is calculated by means of a regression analysis of the experimental data with different expressions for CFRP (Carbon FRP) and GFRP (Glass FRP) confinements. The proposed expression for k_ε is the following:

$$k_\varepsilon = \gamma C^{-0.7} \leq 0.8 \quad (2.26)$$

where $\gamma=0.7$ for CFRP confinement and $\gamma=1.5$ for GFRP confinement. The value of k_ε is conservatively limited to 0.8.

The total confining pressure P_u can be computed as the sum of the contributions due to FRP wrapping f_{fr} and transverse steel reinforcement f_{ls} , reduced with the ratio A_{cc}/A_g , where the A_{cc} is the area of the cross-section included in the transverse steel and A_g the area of the overall cross-section:

$$P_u = f_{fr} + f_{ls} \cdot A_{cc}/A_g \quad (2.27)$$

2.6.2 Stress-strain curve

In the model of Pellegrino & Modena (2010) the experimental trend of the stress-strain curve of FRP confined concrete shows, after a first phase in which it is very similar to that of unconfined concrete, a transition zone followed by a plastic phase with increasing branch according to the effectiveness of the confinement.

According to the results included in the wide experimental database described in Pellegrino & Modena (2010) and considering circular columns as example, it was observed that stress-strain curves mostly have an increasing branch until failure. As shown in Fig. 2.13, after a first increasing branch similar to that of unconfined concrete, another increasing branch, in which confinement becomes active and confining pressure increases almost linearly, is assumed. The model for the confined concrete peak stress f_{cc} is shown in the following equation as a function of the unconfined strength f_{c0} :

$$\frac{f_{cc}}{f_{c0}} = 1 + k_1 \cdot \frac{P_u}{f_{c0}} \quad (2.28)$$

The coefficient k_1 is computed as the product of two coefficients:

$$k_1 = k_A \cdot k_R \quad (2.29)$$

The coefficient k_A is computed with the same formula proposed in Harajli et al. (2006):

$$k_A = A \left(\frac{P_u}{f_{c0}} \right)^{-\alpha} \quad (2.30)$$

with $A=2.95$ and $\alpha=0.40$; A and α are computed by means of a regression analysis of the experimental data included in the experimental database described in Pellegrino & Modena (2010). The reduction coefficient k_R is equal to 1 for circular columns.

According to the common approach of the literature, the ratio $\varepsilon_{cu}/\varepsilon_{c0}$ between confined and unconfined strains is estimated as a function of the confinement pressure P_u :

$$\frac{\varepsilon_{cc}}{\varepsilon_{c0}} = 2 + B \left(\frac{P_u}{f_{c0}} \right) \quad (2.31)$$

The parameter $B=28$ is computed by means of a regression analysis of the experimental data included in the experimental database described in Pellegrino & Modena (2010).

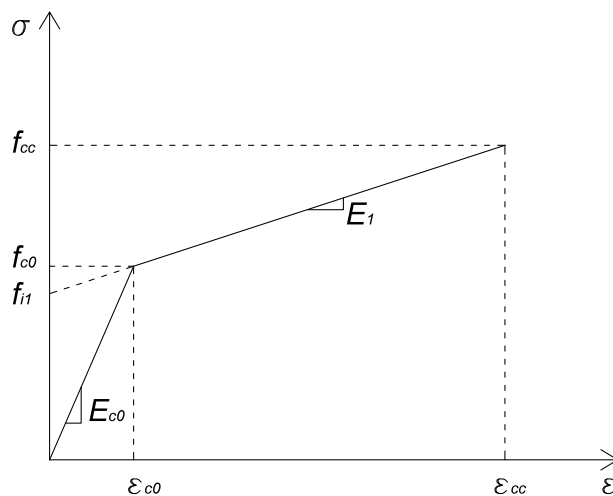


Fig. 2.13 σ - ε diagram for circular columns (Pellegrino & Modena, 2010)

3 PROBABILISTIC FRAMEWORK FOR SEISMIC ASSESSMENT OF MAINSHOCK-DAMAGED BRIDGES

In most cases bridges are the most vulnerable elements in the transportation network during a seismic event, therefore their seismic vulnerability assessment is necessary for a proper aids planning during emergency (immediately after the earthquake) and post-emergency phases and to define a priority fo retrofit interventions.

In this context, a new framework to assess seismic vulnerability of existing bridges after an earthquake mainshock by means of visual inspections on the structures is proposed in the following (Fig. 3.1). The main aim is to provide useful information to owners or Institutions to decide whether or not allowing traffic over a bridge after a seismic event and whether or not repairing mainshock-damaged bridges immediately, in order to manage an optimal budget allocation.

The framework is made up by six steps: the first two steps concern collecting information about existing bridges within a transportation network and calculating the respective fragility curves, the other four steps concern actions planning after a seismic event.

Although the framework can be applied to any kind of civil infrastructure, in particular any typology of bridge, more focus is given to (existing) reinforced concrete (RC) multi-span simply supported girder bridges, a common structural scheme in Italy.



Fig. 3.1 The framework proposed in this study to assess seismic vulnerability of existing bridges after an earthquake mainshock.

3.1 Step 1: collecting bridges information for a database

A web database of the network road bridges with photos, information about materials, static scheme, location and Finite Element Models (FEMs) has to be created. Bridges fragility curves and information about that specific seismogenetic zone (SZ), e.g. hazard curves, have to be embedded, too. This database is useful because, after a seismic event, the velocity to find information about characteristics and structural scheme of bridges is fundamental. An example of database is the I.Br.I.D. (Italian Bridge Interactive Database) Project performed by the Department of Civil, Environmental and Architectural Engineering – University of Padova (VV.AA., 2006-2012). An example of I.Br.I.D. webpage is shown in Fig. 3.2.

The Interactive Bridge Database provides information and data on bridge structures given by the members of the project as well as by the registered users, which are dealing with inspection and maintenance of such structures. The registered users can add new data to the database by filling in the requested forms and browse through the contributions of the other users. The data are available free of charge for further R&D work. The database supplies different types of information. In particular, basing on all the information provided in input, the results of a simplified analysis of the structural seismic vulnerability are available as output. Details on the seismic vulnerability analysis are given in the section 'Research Issues'.

The information is stored in the computer by means of tables in the format of the MySql database software. The layout of the tables is designed to define a number of information objects. Each object has a number of properties (e.g. title, e-mail address, etc.). The objects are combined to deliver the contents of requested entities.

When a user requests an entity, the system extracts the appropriate objects from the MySql tables. The attributes of the entity are assigned the value of their corresponding object property. Hereafter the entity is passed via the Internet to the requesting user.

An advantage with this design is, that it will be possible in the future to define new entities without significant alteration of the existing data tables. (e.g. 'Bridge engineering' could be an entity which draws information from all objects with 'bridge' properties).

The need for continuous maintenance of infrastructure systems, classification and updating of the information on structural conditions makes this database an

important tool to reach these goals. Society depends on the transportation infrastructure for economic, environmental, life-quality, safety and employment protection reasons. The failure of a single bridge can cause a huge loss to society. Considering the number of structures reaching a critical age, innovative test and assessment tools as well as methods are required in order to avoid an infrastructure breakdown.

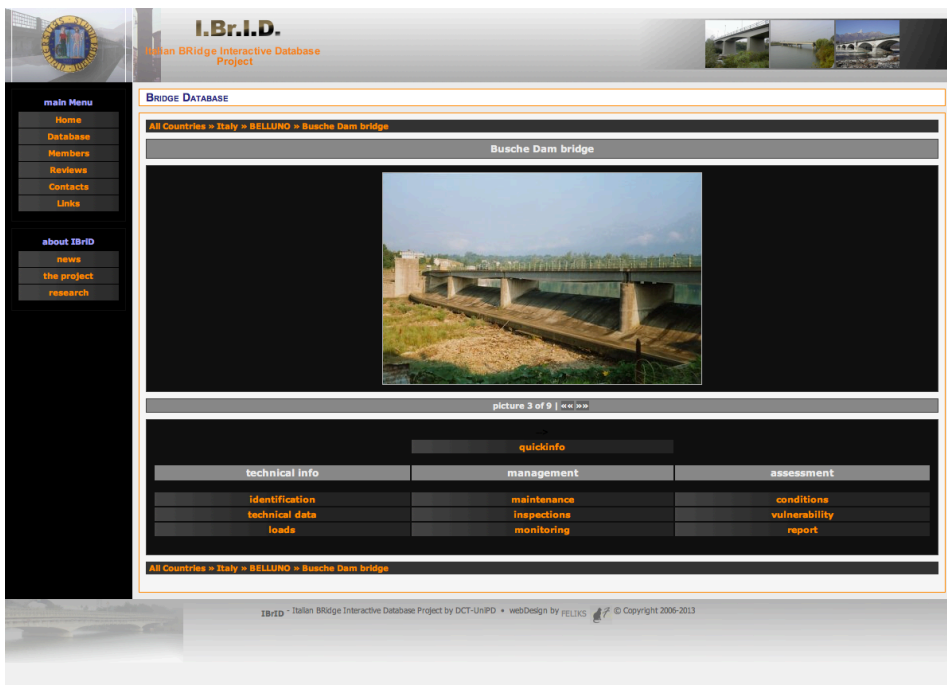


Fig. 3.2 I.Br.I.D. webpage (VV.AA., 2006-2012): example for Busche Dam bridge (Belluno province, northern Italy).

3.2 Step 2: generation of fragility curves

Fragility curves need to be calculated for each bridge in the above-mentioned database in order to integrate it. As shown in previous paragraphs, seismic vulnerability is an essential phase in the earthquake risk assessment procedure, so an investigation about the generation of fragility curves is carried out in the following.

3.2.1 *Investigation on the generation of fragility curves*

An investigation on the calculation of fragility curves is carried out in order to make a comparison between the methods shown in §2.3, taking into account different analytical models of the bridges. Two bridges are considered as example: a case study coming from Fener bridge (between Treviso and Belluno provinces, North-Eastern Italy) and an A27 overpass having a structural scheme usual for bridges that overpass the A27 highway (Venezia-Belluno, North-Eastern Italy). These bridges were built in strategic points on the road network in Veneto region and, furthermore, they are located in moderate/high seismic zones, according to the Italian seismic hazard map by INGV – National Institute of Geophysics and Volcanology (Fig. 3.3).

Since a number of studies mention that longitudinal direction controls bridge response, others declare that transversal direction governs damage on bridge, fragility curves are calculated for both directions in order to define the most vulnerable one.

Lack of data on Italian bridges makes more difficult the identification of damage states, therefore damage states shown in Table 2.2 are considered in this investigation. Consequently piers are considered the most vulnerable elements of the bridges (Shinozuka et al., 2000a; Franchin & Pinto, 2009) taking into account the four damage states presented in Table 2.3: these damage states referred to piers consider a global damage on bridge, as described in the above-mentioned Table 2.2, accounting (in a simple manner) unseating of deck, piers shear failure, movement of the abutments, shear key failure, etc.

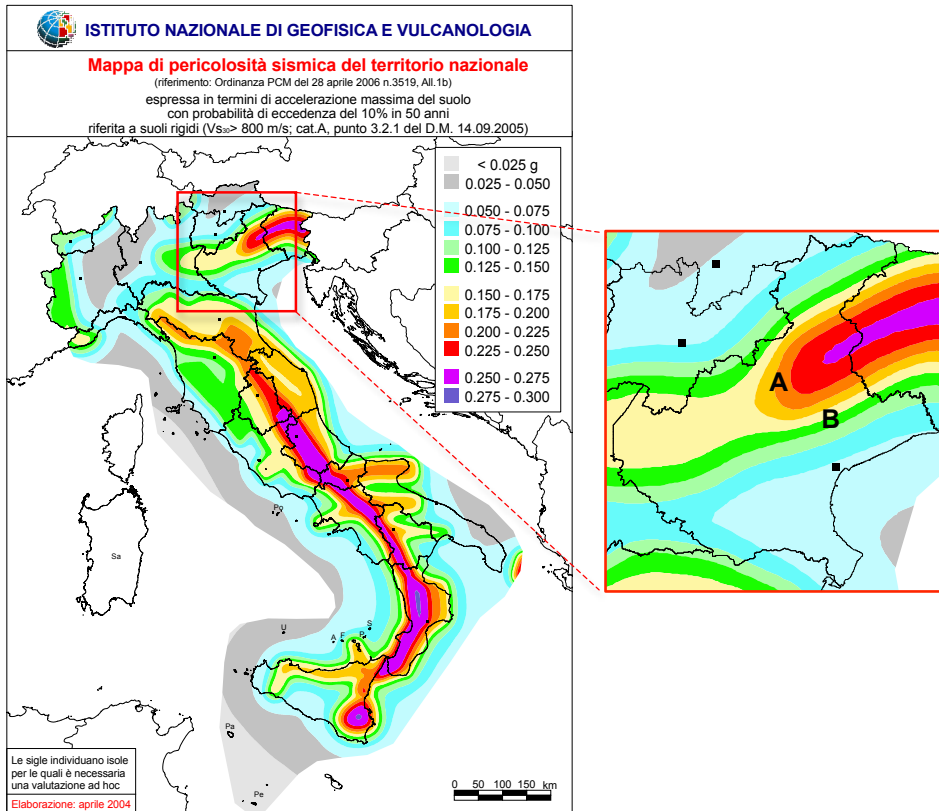


Fig. 3.3 Italian seismic hazard map and geographical position of the bridges (**A** for Fener bridge and **B** for A27 overpass): maximum PGA with probability of exceedance 10% during 50 years, type soil A (source by INGV – (Italian) National Institute of Geophysics and Volcanology).

3.2.1.1 The case study bridge from Fener bridge

First, the vulnerability assessment is developed on a case study, originally built in the Seventies (Fener bridge): the structure consists in a reinforced concrete multi-span simply supported girder bridge. The bridge is 99m long and it has 4 pre-stressed reinforced concrete (PRC) spans with double-tee beams and a cast-in-place RC slab (Fig. 3.4); each span is 24.75m long. The spans are sustained by reinforced concrete framed piers (Fig. 3.4a) with two circular columns (1.50m diameter) and a transverse reverse-T beam (2m high) shown in Fig. 3.4b (taken from the original drawings). The piers are 9m high; deck width

is 9m. Each pier has a transversal framed structure (Fig. 3.4c), therefore it has a different behaviour in the two main directions (the static scheme is a cantilever beam in the longitudinal direction, whereas it is a framed structure in the transversal direction). Foundation structure is set up of plinths and four circular piles (1.25m diameter and 16m long) for each plinth (Fig. 3.5 taken from original drawing). Some geometrical data of the bridge are listed in Table 3.1.

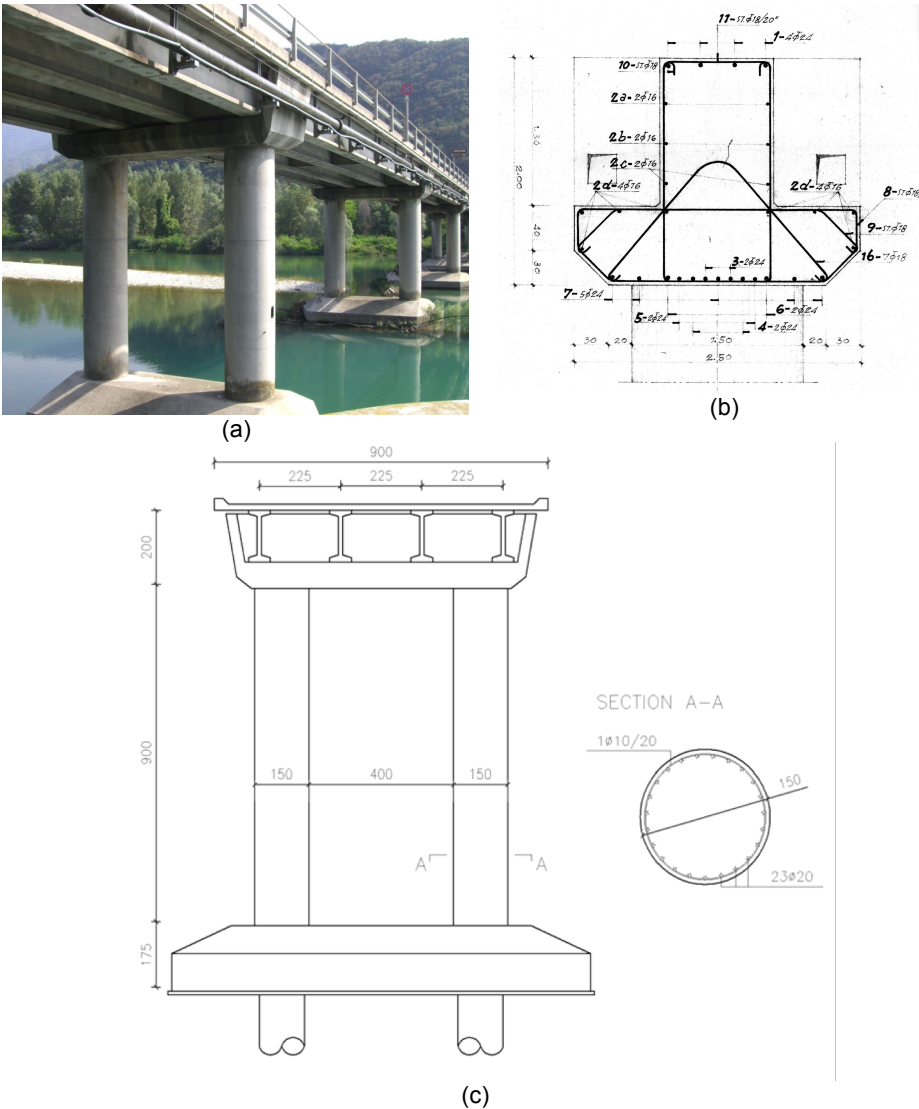


Fig. 3.4 Case study bridge geometrical characteristics: bridge considered as a case study (a), transversal view of the pier (b), original drawing of reinforcement configuration of the pier top (c).

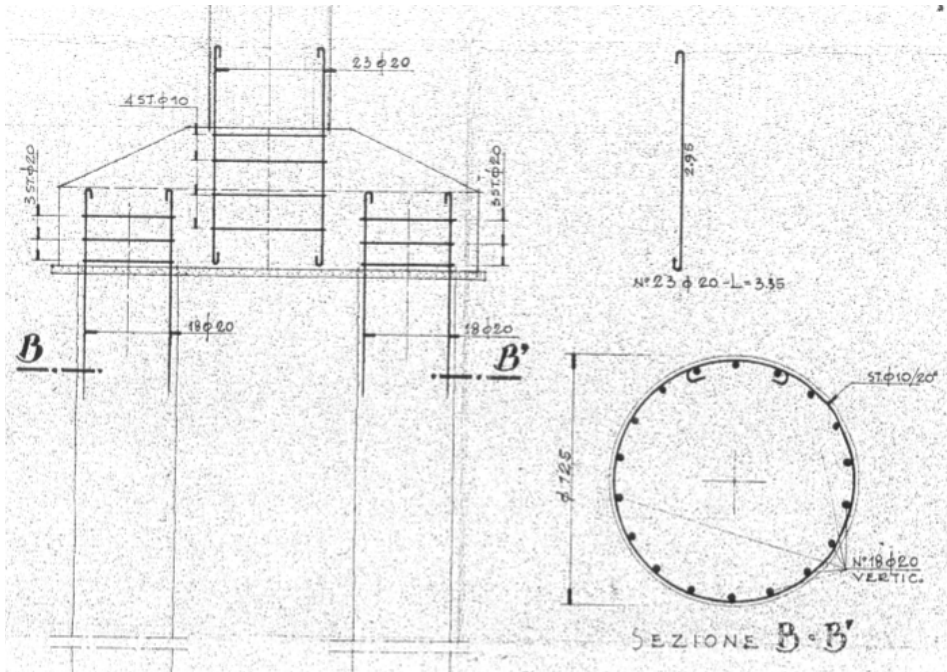


Fig. 3.5 Original drawing of reinforcement configuration of foundation structure (plinth and piles).

Deck length [m]	99.00
Deck width [m]	9.00
Number of spans	4
Span length [m]	24.75
Pier height [m]	9.00
Piles length [m]	16.00

Table 3.1 Case study bridge geometrical characteristics.

Two main variables are considered to build fragility curves: piers unconfined concrete maximum stress f_{c0} and reinforcing steel yielding strength f_y . Concrete is supposed to belong to class C25/30 according to Eurocode 2 (CEN Comité Européen de Normalisation, 2004) with a normal probabilistic distribution (Melchers, 1999). The mean value of the unconfined concrete maximum stress

is equal to 41MPa and the standard deviation is 10MPa (Fig. 3.6a). This distribution is subdivided in five intervals of 14MPa having the following central values: 13MPa, 27MPa, 41MPa, 55MPa and 69MPa. Analogous considerations are made for confined concrete: according to various experimental studies presented in literature, confined concrete maximum stress is incremented by a factor equal to 1.2 in respect to unconfined concrete and the ultimate strain up to 1.6%. Reinforcing steel is FeB32K type (smooth bars commonly used in Italy when the bridge was built) with a lognormal probabilistic distribution (Mirza & MacGregor, 1979). The mean value of the yielding strength is equal to 385MPa and standard deviation is 42MPa (Fig. 3.6b). This distribution is subdivided in three intervals of 82MPa having the following central values: 303MPa, 385MPa and 467MPa. 15 bridge samples are obtained combining these values: their mechanical characteristics and probabilities of occurrence are presented in Table 3.2.

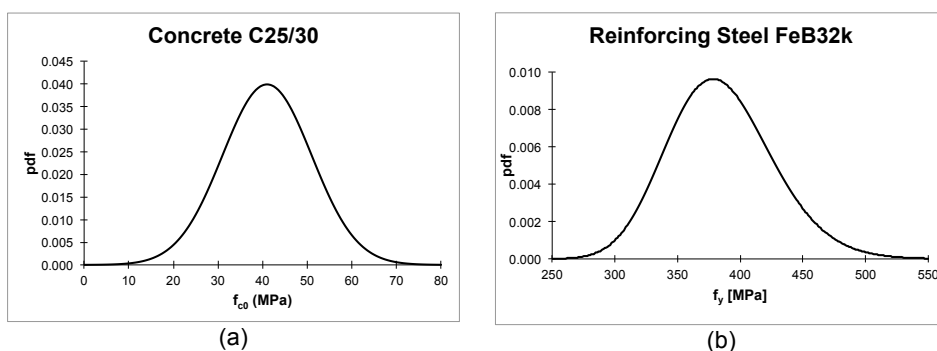


Fig. 3.6 Normal (a) and lognormal (b) probabilistic distribution of unconfined concrete maximum stress f_{c0} (C25/30) and reinforcing steel yielding strength f_y (FeB32K), respectively.

Bridge samples	f_{c0} [MPa]	Prob. (f_{c0})	f_y [MPa]	Prob. (f_y)	Prob. ($f_{c0}; f_y$)
BS1	13	0.011	303	0.099	0.001
BS2	27	0.210	303	0.099	0.021
BS3	41	0.559	303	0.099	0.055
BS4	55	0.210	303	0.099	0.021
BS5	69	0.011	303	0.099	0.001
BS6	13	0.011	385	0.780	0.009

BS7	27	0.210	385	0.780	0.164
BS8	41	0.559	385	0.780	0.436
BS9	55	0.210	385	0.780	0.164
BS10	69	0.011	385	0.780	0.009
BS11	13	0.011	467	0.121	0.001
BS12	27	0.210	467	0.121	0.025
BS13	41	0.559	467	0.121	0.067
BS14	55	0.210	467	0.121	0.025
BS15	69	0.011	467	0.121	0.001
				Sum	1.000

Table 3.2 Characteristics of the 15 considered bridge samples (unconfined concrete) for Fener bridge.

First, four modelling strategies with an increasing level of complexity are developed. The pier modelled as a cantilever with fixed end, the entire bridge with fixed end of the piers at bottom, the entire bridge simulating soil-structure interaction by means of translational and rotational elastic springs at the base of the piers and the entire bridge modelling the whole pier foundation substructure, plinth and piles, are studied to generate and compare the fragility curves.

Considering soil-structure interaction by springs, the stiffness of axial springs (K_v) and rotational springs (K_r) is calculated by means of the following formulas (Priestley et al., 1996a):

$$K_v = m \cdot n \cdot k_p \quad (3.1)$$

$$K_r = m \cdot \sum_{i=1}^n k_p \cdot x_i^2 \quad (3.2)$$

where m is the rows number set up by n piles parallel to load direction, k_p is the axial stiffness of each pile, x_i is the distance from the i -th pile to the foundation center of gravity G .

The stiffness K_h of horizontal springs is calculated taking into account the depth z of the piles by the following formula (Viggiani, 1999):

$$K_h = n_h \left(\frac{z}{D} \right) \quad (3.3)$$

where D is the diameter of the pile and n_h is the soil reaction. Considering the piles 16m long and a mean value for K_h , the springs stiffness values are:

Springs stiffness values	
K_v	$7819.00 \cdot 10^3 \text{ N/mm}$
K_h	$219.78 \cdot 10^3 \text{ N/mm}$
$K_{r,x}$	$5.91 \cdot 10^{13} \text{ Nmm/rad}$ (longitudinal)
$K_{r,y}$	$2.40 \cdot 10^{13} \text{ Nmm/rad}$ (transversal)

Table 3.3 Springs stiffness values for soil-structure interaction.

After that, the entire pier foundation is modelled. Even in this modelling, soil-pile interaction is taken into account by means of springs along the pile length. The stiffness $K_{p,i}$ of the i -th spring is calculated by:

$$K_{p,i} = z_i \cdot B \cdot k_{s,i} \quad (3.4)$$

where z_i is the depth of the i -th spring from the ground levels, B is the dimension of the pile section perpendicular to the spring direction and $k_{s,i}$ is the soil reaction, which depends on z_i . Formulas to calculate $k_{s,i}$ can be found in Viggiani (1999). In this study Bowels formula with Hansen coefficients is considered and the results are shown in the following:

Depth z_i [m]	$K_{p,i}$ [N/mm]
1.75	$7.80 \cdot 10^5$
2.75	$11.49 \cdot 10^5$
3.75	$15.19 \cdot 10^5$
4.75	$18.88 \cdot 10^5$
5.75	$22.57 \cdot 10^5$
6.75	$26.26 \cdot 10^5$
7.75	$29.95 \cdot 10^5$
8.75	$33.64 \cdot 10^5$
9.75	$37.34 \cdot 10^5$
10.75	$41.03 \cdot 10^5$
11.75	$44.72 \cdot 10^5$

12.75	48.41 10 ⁵
13.75	52.11 10 ⁵
14.75	55.80 10 ⁵
15.75	59.49 10 ⁵
16.75	63.18 10 ⁵

Table 3.4 Springs stiffness values for soil-pile interaction.

The deck is simply supported at piers' and abutments' positions: free rotations are allowed around beams' transversal local axes and free longitudinal translations are also allowed at abutments' position.

Considering pier fixed at base for, pier behavior subjected to horizontal loads is investigated. It's observed that, for both horizontal principal directions and for each bridge sample, pier failure comes from a flexural behavior (see Fig. 3.7 as example for BS15). The displacement ductility is calculated as in Eq. (2.6)

Non-linear dynamic analyses (NLDAs), for material and geometry ($P-\Delta$ effects), are carried out by OpenSees code (McKenna et al., 2009), mainly based on fibers formulation of elements: piers and piles are modelled by Force Beam Column Elements having 5 integration points (consistent masses). Kent and Park constitutive law (Kent & Park, 1971), modified by Park et al. (1982), is considered for concrete elements and an elastic-hardening plastic law is considered for reinforcing steel. Piles unconfined concrete is supposed to belong to class C25/30 according to Eurocode 2 (CEN Comité Européen de Normalisation, 2004) and reinforcing steel is FeB32K type (smooth bars): these characteristics are not variable because piles are not considered seismic vulnerable elements. The deck is modelled with beam elements having linear elastic behavior (Young modulus $E_d=34763\text{MPa}$ and shear modulus $G_d=14485\text{MPa}$). Deck dead load and dead/live loads on it are modelled as lumped masses on nodes. Considering the foundation structure, the plinth is modelled as a lumped mass on the center of gravity linked to (columns) piers and piles by means of rigid-links. Each pile is subdivided in 16 elements. Numerical models of the entire bridge without and with foundation structure are shown in Fig. 3.8. Accelerograms for NLDAs are generated as described in §2.3.2.3 and they are spectrum compatible with elastic spectra coming from Italian Code for Constructions (Italian Ministry of Infrastructures, 2008) considering the life-safety limit state (10% exceedance probability during 50 years). The two considered target spectra are shown in Fig. 3.9. As prescribed

in Italian Code, three groups of three accelerograms (one in longitudinal, one in transversal and one in vertical directions) are considered for each bridge sample and the maximum values of recorded results are taken into account for the generation of fragility curves. Since the piers are subjected to flexural failure, the considered damage levels are the same of §2.3.2.1 (Choi, 2002). The comparison between the fragility curves obtained by the four above-mentioned different numerical models and following procedure B in §2.3.2.2 is presented in Fig. 3.10 and Fig. 3.11, Table 3.5 and Table 3.6. Peak Ground Acceleration (PGA) is considered as seismic action and NLDAs are carried out for PGA equal to 0.1g-0.2g-0.3g-0.4g-0.5g-0.6g-0.7g-0.8g-0.9g-1.0g. It is supposed that soil supporting bridge piers is not susceptible to liquefaction.

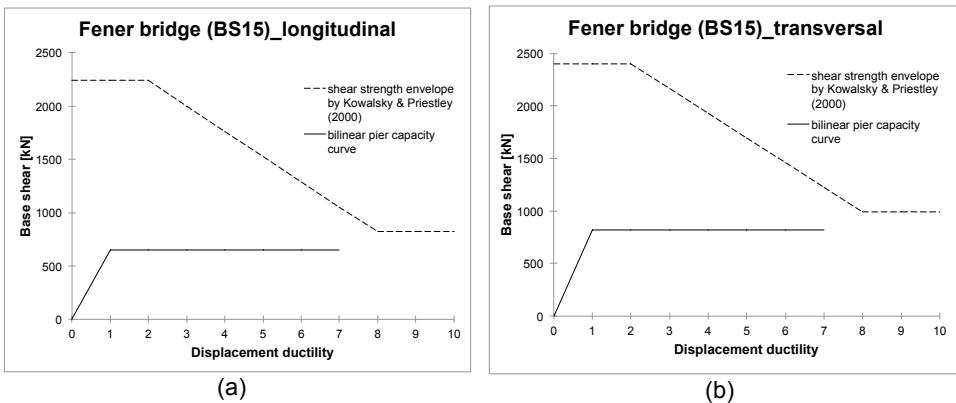
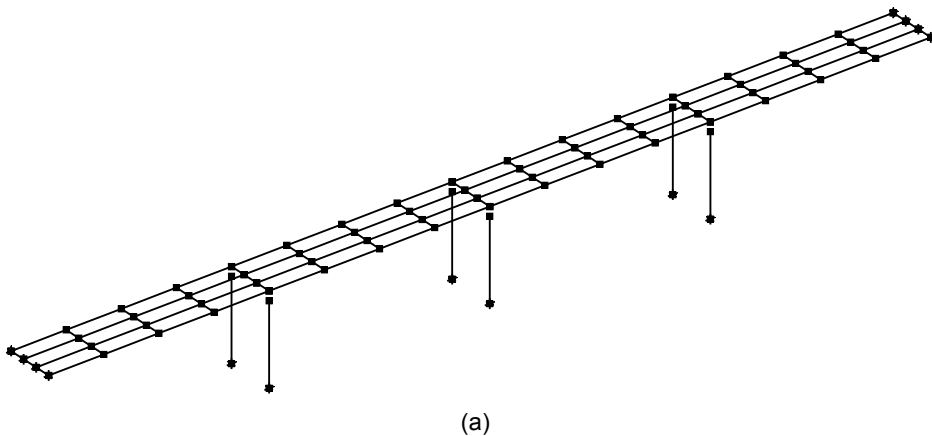
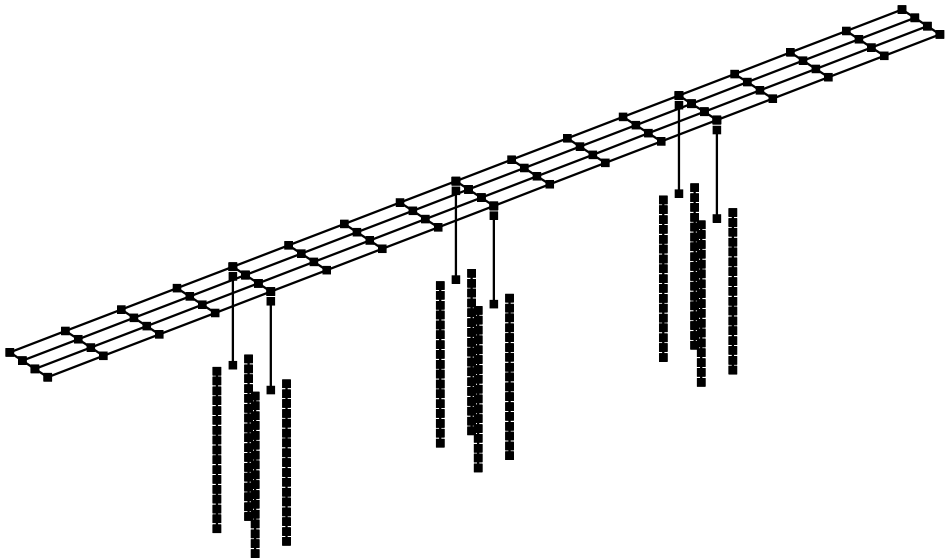


Fig. 3.7 Fener bridge pier behavior subjected to horizontal loads: longitudinal (a) and transversal (b) directions (BS15, piers fixed at base).





(b)

Fig. 3.8 Numerical models of the case study bridge without (a) and with foundation structure (b).

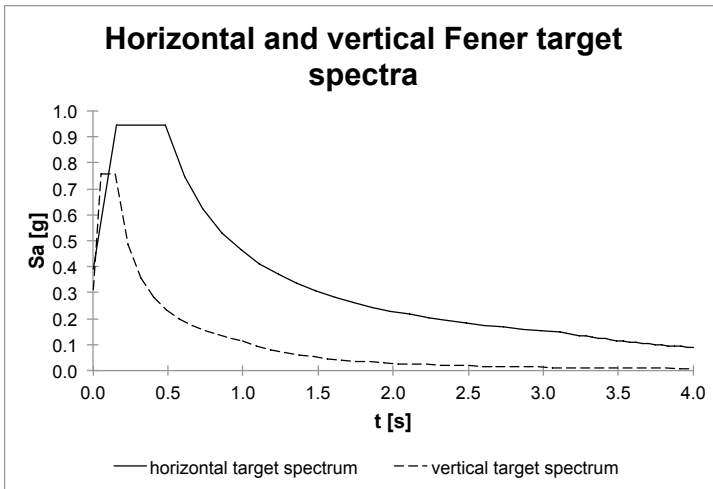


Fig. 3.9 Horizontal and vertical elastic target spectra (life-safety limit state) considered for Fener bridge.

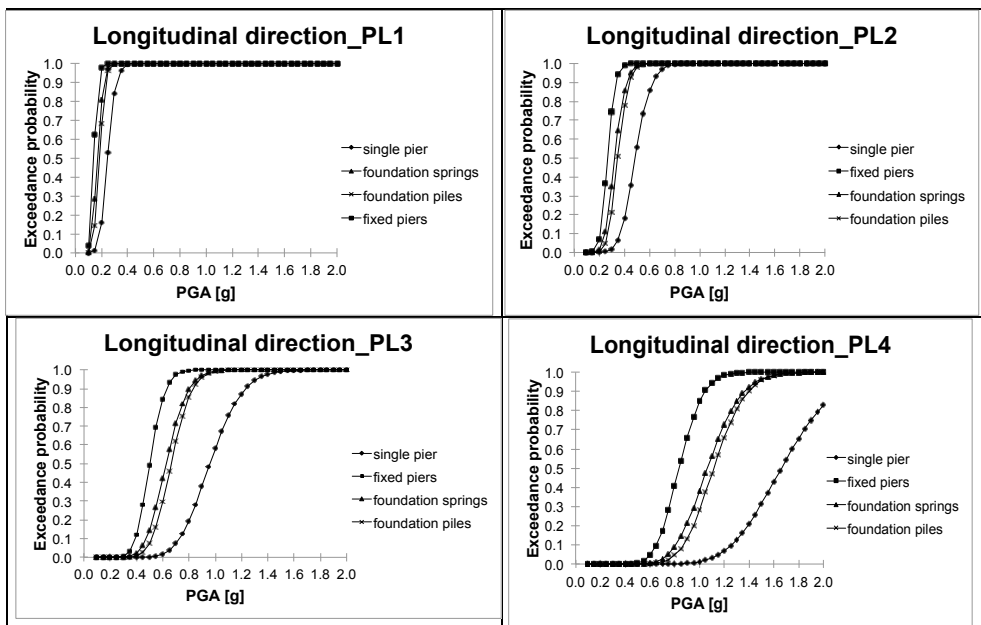


Fig. 3.10 Fragility curves (longitudinal direction). Comparison between 4 analytical models: single pier with fixed end, the entire bridge with fixed end of the piers at bottom, the entire bridge simulating soil-structure interaction by means of translational and rotational springs at the base of the piers and the entire bridge modelling the whole foundation structure.

	PL1		PL2	
	Median	St. dev.	Median	St. dev.
Single pier	0.24	0.28	0.48	0.28
Fixed piers	0.13	0.35	0.27	0.35
Found. springs	0.18	0.38	0.34	0.38
Found. piles	0.19	0.27	0.35	0.27
	PL3		PL4	
	Median	St. dev.	Median	St. dev.
Single pier	0.96	0.28	1.66	0.28
Fixed piers	0.51	0.35	0.83	0.35
Found. springs	0.64	0.38	1.09	0.38
Found. piles	0.67	0.27	1.13	0.27

Table 3.5 Fragility curves parameters, median and standard deviation, (longitudinal direction) for the 4 numerical models.

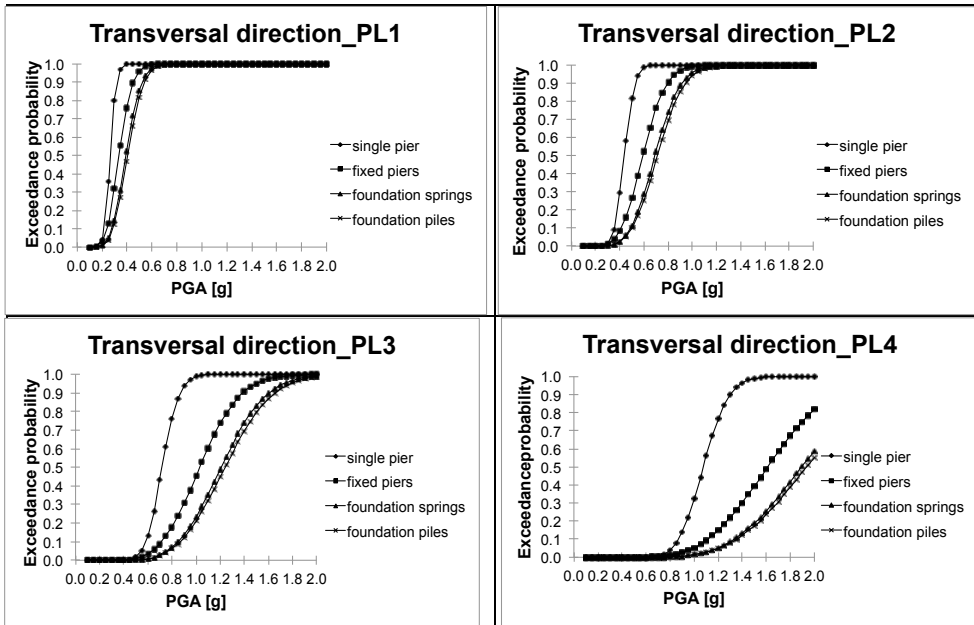


Fig. 3.11 Fragility curves (transversal direction). Comparison between 4 analytical models: single pier with fixed end, the entire bridge with fixed end of the piers at bottom, the entire bridge simulating soil-structure interaction by means of translational and rotational springs at the base of the piers and the entire bridge modelling the whole foundation structure.

	PL1		PL2	
	Median	St. dev.	Median	St. dev.
Single pier	0.27	0.29	0.42	0.29
Fixed piers	0.34	0.37	0.59	0.37
Found. springs	0.39	0.36	0.68	0.36
Found. piles	0.41	0.36	0.72	0.36
	PL3		PL4	
	Median	St. dev.	Median	St. dev.
Single pier	0.73	0.29	1.09	0.29
Fixed piers	0.99	0.37	1.61	0.37
Found. springs	1.21	0.36	1.90	0.36
Found. piles	1.25	0.36	1.95	0.36

Table 3.6 Fragility curves parameters, median and standard deviation, (transversal direction) for the 4 numerical models.

After that, the focus is to investigate how input loads (accelerograms) and piers height influence fragility curves trend.

Since accelerograms are spectrum compatible but random, first we investigate how these seismic loads modify fragility curves. Following procedure B (§2.3.2.2), NLDAs are carried out on the above-mentioned entire bridge with fixed end of the piers. Only longitudinal direction is taken into account to reduce computational effort. Three groups of three artificial accelerograms (one in longitudinal, one in transversal and one in vertical directions) are considered and they are generated as described in §2.3.2.3, being spectrum compatible with elastic spectra coming from Italian Code for Constructions (Italian Ministry of Infrastructures, 2008). The outcomes are shown in Fig. 3.12 and Table 3.7.

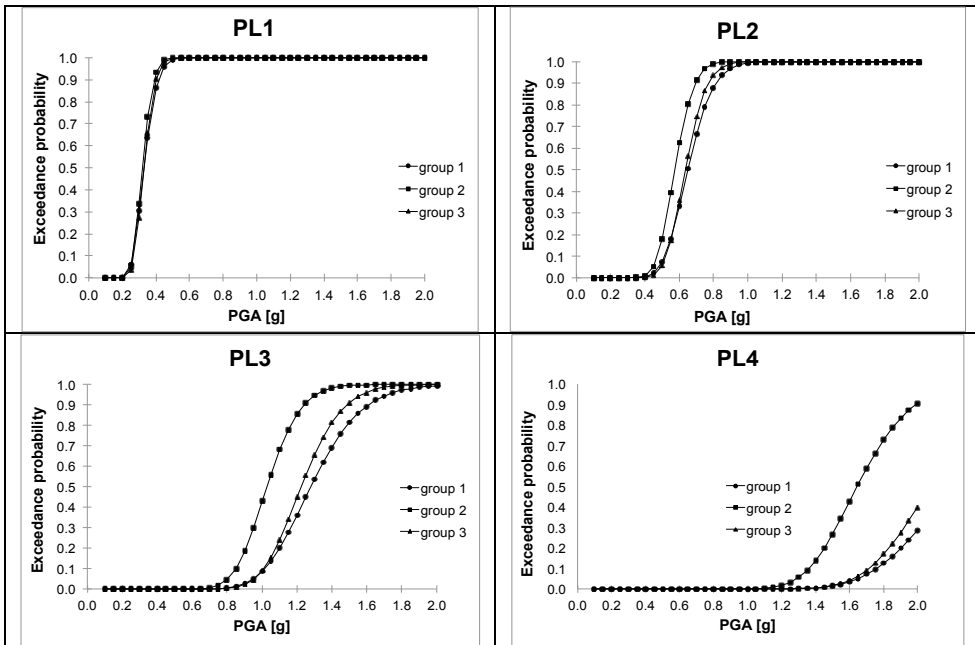


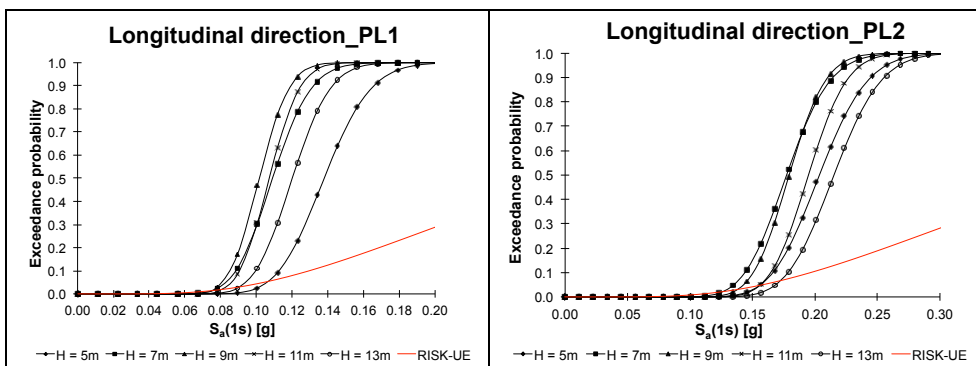
Fig. 3.12 Fragility curves (longitudinal direction): comparison between three groups of three accelerograms (entire bridge with fixed end of the piers).

	PL1		PL2	
	Median	St. dev.	Median	St. dev.
group 1	0.35	0.29	0.65	0.29
group 2	0.34	0.35	0.57	0.35
group 3	0.35	0.31	0.64	0.31

	PL3		PL4	
	Median	St. dev.	Median	St. dev.
group 1	1.29	0.29	2.09	0.29
group 2	1.02	0.35	1.65	0.35
group 3	1.23	0.31	2.18	0.31

Table 3.7 Fragility curves parameters, median and standard deviation, (longitudinal direction) for the three groups of three accelerograms (entire bridge with fixed end of the piers).

Then, considering the model of the entire bridge with fixed end of the piers at bottom, piers height influence on fragility curves trend is investigated. The following piers heights are considered: 5m, 7m, 9m, 11m and 13m. Flexural failure is assumed for each numerical modelling. Fragility curves are generated considering procedure B in §2.3.2.2. NLDAs are carried out for different intensities of $S_a(1s)$ in order to compare analytical fragility curves with empirical fragility curves from RISK-UE method (Mongeo et al., 2003), which doesn't consider this geometrical parameter (pier height) to generate the curves. Artificial accelerograms are considered as in the investigations before presented. The results are shown in Fig. 3.13, Fig. 3.14, Table 3.8 and Table 3.9.



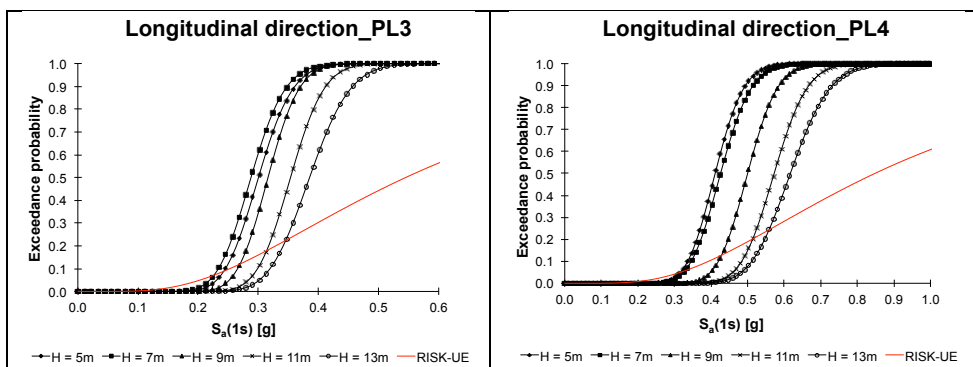


Fig. 3.13 Fragility curves (longitudinal direction): comparison between numerical models with different pier height and RISK-UE method (Mongeo et al., 2003).

	PL1		PL2	
	Median	St. dev.	Median	St. dev.
H = 5m	0.14	0.35	0.20	0.35
H = 7m	0.11	0.29	0.17	0.29
H = 9m	0.10	0.32	0.18	0.32
H = 11m	0.11	0.34	0.19	0.34
H = 13m	0.12	0.36	0.22	0.36
RISK-UE	0.28	0.60	0.42	0.60
	PL3		PL4	
	Median	St. dev.	Median	St. dev.
H = 5m	0.30	0.35	0.41	0.35
H = 7m	0.29	0.29	0.43	0.29
H = 9m	0.31	0.32	0.50	0.32
H = 11m	0.35	0.34	0.56	0.34
H = 13m	0.39	0.36	0.62	0.36
RISK-UE	0.54	0.60	0.85	0.60

Table 3.8 Fragility curves parameters, median and standard deviation, (longitudinal direction) for the 6 numerical models.

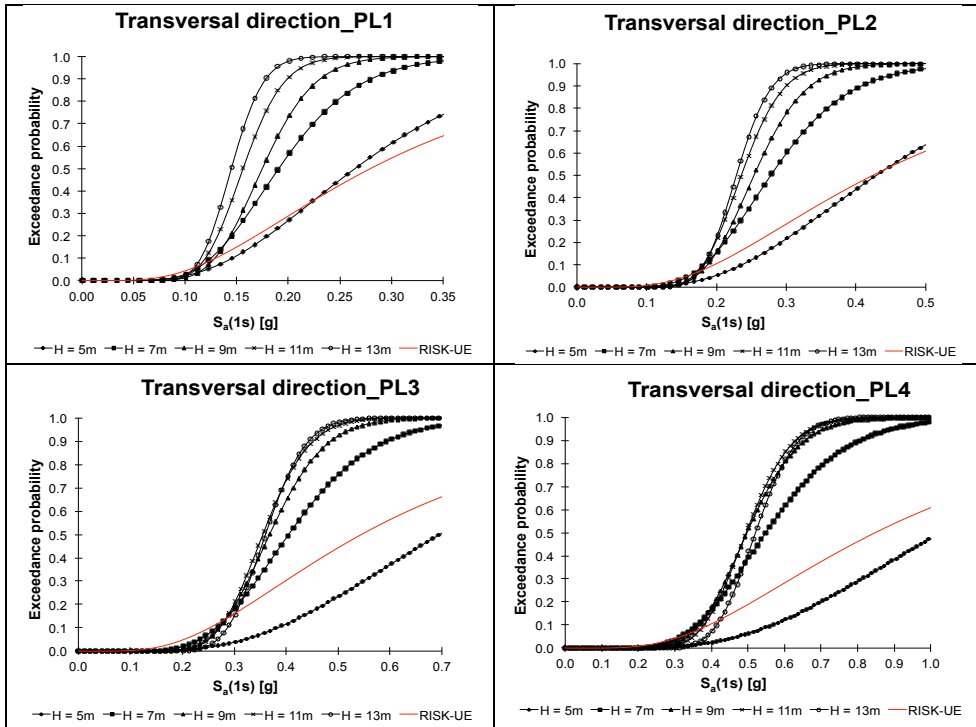


Fig. 3.14 Fragility curves (transversal direction): comparison between numerical models with different pier height and RISK-UE method (Mongeo et al., 2003).

	PL1		PL2	
	Median	St. dev.	Median	St. dev.
H = 5m	0.27	0.33	0.43	0.33
H = 7m	0.19	0.28	0.28	0.28
H = 9m	0.17	0.36	0.25	0.36
H = 11m	0.16	0.32	0.24	0.32
H = 13m	0.14	0.31	0.23	0.31
RISK-UE	0.28	0.60	0.42	0.60
	PL3		PL4	
	Median	St. dev.	Median	St. dev.
H = 5m	0.70	0.33	1.03	0.33
H = 7m	0.41	0.28	0.55	0.28
H = 9m	0.37	0.36	0.49	0.36
H = 11m	0.35	0.32	0.50	0.32

H = 13m	0.36	0.31	0.52	0.31
RISK-UE	0.55	0.60	0.85	0.60

Table 3.9 Fragility curves parameters, median and standard deviation, (transversal direction) for the 6 numerical models.

As above-mentioned, a number of existing RC bridges need retrofitting or strengthening because of improper design or construction, change of the design loads, damage caused by environmental factors or seismic events (Priestley et al., 1996a; Kim & Shinozuka, 2004; Zhou et al., 2010; Morbin et al., 2012). Taking into account the increasing use of FRP (Fiber Reinforced Polymer) composites particularly for seismic retrofit interventions, the effects of FRP pier jacketing, in terms of seismic vulnerability reduction, is studied. Considering the model of the entire bridge with fixed end of the piers at bottom, analytical fragility curves have been generated for the retrofitted bridge (procedure B, §2.3.2.2) and compared to those of the existing bridge, also taking into account the analytical models of FRP-jacket. In fact, two analytical models for the estimation of the constitutive law of the FRP confined RC element have been considered: the model in National Research Council (2004) and the model proposed in Pellegrino & Modena (2010). The seismic retrofit intervention is made by means of 4 layers of CFRP (Carbon Fiber Reinforced Polymer) continuously wrapped along the height of the piers. The CFRP characteristics are: Young modulus = 230GPa, ultimate stress = 3430MPa, ultimate strain = 1.5%, density = 1820kg/m³ and thickness of one layer = 0.165mm. This seismic retrofit intervention by means of FRP allows to increase the confined concrete ultimate strain (National Research Council, 2004) according to the values presented in Table 3.10. FRP characteristics are not considered main variables (no pdf is associated to them) because FRP material comes from a strictly controlled industrial production where variability is minimum. The entire bridge modelling with fixed end of the piers at bottom is considered to generate fragility curves. The results, following procedure B in §2.3.2.2, are shown in Fig. 3.15 and Fig. 3.16, Table 3.11 and Table 3.12.

f_{c0} [MPa]	ϵ_{cc} [‰]
3	9.1
27	7.4
41	6.7
55	6.2
69	5.9

Table 3.10 FRP confined concrete ultimate strain (National Research Council, 2004).

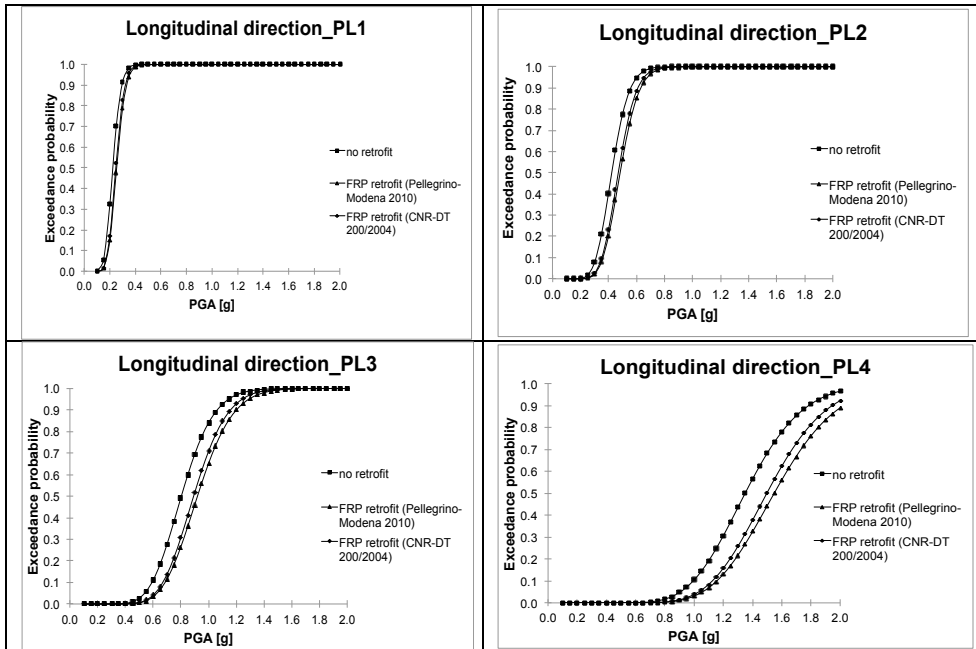


Fig. 3.15 Fragility curves (longitudinal direction): comparison between entire bridge without retrofit and retrofitted bridge: models by Pellegrino & Modena (2010) and by National Research Council (2004) are used for modelling the constitutive law of the bridge with confined piers.

	PL1		PL2	
	Median	St. dev.	Median	St. dev.
Entire bridge	0.13	0.35	0.27	0.35
Retrofit by Pellegrino & Modena (2010)	0.26	0.31	0.49	0.31
Retrofit by National Research Council (2004)	0.24	0.33	0.48	0.33

	PL3		PL4	
	Median	St. dev.	Median	St. dev.
Entire bridge	0.51	0.35	0.83	0.35
Retrofit by Pellegrino & Modena (2010)	0.93	0.31	1.55	0.31
Retrofit by National Research Council (2004)	0.89	0.33	1.50	0.33

Table 3.11 Fragility curves parameters, median and standard deviation, (longitudinal direction) for the 3 numerical models.

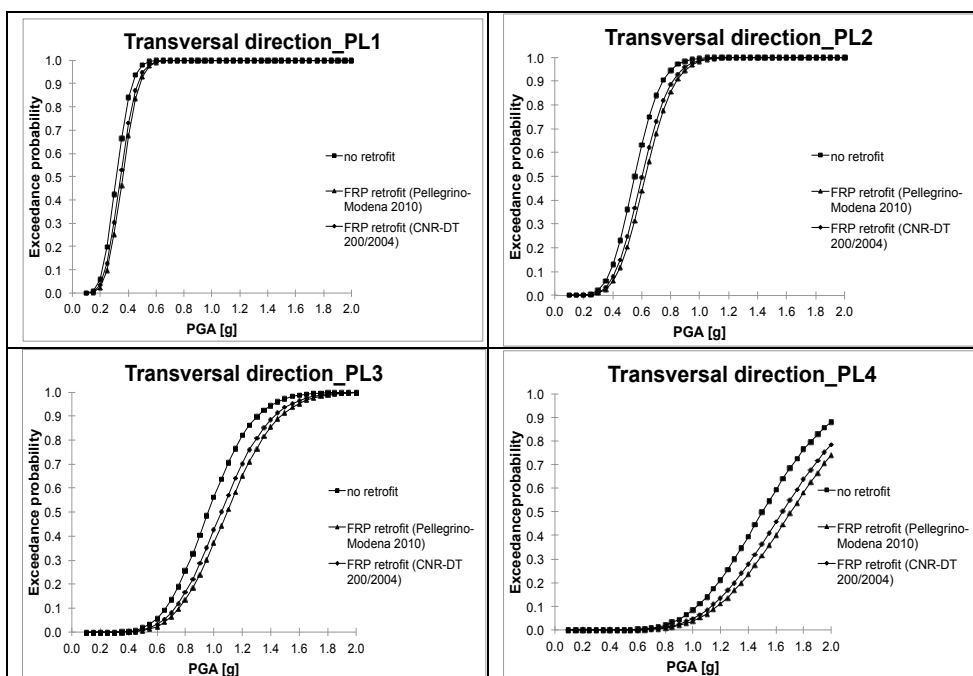


Fig. 3.16 Fragility curves (transversal direction): comparison between entire bridge without retrofit and retrofitted bridge: models by Pellegrino & Modena (2010) and by National Research Council (2004) are used for modelling the constitutive law of the bridge with confined piers.

	PL1		PL2	
	Median	St. dev.	Median	St. dev.
Entire bridge	0.34	0.37	0.59	0.37
Retrofit by Pellegrino & Modena (2010)	0.36	0.38	0.64	0.38
Retrofit by National Research Council (2004)	0.34	0.39	0.61	0.39

	PL3		PL4	
	Median	St. dev.	Median	St. dev.
Entire bridge		0.37	1.61	0.37
Retrofit by Pellegrino & Modena (2010)	1.10	0.38	1.71	0.38
Retrofit by National Research Council (2004)	1.05	0.39	1.65	0.39

Table 3.12 Fragility curves parameters, median and standard deviation, (transversal direction) for the 3 numerical models.

3.2.1.2 The A27 overpass bridge

Influence of the deck skew angle on seismic vulnerability assessment is investigated. A 3-spans simply supported girder bridge is considered: this structural scheme is usual for bridges that overpass A27 highway (Venezia-Belluno, North-Eastern of Italy). Their main difference is the skew angle. A bridge-type is considered to study the influence of the skew angle and, then, the results should be related to other similar bridges. As mentioned, the structure consists in a 3-spans simply supported girder bridge: the spans lengths are respectively 12.0m, 37.5m and 12.0m (Fig. 3.17a). Each lateral span has 4 pre-stressed reinforced concrete (PRC) double-tee beams 1.25m high and a cast-in-place RC slab 20cm high (Fig. 3.17b). The main span is a steel-concrete composite structure having two steel double-tee (not symmetrical) strengthened transversally beams 1.9m high and a cast-in-place RC slab 20cm high (Fig. 3.17c). The spans are sustained by reinforced concrete framed piers with two squared columns (section 0.9m \times 0.9m) 3.75m high with a transverse rectangular beam 1.9m high (Fig. 3.17d). As the previous case study bridge, each pier has a transversal framed structure, therefore it has a different behavior in the two main directions: the static scheme is a cantilever beam in the longitudinal direction, whereas it is a framed structure in the transversal direction. Deck width is 8.50m. Some geometrical data of the bridge are listed in Table 3.13.



(a)



(b)



(c)



(d)

Fig. 3.17 A27 highway overpass images: view from the highway (a), view of the main span (b), view of a lateral span (c) and view of a RC framed pier (d).

Deck length [m]	61.50
Deck width [m]	8.50
Number of spans	3
Max span length [m]	37.50
Pier height [m]	3.75

Table 3.13 A27 overpass geometrical characteristics.

As the previous example, two main variables are considered to build fragility curves: unconfined concrete maximum stress f_{c0} and reinforcing steel yielding strength f_y . Concrete is supposed to belong to class C25/30 according to Eurocode 2 (CEN Comité Européen de Normalisation, 2004) with a normal probabilistic distribution (Melchers, 1999). The mean value of the unconfined

concrete maximum stress is equal to 38MPa and the standard deviation is 4.85MPa (Fig. 3.18a). This distribution is subdivided in five intervals having the following central values: 24MPa, 31MPa, 38MPa, 45MPa and 52MPa. Analogous considerations are made for confined concrete: according to various experimental studies presented in literature, confined concrete maximum stress is incremented by a factor equal to 1.2 in respect to unconfined concrete and the ultimate strain up to 1.6%. Reinforcing steel (smooth bars commonly used in Italy when the bridge was built) is considered with a lognormal probabilistic distribution (Mirza & MacGregor, 1979). The mean value of the yielding strength is equal to 540MPa and standard deviation is 72MPa (Fig. 3.18b). This distribution is subdivided in three intervals of 82MPa having the following central values: 390MPa, 540MPa and 690MPa. 15 bridge samples, nominally identical but statistically different, are obtained combining these values (Table 3.14).

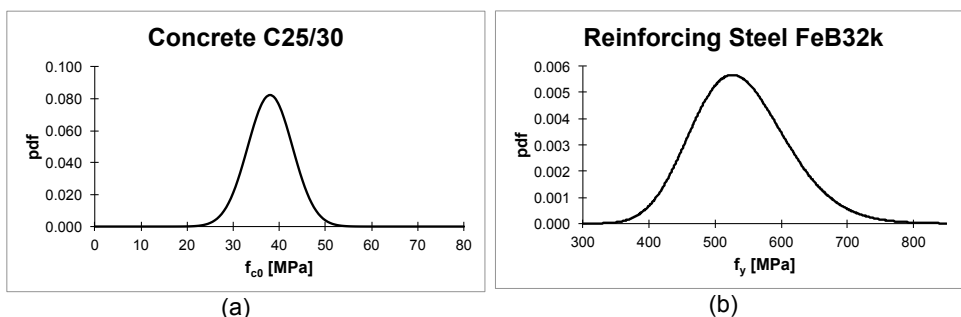


Fig. 3.18 Normal (a) and lognormal (b) probabilistic distribution of unconfined concrete maximum stress f_{c0} (C25/30) and reinforcing steel yielding strength f_y (FeB32K), respectively.

Bridge samples	f_{c0} [MPa]	Prob. (f_{c0})	f_y [MPa]	Prob. (f_y)	Prob. ($f_{c0}; f_y$)
BS1	24	0.009	390	0.067	0.001
BS2	31	0.203	390	0.067	0.014
BS3	38	0.576	390	0.067	0.039
BS4	45	0.203	390	0.067	0.014
BS5	52	0.009	390	0.067	0.001
BS6	24	0.009	540	0.833	0.007
BS7	31	0.203	540	0.833	0.169
BS8	38	0.576	540	0.833	0.480
BS9	45	0.203	540	0.833	0.169

BS10	52	0.009	540	0.833	0.007
BS11	24	0.009	690	0.105	0.001
BS12	31	0.203	690	0.105	0.021
BS13	38	0.576	690	0.105	0.060
BS14	45	0.203	690	0.105	0.021
BS15	52	0.009	690	0.105	0.001
				Sum	1.000

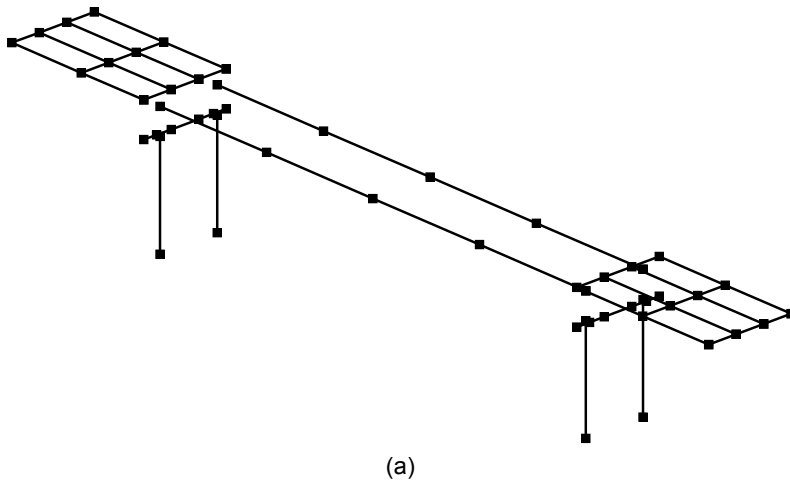
Table 3.14 Characteristics of the 15 considered bridge samples (unconfined concrete) for A27 highway overpass.

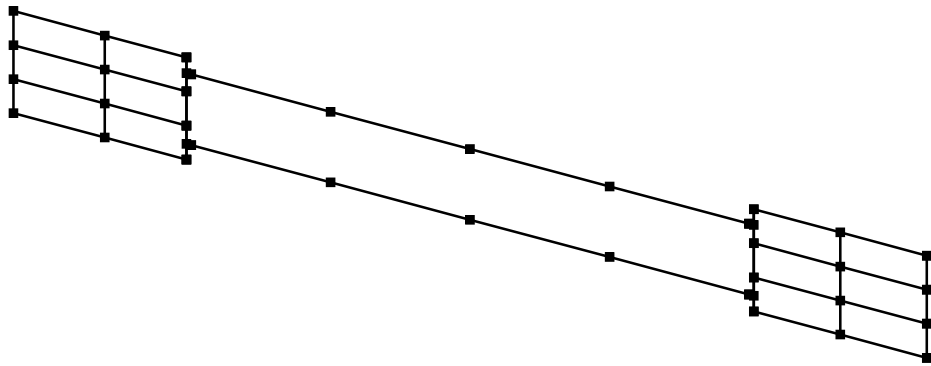
Taking into account results from the previous comparison of fragility curves, the model of the entire bridge with fixed end of the piers at bottom is considered. The deck is simply supported at piers' and abutments' positions: free rotations are allowed around beams' transversal local axes and free longitudinal translations are also allowed at abutments' position. Different skew angles are considered in the analyses: 0°, 7.5°, 15° and 30°.

Considering pier fixed at base for, pier behavior subjected to horizontal loads is investigated. It's observed that, for both horizontal principal directions and for each bridge sample, pier failure comes from a flexural behavior.

As the previous example, non-linear dynamic analyses (NLDAs), for material and geometry (P- Δ effects), are carried out by OpenSees code (McKenna et al., 2009), mainly based on fibers formulation of elements: piers and piles are modelled by Force Beam Column Elements having 5 integration points (consistent masses). Kent and Park constitutive law (Kent & Park, 1971), modified by Park et al. (1982), is considered for concrete elements and an elastic-hardening plastic law is considered for reinforcing steel. The deck is modelled with beam elements having linear elastic behavior, transversal beams of the main span are modeled as rigid-link. Deck dead load and dead/live loads on it are modelled as lumped masses on nodes. Numerical model of the entire bridge (15° skew angle) is shown in Fig. 3.19. Accelerograms for NLDAs are generated as described in §2.3.2.3 and they are spectrum compatible with elastic spectra coming from Italian Code for Constructions (Italian Ministry of Infrastructures, 2008) considering the life-safety limit state (10% exceedance probability during 50 years). The two considered target spectra are shown in Fig. 3.20. As prescribed in Italian Code, three groups of three accelerograms (one in longitudinal, one in transversal and one in vertical directions) are considered for each bridge sample and the maximum values of recorded results

are taken into account for the generation of fragility curves. Since the piers are subjected to flexural failure, the considered damage levels are the same of §2.3.2.1 (Choi, 2002). The comparison between the fragility curves obtained by the four above-mentioned different numerical models and following procedure A in §2.3.2.2 is presented in Fig. 3.21 and Fig. 3.22, Table 3.15 and Table 3.16. In the same pictures, a comparison between analytical fragility curves and empirical fragility curves, in particular RISK-UE method presented in §2.3.1, is shown for the 15° skew angle A27 highway overpass (RISK-UE method doesn't change between longitudinal and transversal direction). Spectral acceleration at 1s, $S_a(1s)$, is considered as seismic action and NLDAs are carried out for $S_a(1s)$ equal to 0.1g-0.2g-0.3g-0.4g-0.5g-0.6g-0.7g-0.8g-0.9g-1.0g. It is supposed that soil supporting bridge piers is not susceptible to liquefaction.





(b)

Fig. 3.19 Numerical model of the A27 highway overpass (15° skew angle): global view (a) and plant view (b).

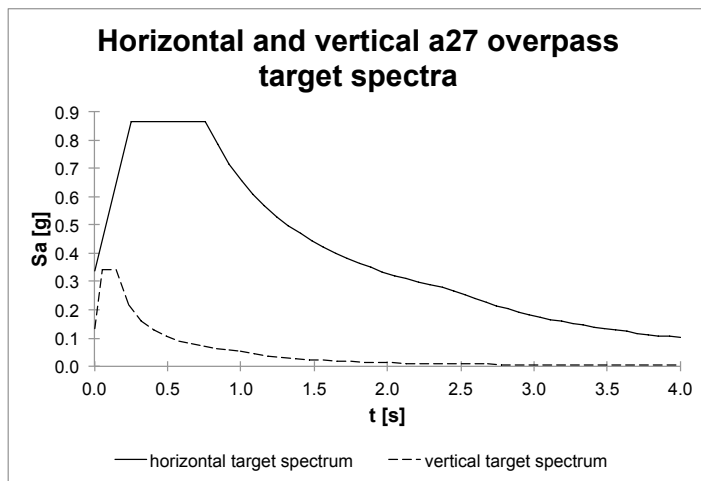


Fig. 3.20 Horizontal and vertical elastic target spectra (life-safety limit state) considered for A27 overpass.

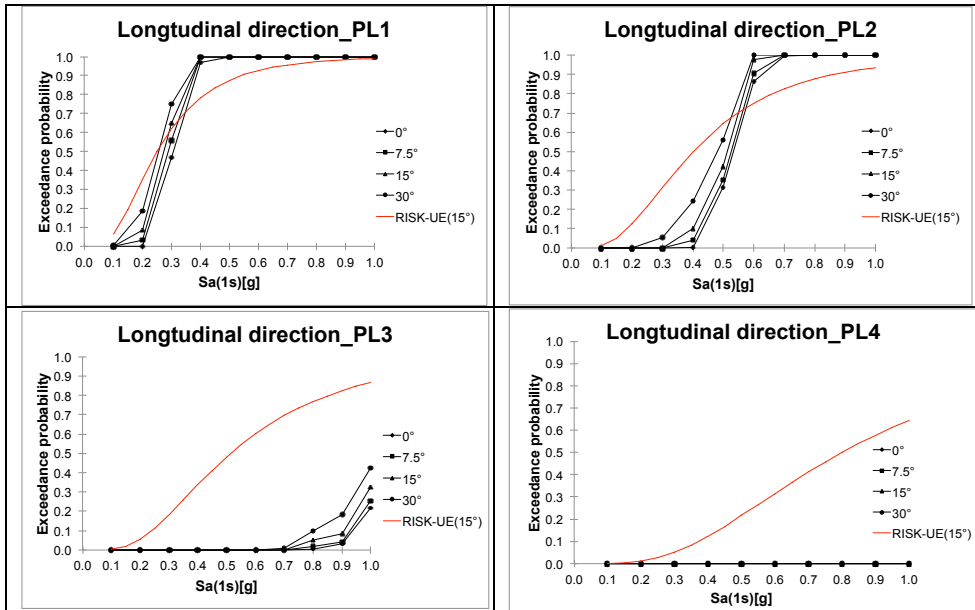


Fig. 3.21 Fragility curves (longitudinal direction): comparison between numerical models with different skew angles and RISK-UE method (Mongeo et al., 2003) with 15° skew angle. PL4 analytical fragility curves are overlapped.

	PL1		PL2	
	Median	St. dev.	Median	St. dev.
0°	0.32	0.33	0.54	0.33
7.5°	0.28	0.35	0.52	0.35
15°	0.26	0.36	0.49	0.36
RISK-UE (15°)	0.25	0.60	0.40	0.60
30°	0.23	0.40	0.45	0.40
	PL3		PL4	
	Median	St. dev.	Median	St. dev.
0°	1.30	0.33	2.10	0.33
7.5°	1.24	0.35	2.03	0.35
15°	1.17	0.36	1.90	0.36
RISK-UE (15°)	0.51	0.60	0.80	0.60
30°	1.10	0.40	1.79	0.40

Table 3.15 Fragility curves parameters, median and standard deviation, (longitudinal direction) for the studied numerical models.

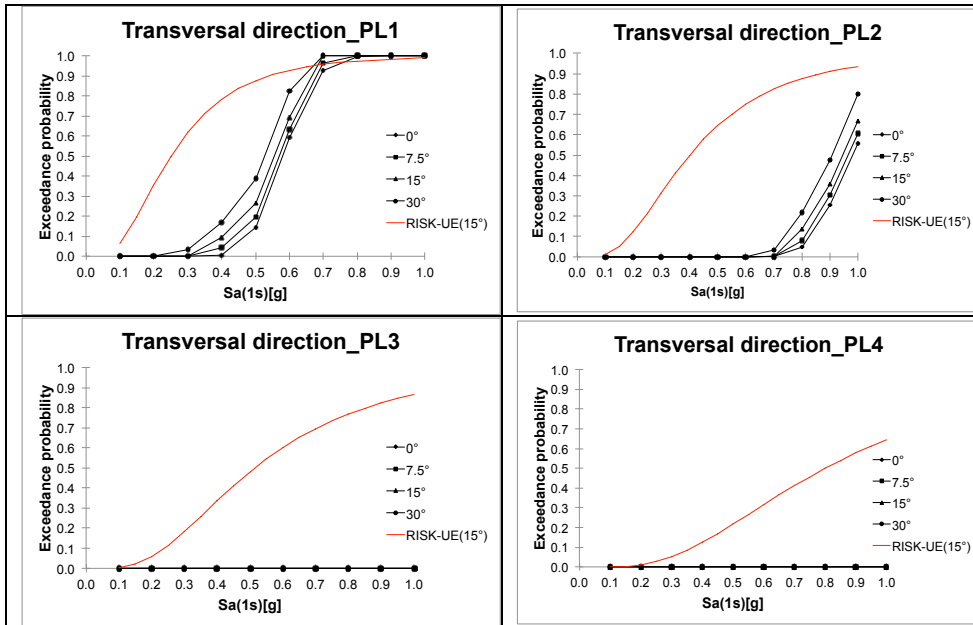


Fig. 3.22 Fragility curves (transversal direction): comparison between numerical models with different skew angles and RISK-UE method (Mongeo et al., 2003) with 15° skew angle. PL3 and PL4 analytical fragility curves are overlapped.

	PL1		PL2	
	Median	St. dev.	Median	St. dev.
0°	0.58	0.30	0.99	0.30
7.5°	0.56	0.32	0.95	0.32
15°	0.53	0.35	0.91	0.35
RISK-UE (15°)	0.25	0.60	0.40	0.60
30°	0.51	0.39	0.88	0.39
	PL3		PL4	
	Median	St. dev.	Median	St. dev.
0°	1.48	0.30	2.31	0.30
7.5°	1.41	0.32	2.25	0.32
15°	1.33	0.35	2.13	0.35
RISK-UE (15°)	0.51	0.60	0.80	0.60
30°	1.25	0.39	1.94	0.39

Table 3.16 Fragility curves parameters, median and standard deviation, (transversal direction) for the studied numerical models

3.2.1.3 Conclusions

In this first part of the study, the following conclusions can be drawn regarding the modelling strategy for obtaining seismic fragility curves, the FRP retrofit interventions consisting in pier jacketing, the different skew angles and piers height:

- the choice of accelerograms affects fragility curves trend, hence the more accelerograms are considered, the more uncertainties in seismic loads are reduced;
- the probabilistic distribution of strength values of considered materials has to be taken into account for a proper estimation of the fragility curves. A proper survey, e.g. in-field tests and laboratory analyses on bridge specimens, may be recommended to reduce uncertainties;
- non-linear dynamic analysis can be used for the determination of seismic fragility of the structure, but it requires a consistent computational effort with respect to other simplified analyses;
- bridge vulnerability estimation can be improved if the entire bridge model is considered. In particular, for the considered case, the bridge vulnerability is underestimated in longitudinal direction and overestimated in transversal direction if only the highest pier is analyzed, particularly for high levels of damage where non-linear effects are significant;
- piers height is an important geometrical parameter which has to be taken into account for a proper assessment of fragility analysis. Varying this parameter, a particular trend is not noticed. In particular, piers height influences the stiffness of the entire structure and, consequently, the bridge proper period changes. If the piers height increases (the pier flexural stiffness decreases), the proper period of the bridge also tends to increase and move towards low spectral acceleration, causing a reduction of seismic action. On the contrary, the bending moment at the fixed bottom of the pier could increase because the arm of the seismic force increases. Since flexural failure is predominant, these two reasons make piers height a relevant parameter for the vulnerability assessment, in particular for high damage levels when non-linear effects are important;
- as expected, seismic vulnerability decreases for FRP retrofitted bridges with respect to the bridge without FRP confinement;
- the model proposed by Pellegrino & Modena (2010) shows a reduction of the vulnerability more evident than that obtained with the model proposed adopted in the National Research Council (2004) since the

former is more accurate than the latter taking into account the contribution of the steel stirrups confinement and the interaction mechanisms between internal reinforcing steel and external FRP retrofit;

- skew angle affects fragility curves both in longitudinal and transversal direction: in particular the wider the skew angle is, the more the bridge seismic vulnerability increases: in particular, considering the main span and horizontal forces at piers bearings during seismic motion, as skew angle increases, the arm of the horizontal forces increases causing major deck rotation and so making worse the performance of the bridge, for example in terms of major displacement for the piers;
- RISK-UE method is noticed that it mainly makes a rough approximation in respect to analytical fragility curves. Considering different piers height, RISK-UE method tends to underestimate fragility of the structure for each considered numerical modelling both in longitudinal and transversal direction. RISK-UE method doesn't take into account piers height and horizontal directions for generating empirical fragility curves. Whereas, regarding 15° skew angle, the empirical method overestimates seismic vulnerability, in particular for PL3 and PL4 in longitudinal direction and all PLs in transversal direction, as compared with analytical fragility curves. The RISK-UE method for PL1 and PL2 in longitudinal direction reflects analytical fragility curves trend, but the difference is mostly due to the different standard deviation between the two methods.

3.3 Step 3: inspections beginning

A preliminary work is carried out in past paragraphs in order to organize a functional database to be used in emergency and post-emergency phases. As above-mentioned, in this study a new framework based on visual inspections is presented.

If an earthquake occurs, it's important to set a criterion when inspections on bridges can start. This criterion is suggested: inspections, or other NDE methods, start on a bridge if earthquake reaches or overcomes a specific seismic intensity measure, for example expressed in PGA (Peak Ground Acceleration) or $S_a(1s)$ (Spectral acceleration at 1s). This intensity threshold depends on the definition of Performance Levels (PLs): in this work it is defined

as the seismic intensity measure at which there is a 10% seismic risk probability of observing the most vulnerable PL between moderate damage and shear failure, referred to a time period equal to the service life of the structure. This probability is calculated in Eq. (2.4) that defines the total PL probability in seismic risk assessment.

Shear failure is considered because is a brittle failure and moderate damage (PL2) is considered because, according to the definition of PLs in §2.3.1, it is the first PL that affects structural stability, minor damage (PL1) is mostly a cosmetic damage.

Moreover, the 10% value (concerning seismic risk probability) is considered by analogy with life-safety limit state: according to Ellingwood (2009), life-safety limit state provided by building codes is considered the performance level that strikes a good balance between uncertainty and risk acceptance.

3.3.1 Step 3 example

In order to clarify the proposed criterion, an example based on the case study bridge coming from Fener bridge (§3.2.1.1) is presented in the following.

The considered hazard curve of Fener bridge comes from Grendene (2006). According to §2.2, the PSHA for the studied site was carried out by the standard approach (Cornell, 1968) using the computer formulation by Bender & Perkins (1987). This approach is based on two work hypotheses: the earthquake recurrence times follow a Poisson distribution (made up by independent, non-multiple events, and the process is stationary in time) and the magnitude is exponentially distributed (the Gutenberg - Richter relation holds). In addition, the seismicity is considered uniformly distributed over the seismogenic zone (SZ). The Cornell method, then, needs the following input data: the SZ geometry definition, the seismicity models (in terms of average number of earthquakes related to magnitude interval, and maximum possible magnitude), and the attenuation relation of the chosen parameter of ground motion.

Considering that case study bridge seismic vulnerability analysis is carried out for life-safety limit state (10% exceedance probability during 50 years), Hazard and Δ -Hazard curves for Fener bridge site and for a 50 years period are shown in Fig. 3.23.

Moderate damage (PL2) fragility curve is considered to calculate PGA threshold beyond which visual inspections (or other NDE methods) can start; entire bridge

modelling with fixed end of the piers at bottom (§3.2.1.1) is considered. Solving Eq. 2.4, the PGA threshold value results 0.26g, obtained by linear interpolation between 0.25g and 0.30g (Fig. 3.24 red line).

The PGA threshold values can be embedded in the above-mentioned database (§3.1) in order to make quicker interventions in emergency phase.

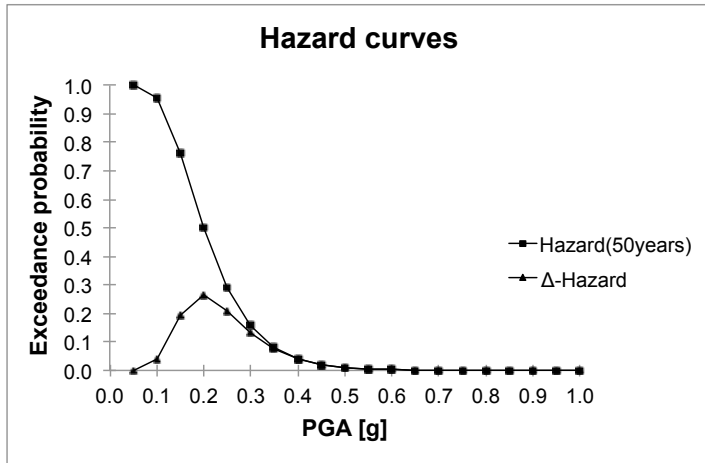


Fig. 3.23 Hazard and Δ -Hazard curves for Fener bridge site (50 years).

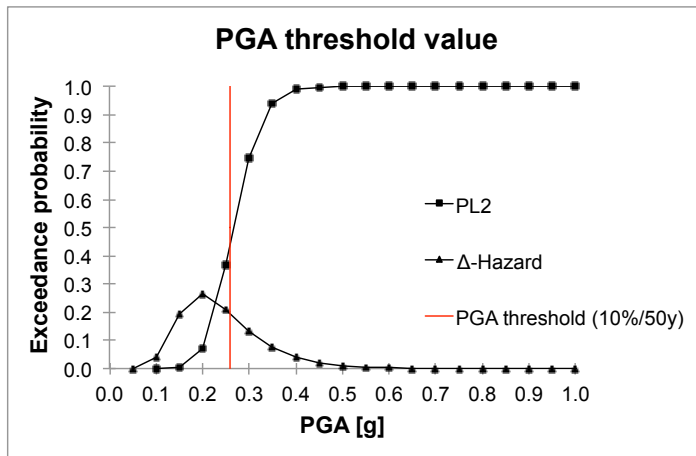


Fig. 3.24 10% PL2 probability in 50 years: PGA threshold value (red line) beyond which visual inspections can start in case study bridge from Fener bridge (§3.2.1.1).

3.4 Step 4: inspections progress

This step concerns the execution of the inspections and if the seismic intensity threshold is reached. Since in this study piers are considered the most vulnerable elements in a bridge, inspections are referred to bridge piers.

If the considered bridge has an unseated span or a pier is detected as collapsed, the bridge will be immediately closed. Otherwise piers visual inspections, NDE method, are performed under a probabilistic point of view, considering uncertainties by analogy with a defect detectability function (DDF), as presented in §2.5 (Mori & Ellingwood, 1994): in this study a step defect detectability function is considered (Fig. 3.25) and the defect sizes are the damage states shown in Table 3.17, similar to the above-mentioned fragility curves performance levels, but conceptually different: the former are detected, the others are predicted. We notice that these damage states are not comparable with defect sizes considered in Mori & Ellingwood (1994), they have a major extent, however DDF is accounted as a means to consider visual inspections uncertainties. Moreover, as shown in the following paragraph, it is not completely applied as mentioned in the reference (Mori & Ellingwood, 1994). These damage states should be both analytically and visually detectable (Franchin & Pinto, 2009): θ is the chord rotation at the pier (supposed fixed at the base), θ_y is the chord rotation corresponding to steel yielding at the pier base cross section, γ is the shear deformation, γ_{crack} is the cracking strain and γ_{peak} is the strain corresponding to the maximum shear force value in a shear force-deformation law. The chord rotation is defined as the angle between the tangent to the axis at the end of column subjected to steel yielding and the chord connecting that end with the point having null flexural moment (point of contraflexure), i.e. the end of shear span calculated as the ratio between flexural moment and shear at the end section.

Damage states shown in Table 3.17 are referred to a general structure: it's noticed that, if piers with fixed ends are considered, damage states calculated in chord rotation are the same of the damage levels calculated by Eq. (2.6) in Table 2.3, in both longitudinal and transversal direction, also if the pier has a framed structure. During inspections it's needed to identify where the damage is localized on the pier and how much it is extensive.

In this first approach, the probability to detect a damage $d(x)$ is equally partitioned between the considered damage states. Each of these damage states has a certain probability to be detected: the smaller the defect is, the

more the damage is difficult to detect with accuracy and the visual inspection is affected by uncertainty. Other studies (Ranf et al., 2007; Jerome & O'Connor, 2010; Terzic & Stojadinović, 2010; Alessandri et al., 2011) take into account inspections on bridges after a seismic event, but under a deterministic point of view.

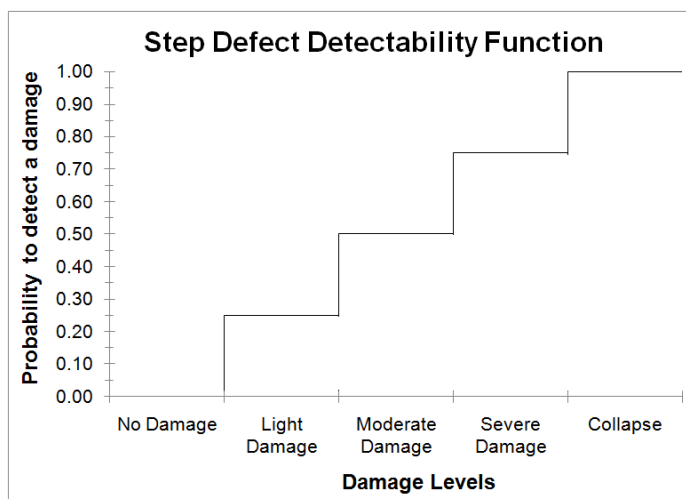


Fig. 3.25 The considered step defect detectability function for visual inspections.

Damage state	Description (physical and analytical)		Probability of detecting a damage
	Flexural	Shear	
No Damage (N)	No damage.		0.00
Light Damage (LD)	Light concrete spalling. ($\theta = \theta_y$)	Hairline diagonal cracks. ($Y_s = Y_{crack}$)	0.25
Moderate Damage (MD)	Moderate concrete spalling. ($\theta = 2\theta_y$)	Some moderate open diagonal cracks. ($Y_{crack} < Y_s < Y_{peak}$)	0.50

Extensive Damage (ED)	Severe spalling, bar yield and some bar buckling. ($\theta = 4\theta_y$)	Open diagonal cracks. ($V_s = V_{peak}$)	0.75
Collapse (CO)	Pier without load-bearing capacity, imminent deck collapse.		1.00

Table 3.17 Damage states considered for piers visual inspections: visual and analytical description, partially from Franchin & Pinto (2009), and their probability to be detected.

3.4.1 Updating fragility curves

After inspections, fragility curves have to be updated taking into account damaged bridge, in relation to Light, Moderate and Extensive above-mentioned inspections damage states, and the probability associated to each detected damage. Inspection of a pier is considered an independent event not related to other piers inspections of the same bridge or other bridges.

Updating fragility curves needs to create a numerical model of the damaged bridge. An approach to model (damaged) structures taking into account flexural and shear responses (Table 3.17) is presented in Franchin & Pinto (2009). If a fiber formulation element is considered having a certain number of integration points along it (e.g. force-beam column element with 5 integration points), at each integration point a section aggregator can be used to construct a section coupling axial/flexural response (given by a fiber-discretized section) with shear response (given by a uniaxial hysteretic law). Axial/flexural and shear responses are uncoupled in the section aggregator, but they are still coupled through the element equilibrium. The shear force-deformation law can be accounted in Priestley et al. (1994). More details can be found in the above-mentioned Franchin & Pinto (2009).

After generating the numerical model of the damaged bridge, updated fragility curves are calculated by means of the procedures shown in the past paragraphs, taking into account the same seismic action intensity of the fragility curves embedded in the database (§3.1), as if the damaged bridge was

subjected to another seismic event of the same intensity. Inspection uncertainty is considered as described in the following.

The probability of detecting a damage is thought as the probability that the updated fragility curve is not equal to the old (not updated) fragility curve; calculating fragility curve for each pier of the considered damaged bridge, the above-mentioned probability is applied (multiplied) to the difference value between pier updated fragility curve and the old fragility curve, reducing the gap, obtaining the updated fragility curve affected by inspection uncertainty (totally independent events). After that, the fragility curve of the entire bridge is calculated by the Eq. (2.15).

3.4.2 Step 4 example

In order to clarify this criterion, an example based on the case study bridge coming from Fener bridge (§3.2.1.1) is presented in the following.

It is supposed that an earthquake occurred, the 3 bridge piers are damaged and the damage is detected as Extensive Damage (ED) for every pier. The damage is localized within 1m from the pier base section. A simplified approach is taken into account to model damaged piers: reminding that the bridge piers failure comes from a flexural failure (§3.2.1.1) and a damaged RC element is less rigid in comparison with the same one in good condition, we consider a reduced concrete Young modulus (E_r) for the damaged material, as usual in this context (we assume $E_r = E/6$ for ED state, where E is the concrete Young modulus at 28 days). After having generated the bridge numerical model (fixed at piers base section), fragility curve are calculated following procedure B in §2.3.2.2. The new (updated) and the old (not updated) fragility curves for the PL2 (longitudinal direction) of the central pier are shown in Fig. 3.26. After that, we calculate the gap (value) between the new and old fragility curves probabilities of exceedance for each seismic action considered (PGA is considered in this example). These gap values are multiplied for the probability respective to the detected damage for the considered pier (0.75 in this example, because ED state is detected) and, then, the reduced gap values are summed to the old fragility curve values in order to obtain the new (updated) pier fragility curve which considers uncertainties about inspections (Fig. 3.26, red curve). After that, following this procedure for each bridge pier, the fragility curve of the entire bridge is calculated by the upper bound of Eq. (2.15).

These updated fragility curves can be embedded in the database presented in §3.1.

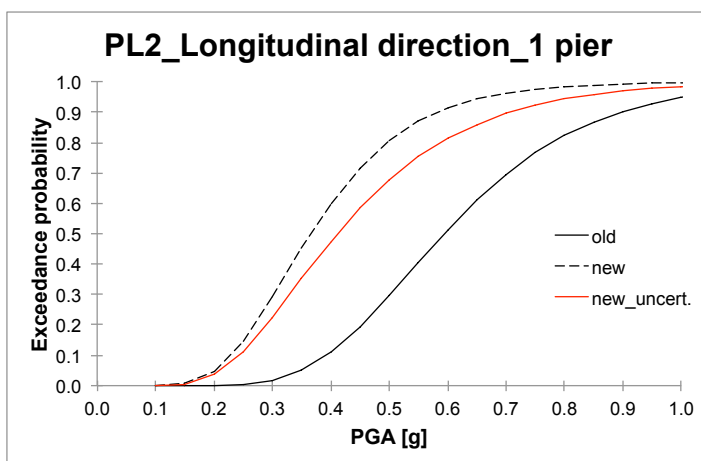


Fig. 3.26 Case study bridge from Fener bridge PL2 (longitudinal direction, 1 pier): calculation of fragility curve taking into account inspection uncertainties (red curve).

3.5 Step 5: allowing traffic

After updating fragility curves taking into account inspection uncertainties, this step concerns the calculation of a safety index in order to decide whether or not allowing traffic over the bridge.

Decision to closure a bridge after a seismic event cannot be only based on visual (often rapid) damage inspections or observations without performing any analysis, because large uncertainties lead the relation between damage patterns and loss of capacity (Franchin & Pinto, 2009). These uncertainties are present even if monitoring instruments (that record displacements and damage on structures) are placed at each bridge and these real time data (together with prior analysis) are used to make a decision about the closure.

Mackie & Stojadinović (2006), considering a Pacific Earthquake Engineering Research (PEER) approach, suggests a functional relationship which links

reduction traffic volume and loss of vertical load-bearing capacity of bridge; however, calculation of loss of vertical load-bearing capacity related to seismic intensity measure is affected by important uncertainties in all the different approaches of the study.

Taking into account the lack of literature on this topic and the impossibility to define both by means of inspection or monitoring systems and analytically without significant uncertainties loss of vertical load-bearing capacity, this study gives up to determine probability for partial traffic limitation and it considers an index to decide whether or not bridge is fully operational.

The index is defined as Eq. (3.4): considering the most vulnerable fragility curve between collapse (PL4) and shear failure, a ratio between updated risk ($P_{PL,new}$) and old risk ($P_{PL,old}$) is calculated (Franchin & Pinto, 2009).

$$\frac{P_{PL,new}}{P_{PL,old}} \leq 1 \rightarrow \text{bridge fully operational} \quad (3.4)$$

$P_{PL,new}$ is the updated risk calculated as in §3.3, considering new (updated) fragility curve with inspections uncertainties (§3.4.1), whereas the $P_{PL,old}$ is the maximum value between the old (pre-earthquake) risk of the considered bridge and the average pre-earthquake risk among the bridge population of that seismogenetic zone (SZ).

If $P_{PL,old}$ of the considered bridge is larger than the average pre-earthquake risk among the bridge population, it means that this bridge needs a seismic retrofit; however, the bridges on the considered SZ were open to traffic before the seismic event, so it's rational to consider their average pre-earthquake risk in terms of allowing traffic, since this risk level was (indirectly) accepted by the civil society.

If the index in Eq. (3.4) is larger than 1, the bridge is not fully operational and, not considering partial traffic limitation, the bridge can be opened for emergency operators or totally closed. Some index values for the bridge not fully operational are suggested in Franchin & Pinto (2009): e.g. 3÷5 bridge open for emergency operators. These values are affected by a significant variability and uncertainty that depend on different aspects about the single bridge and the characteristics of the considered SZ, therefore in this study bridge can be considered only opened (fully operational) or closed (not fully operational), according to Eq. (3.4).

It's highlighted that this criterion can be always considered valid or only in emergency and post-emergency phases after a seismic event; more investigations about bridge load-bearing capacity can be carried out in following periods and the bridge could be opened without any retrofit intervention, in accordance with Institutions and engineers investigations.

3.5.1 Step 5 example

Considering the case study bridge coming from Fener bridge (§3.2.1.1), this criterion is developed. Taking into account the bridge damaged as described in §3.4.1, PL4 (longitudinal direction because the most vulnerable) old and new fragility curves and Δ -Hazard curve presented in §3.3 (see also Fig. 3.27) are considered to calculate the seismic risk probability as in Eq. (2.4). The results are in the following:

$$\begin{aligned} P_{PL,old_bridge} &= 0.18 \% \\ P_{PL,new} &= 0.42 \% \end{aligned}$$

The average pre-earthquake risk among the bridge population of that SZ is calculated from a previous study regarding seismic vulnerability of bridges in that area (Grendene, 2006):

$$P_{PL,old_SZ} = 0.34\%$$

Since P_{PL,old_SZ} is larger than P_{PL,old_bridge} , the ratio in Eq. (3.4) results equal to 1.23, larger than 1, therefore the bridge is suggested to be closed.

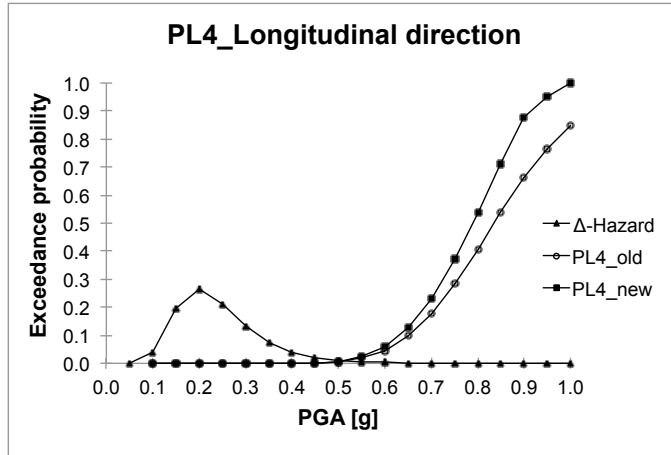


Fig. 3.27 PL4 fragility curves and Δ -Hazard curve for the case study bridge from Fener bridge.

3.6 Step 6: costs probability evaluation

The last step of the framework concerns repair costs to be sustained for the damaged bridge. This step is mostly important for Institutions that manage the (road or railway) network and owners of the bridges.

Number of studies in literature take into account costs evaluation after a seismic event under different points of view: e.g. Mackie & Stojadinović (2006) considers a component-level decision for repair cost based on limit states (PEER approach), Franchin et al. (2006) concerns costs evaluation in terms of human losses, Zhou et al. (2010) and Carturan et al. (2010a) consider costs for the entire road network, mostly in terms of social cost (traffic delay, etc.). Although these approaches are important for the evaluation of the entire road or railway network, costs evaluation of the single bridge in the network is as much important to get this result.

In this context, more focus is given to repair cost (C_{repair}), in particular when it is more expensive than replace cost (C_{replace}). This aspect is performed under a probabilistic point of view (Li, 2006).

Considering that (in this study) piers are considered the most vulnerable elements of the bridges and the use of FRP composites is getting wider and wider, particularly for seismic retrofit interventions, the repair cost could be referred to FRP retrofit interventions on the piers as representative of the entire bridge damage (Mackie & Stojadinović, 2006).

First, FRP retrofit interventions cost (C_{repair} in this study) needs to be defined: this cost mainly depends on piers geometry and the number of FRP layers. It's supposed that seismic retrofit intervention is made by means of CFRP (Carbon Fiber Reinforced Polymer), continuously wrapped along the height of the piers, having the following characteristics: Young modulus = 230GPa, ultimate stress = 3430MPa, ultimate strain = 1.5%, density = 1820kg/m³, thickness of one layer = 0.165mm.

After that, in accordance with fragility curves PLs visual (Table 2.2) and analytical (Table 2.3) descriptions, CFRP retrofit interventions are estimated for PL2 and PL3. PL1 and PL4 are neglected because PL1 is mostly a cosmetic damage, so C_{repair} is always cheaper than C_{replace} , whereas PL4 concerns the bridge collapsed, therefore other intervention typologies (e.g. replace the bridge) are needed. 1 CFRP layers are accounted for PL2 and 3 CFRP layers for PL3.

After having conducted a cost analysis considered different Italian regional pricelists, we estimate the following costs: 300€/m² for the first CFRP layer and 150€/m² for other layers, 750÷1200€/m² for replacing an ordinary RC multi-span simply supported girder bridge, it depends on foundations, piers geometry, deck, etc. So, the considered repair costs for the above-mentioned PLs are:

$$\begin{aligned} C_{\text{repair,PL2}} &= 300 \text{ €/m}^2 \rightarrow \text{estimated repair cost for PL2 (1 CFRP layer)} \\ C_{\text{repair,PL3}} &= 600 \text{ €/m}^2 \rightarrow \text{estimated repair cost for PL3 (3 CFRP layers)} \end{aligned}$$

Repair cost and replace cost (for each PL and each bridge) are compared to determine the most expensive one by the following costs ratio:

$$C_r = \frac{C_{\text{repair}}}{C_{\text{replace}}} \quad (3.5)$$

If $C_r > 1$ repair cost exceeds replace cost, whereas replace cost are the same ($C_r = 1$) or more expensive ($C_r < 1$) than repair cost

Since these repair costs are also related to PLs, they are affected by uncertainty. The uncertainty is calculated by seismic risk associated to the PLs (Eq. 2.4): updated fragility curves (§3.4.1) and Δ -Hazard curve (§3.3) are considered and the seismic risk value is strictly related to the results in Eq. (3.5).

The criterion in Eq. (3.5) is mainly applied for fully operational (damaged) bridges. Considering updated fragility curves, the costs forecast refers to the bridge condition after another seismic event: it's useful for Institutions or bridge owners in order to decide whether or not retrofitting the bridge before another seismic event occurs. Then, the decision to make seismic retrofit interventions depends on different aspects: budget availability (at that moment), bridge importance within the road or railway network, acceptance of the risk from Institutions or bridges owners, etc.

Taking into account not fully operational (damaged) bridges, this criterion could be applied if it's decided to make the bridge opened after further (rapid) investigations on it.

3.6.1 Step 6 example

Considering the case study bridge coming from Fener bridge (§3.2.1.1) and the results obtained in §3.5.1, this criterion is developed.

Since the bridge is suggested to be closed (not fully operational), we assume that the bridge is made opened after further rapid investigations.

First, PL2-PL3 repair costs and replace cost are to be calculated from geometrical characteristics of the bridge (§3.2.1.1) and cost data in §3.6. The considered surfaces to calculate costs are the following (CFRP is continuously wrapped along the height of the circular piers columns):

$$\begin{aligned} \text{Plant bridge} &= 891 \text{ m}^2 \\ \text{3 piers surface} &= 254.34 \text{ m}^2 \end{aligned}$$

The costs of the bridge, considering 900 €/m² for replace cost, result:

$$\begin{aligned} C_{\text{repair,PL2}} &= \text{€ } 76,302 \\ C_{\text{repair,PL3}} &= \text{€ } 152,604 \\ C_{\text{replace}} &= \text{€ } 801,900 \end{aligned}$$

The cost ratios are (Eq. 3.5):

$$C_{r,PL2} = 0.10$$

$$C_{r,PL3} = 0.19$$

These cost ratios highlight that retrofitting the bridge is cheaper than replacing it, for both PLs considered. Finally, PL2 and PL3 seismic risks are calculated (Eq. 2.4) considering updated fragility curves (§3.4.1) and Δ -Hazard curve (§3.3.1):

$$P_{PL2,new} = 58.3\%$$

$$P_{PL3,new} = 28.1\%$$

Taking into account that Δ -Hazard curve is referred to 50 years, these results mean that, if a seismic event occurs in the following 50 years, there is a probability of 58.3% to spend €76,302 and a probability of 28.1% to spend €152,604 for retrofitting the bridge. It's noticed that these costs are much lower than bridge replace cost, respectively 10% and 19% of the estimated replace cost. Considering this evaluation and the above-mentioned motivations regarding road network, budget availability, importance of the structure, etc., Institutions or owners of the bridges can decide to accept these risks and not immediately retrofit the bridge or, on the contrary, they can decide to make interventions on the bridge in order to reduce these risks.

4 CONCLUSIONS AND RECOMMENDATIONS

This study presents some insights about seismic assessment of existing RC bridges with a common structural typology in Italy. In particular, a probabilistic framework for RC mainshock-damaged bridges is proposed in order to give useful information to owners or Institution to decide whether or not allowing traffic over a bridge after a seismic event and retrofitting immediately damaged bridges. This procedure is mainly based on analytical fragility curves and on bridge visual inspections (non-destructive evaluation methods) considered under a probabilistic point of view by means of a defect detectability function.

Within this framework, an investigation about generation of fragility curves is carried out. In particular, fragility curves are found for multi-span simply supported RC girder bridges by means of non-linear dynamic analyses. Different modelling strategies with an increasing level of complexity have been developed: the highest pier modelled as a cantilever with fixed end, the entire bridge with fixed end, the entire bridge with foundation springs at bottom of the piers and the entire bridge with foundation substructure. Numerical modellings with different piers height and skew angles are investigated, too. Some of these analytical fragility curves are compared with the empirical ones coming from RISK-UE method.

Moreover, a particular focus is given to common FRP retrofit interventions, consisting in pier confinement, and their effects on seismic vulnerability reduction: two analytical models for FRP confined RC piers have been considered and their predictions are compared.

In the first part of the study, the first two steps, the following conclusions can be drawn regarding the modelling strategy for obtaining seismic fragility curves, bridge geometrical parameters, FRP retrofit interventions consisting in pier jacketing and the different skew angles:

- the choice of accelerograms affects fragility curves trend, hence the more accelerograms are considered, the more uncertainties in seismic loads are reduced;
- the probabilistic distribution of strength values of considered materials has to be taken into account for a proper estimation of the fragility curves. A proper survey, e.g. in-field tests and laboratory analyses on bridge specimens, may be recommended to reduce uncertainties;

- non-linear dynamic analysis can be used for the determination of seismic fragility of the structure, but it requires a consistent computational effort with respect to other simplified analyses;
- bridge vulnerability estimation can be improved if the entire bridge model is considered. In particular, for the considered case, the bridge vulnerability is underestimated in longitudinal direction and overestimated in transversal direction if only the highest pier is analyzed, particularly for high levels of damage where non-linear effects are significant. It is shown that entire bridge modeling with fixed end of the piers at bottom has a good approximation in comparison with numerical modellings that consider soil-structure interaction;
- piers height is an important geometrical parameter which has to be taken into account for a proper assessment of fragility analysis. Varying this parameter, a specific trend is not noticed. In particular, piers height influences the stiffness of the entire structure and, consequently, the proper period of bridge changes. Considering the pier as a simple oscillator (multi span simply-supported girder bridge), the formula to calculate its proper period is the well-known:

$$T = 2\pi\sqrt{\frac{M}{K}} \quad (3.6)$$

where M is the mass of the pier and the masses associated to that pier coming from deck dead and live loads, K is the pier stiffness (shear and flexural). If the piers height increases (the pier flexural stiffness decreases), the proper period of the bridge also tends to increase and move towards low spectral acceleration, causing a reduction of seismic action. On the contrary, the bending moment at the fixed bottom of the pier could increase because the arm of the seismic force increases.

Since flexural failure is predominant, these two reasons make piers height a relevant parameter for the vulnerability assessment, in particular for high damage levels when non-linear effects are important;

- as expected, seismic vulnerability decreases for FRP retrofitted bridges with respect to the bridge without FRP confinement;
- the model proposed by Pellegrino & Modena (2010) shows a reduction of the vulnerability more evident than that obtained with the model proposed adopted in the National Research Council (2004) since the

former is more accurate than the latter taking into account the contribution of the steel stirrups confinement and the interaction mechanisms between internal reinforcing steel and external FRP retrofit;

- skew angle affects fragility curves both in longitudinal and transversal direction: in particular the wider the skew angle is, the more the bridge seismic vulnerability increases. Considering a span and horizontal forces at piers bearings during seismic motion, as skew angle increases, the arm of the horizontal forces increases causing major deck rotation and so making worse the performance of the bridge, for example in terms of major displacement for the piers;
- RISK-UE method is noticed that it mainly makes a rough approximation in respect to analytical fragility curves. Considering different piers height, RISK-UE method tends to underestimate fragility of the structure for each considered numerical modelling both in longitudinal and transversal direction. RISK-UE method doesn't take into account piers height and main horizontal directions for generating empirical fragility curves. Whereas, regarding 15° skew angle, the empirical method overestimates seismic vulnerability, in particular for PL3 and PL4 in longitudinal direction and all PLs in transversal direction, as compared with analytical fragility curves. The RISK-UE method for PL1 and PL2 in longitudinal direction reflects analytical fragility curves trend, but the difference is mostly due to the different standard deviation between the two methods.

After this investigation on the generation of fragility curves, other steps of the framework concern activities after a seismic event, in particular the activities are based on visual inspections for damaged bridges.

A criterion to begin visual inspections is suggested in step 3: if the earthquake has reached the seismic intensity corresponding to 10% of specific risk, considering the most vulnerable fragility curve between PL2 and shear failure and the hazard curve referred to a time period equal to the service life of the structure, visual inspections on bridges can start. The 10% probability is considered in accordance to (Ellingwood, 2009): by analogy with life safety limit state of building codes, 10% probability strikes a good balance between uncertainty and risk acceptance.

If the threshold is reached, visual inspections on piers, considered the most vulnerable element of the bridge, start taking into account four damage states both analytically and visually detectable (step 4). These four damage states are accounted under a probabilistic point of view considering, by analogy, a step defect detectability function (Mori & Ellingwood, 1994). Fragility curves of damaged bridge are updated taking into account visual inspections (damaged bridge) and uncertainties associated to them. In the example shown in §3.4.2, damaged bridge is seismically more vulnerable than undamaged bridge. The damaged bridge fragility curves depend on the inspected damage, which modifies the stiffness of the entire structure and, so, its proper period: in particular, it's well known that damaged structure stiffness is lower than undamaged structure one, therefore, according to Eq. (3.6), the proper period of the damaged structure could shift to low spectral acceleration which entail low seismic loads. These two aspects can make damaged structure fragility curves not always more vulnerable than undamaged structure ones.

The last two steps give useful information to owners and Institutions in order to whether or not allow traffic over the bridge and repair immediately damaged bridges after a seismic event.

The criterion in step 5, based on a ratio between bridge specific risk before and after a seismic event, proposes to consider the bridge fully operational or not fully operational, without accounting any partial traffic limitation. Other studies, e.g. Mackie & Stojadinović (2006), calculate the loss of vertical load-bearing capacity related to seismic intensity measure in order to consider partial traffic limitation, but the procedure is affected by important uncertainties in all the approaches of the study. For this reason, this study considers only one complete traffic limitation.

Step 6 refers to an assessment about costs that have to be sustained for damaged bridge. Considering piers as the most vulnerable elements of the bridges, repair costs are referred to retrofit intervention made by CFRP continuously wrapped along the height of the piers. The main goal of this step is to give indications about economical benefits if the bridge is struck by another earthquake, in particular if the bridge repair costs can exceed replace costs. This costs assessment is given under a probabilistic point of view, because it's associated to a specific seismic risk. Decisions whether or not retrofitting or replace the bridge need to be taken in relation to other aspects as economical budget availability, importance of the structure, risk analysis of the whole road

network, etc. Anyway, this costs indications are useful for a proper budget allocation.

4.1 Recommendation for further studies

Results coming from this study identify several topics worthy of further investigation:

- generation of analytical fragility curves could consider as vulnerable other elements of the bridge in order to improve the seismic assessment (Nielsen & DesRoches, 2007): pounding between adjacent spans, fixed and expansion bearings, abutments failure, deck unseating, etc. Specific PLs have to be defined for each element considered as vulnerable;
- moreover, concrete damages due to carbonatation, deicing salts, corrosion (Biondini et al., 2013; Zanini et al., 2013) could be considered on the generation of fragility curves in order to obtain a proper seismic estimation;
- influence of other bridge geometrical parameters could be investigated (e.g. piers section, pier reinforcing steel typologies, span length, etc.) in order to give simple analytical laws to generate quickly fragility curves;
- fragility curves coming from natural seismic action could be compared to the ones coming from artificial accelerograms in order to investigate the approximation of the artificial accelerograms approach. Moreover, more than three groups of accelerograms, as suggested in Italian Code for Constructions (Italian Ministry of Infrastructures, 2008), can be considered to reduce uncertainties on seismic actions;
- considering step 4 of the probabilistic framework, other real time monitoring techniques can be accounted to quickly inspect the bridge and reduce uncertainties of inspections. Monitoring techniques can be exploited also in the long term with the aim of reducing uncertainties in the assessment of the infrastructure since dispersion of the data reduces when significant data is acquired. Long term monitoring data

can also give information on the degradation of structural performances during the entire life-cycle of the infrastructure;

- taking into account step 5 to allow traffic over mainshock-damaged bridges, the criterion could be improved giving some indications, when the bridge is not fully operational, if the bridge could be open only for emergency traffic;
- repair costs in step 6 could consider not only CFRP piers retrofitting, but also other typologies of retrofitting and other elements of the bridge in order to make a better repair costs evaluation and eventually decide interventions on bridge;
- the whole probabilistic framework could be implemented in a code and included in an Internet-based Bridge Management Systems (BMS) to define a priority for an optimal budget allocation.

NOTATIONS

A	scalar parameter;
A_{cc}	area of the cross-section included inside the transverse steel;
A_e	effective shear area;
A_g	area of the overall cross-section;
A_{st}	steel shear area;
B	scalar parameter;
C	scalar parameter;
C_r	cost ratio;
C_{repair}	repair cost;
$C_{replace}$	replace cost;
CFRP	carbon fiber reinforced polymer;
CO	collapse;
c	depth of compression zone;
c_m	cover to main steel bars of the RC cross section;
cdf	cumulative density function;
D	damage;
d	diameter of the circular cross-section or column depth;
d'	reduced diameter or column width;
d(x)	probability to detect a damage of size x;
d_{PL}	pier ductility demand;
DV	decision variable;
E_d	Young modulus of deck elements;
E_c	concrete Young modulus;
E_{c0}	unconfined concrete Young modulus;
E_f	FRP Young modulus;
E_s	reinforcing steel Young modulus;
$E_{y,long}$	longitudinal reinforcing steel Young modulus;
ED	extensive damage;
E[D]	Mean value of the damage function;
FRP	fiber reinforced polymer;
f_{c0}	unconfined concrete maximum stress;
f_{cc}	confined concrete peak stress;
f_D	lognormal probability function;
f_{if}	confinement pressure due to FRP;

f_{ls}	confinement pressure due to transverse reinforcement;
f_y	reinforcing steel yielding strength;
$f_{y,st}$	transverse reinforcing steel yielding strength;
G	mechanical model of the structure
G_d	shear modulus of deck elements;
G_{c0}	unconfined concrete shear modulus;
GFRP	glass fiber reinforced polymer;
IM	Intensity Measure;
K	structural stiffness;
k_1	scalar coefficient;
k_A	scalar coefficient;
k_f	coefficient of efficiency of the confinement;
k_R	reduction coefficient;
k_s	coefficient of efficiency for the confining transverse steel;
k	coefficient of efficiency of the FRP retrofit;
L	column shear span;
LD	light damage;
M	mass;
MD	moderate damage;
N	no damage;
NDE	non-destructive evaluation;
NLDA	non-linear dynamic analysis;
n_f	number of FRP layers;
PGA	peak ground acceleration;
pdf	probability density function;
$pk(f_c)$	probability of occurrence with f_c central value;
$pk(f_y)$	probability of occurrence with f_y central value;
$pk(f_y;f_{c0})$	combined probability of occurrence with f_y and f_c central values;
P_{PL}	specific seismic risk (probability of PL in a defined period)
$P_{PL,new}$	update specific seismic risk (probability of PL in a defined period)
$P_{PL,old}$	not update specific seismic risk (probability of PL in a defined period)
PL	Performance Level;
P_u	total confining pressure at failure;
RC	reinforced concrete;
S_a	spectral acceleration;
S_d	average seismic structural demand;
s	spacing of transverse reinforcement [mm];

T	proper period of a structure;
t_f	thickness of a single FRP layer;
V_A	shear strength of a concrete member;
V_c	shear resisting concrete mechanism;
V_p	shear resisting axial load contribution;
V_s	shear resisting steel truss mechanism;
$\text{Var}[D]$	variance of the damage function;
x_{\max}	maximum horizontal displacement of a target point;
x_y	horizontal displacement of a target point for steel yielding.
α	scalar parameter or aspect ratio factor;
β	lognormal standard deviation or longitudinal steel ratio factor;
β_c	structural capacity lognormal standard deviation;
β_d	structural demand lognormal standard deviation;
ε	dispersion of data for the linear regression;
ε_{c0}	unconfined concrete maximum strain;
ε_{cu0}	unconfined concrete ultimate strain;
ε_{cc}	confined concrete ultimate strain;
$\varepsilon_f^{\text{eff}}$	effective hoop FRP strain;
ε_{fu}	ultimate FRP strain;
ε_{sy}	reinforcing steel yielding strain;
ε_{su}	reinforcing steel ultimate strain;
θ	chord rotation or inclination of diagonal shear cracks;
θ_y	steel yielding chord rotation;
γ	scalar parameter or displacement ductility factor;
γ_{crack}	concrete cracking shear strain;
γ_s	shear strain;
γ_{peak}	concrete strain corresponding to the maximum shear force value in a shear force-deformation law;
λ	average value related to a specific IM value;
ν_c	concrete Poisson ratio;
ρ_{st}	transverse steel ratio;
ρ_f	FRP retrofit ratio;
$\rho_{y,\text{long}}$	longitudinal steel ratio.

LIST OF FIGURES

Fig. 2.1 PEER Performance-Based methodology (source by Deierlein, G.).....	21
Fig. 2.2 Example of seismic hazard curve (50 years).	22
Fig. 2.3 Capacity-Demand Acceleration-Displacement spectra showing uncertainty in structural behavior and ground motion [source by VV.AA. (1999), in particular Mander, J.B.]	24
Fig. 2.4 Example of fragility curves for existing bridges considering four Performance Levels (PLs).	24
Fig. 2.5 Example of linear regression in a $\ln(\text{PGA}/g)$ vs. $\ln(\text{Damage})$ diagram.	31
Fig. 2.6 Example of a horizontal target spectrum with a matched accelerogram by Vanmarcke (1976) method.	33
Fig. 2.7 RC column failure modes classification according to (Applied Technology Council, 1981): flexural failure (a), flexural-shear failure (b) and brittle shear failure (c). Source by Miranda et al. (2005).....	35
Fig. 2.8 Reinforced concrete column failure modes: flexural failure (a) and brittle shear failure (b). Source by Miranda et al. (2005).	36
Fig. 2.9 Total force-deformation response according to Calvi et al. (2005). Source by Miranda et al. (2005).	37
Fig. 2.10 Factors for calculating shear strength: γ factor for shear strength of concrete (a), α factor for column aspect ratio (b) and β factor for longitudinal steel ratio (c). Source by Kowalsky & Priestley (2000).....	39
Fig. 2.11 Axial load contribution in columns with double bending (a) and single bending (b). Source by Priestley et al. (1994).	39
Fig. 2.12 Example of defect detectability function (DDF).	43
Fig. 2.13 σ - ϵ diagram for circular columns (Pellegrino & Modena, 2010).....	47
Fig. 3.1 The framework proposed in this study to assess seismic vulnerability of existing bridges after an earthquake mainshock.	49
Fig. 3.2 I.Br.I.D. webpage (VV.AA., 2006-2012): example for Busche Dam bridge (Belluno province, northern Italy).	51
Fig. 3.3 Italian seismic hazard map and geographical position of the bridges (A for Fener bridge and B for A27 overpass): maximum PGA with probability of exceedance 10% during 50 years, type soil A (source by INGV – (Italian) National Institute of Geophysics and Volcanology).	53

Fig. 3.4 Case study bridge geometrical characteristics: bridge considered as a case study (a), transversal view of the pier (b), original drawing of reinforcement configuration of the pier top (c).	54
Fig. 3.5 Original drawing of reinforcement configuration of foundation structure (plinth and piles).	55
Fig. 3.6 Normal (a) and lognormal (b) probabilistic distribution of unconfined concrete maximum stress f_{c0} (C25/30) and reinforcing steel yielding strength f_y (FeB32K), respectively.	56
Fig. 3.7 Fener bridge pier behavior subjected to horizontal loads: longitudinal (a) and transversal (b) directions (BS15, piers fixed at base).	60
Fig. 3.8 Numerical models of the case study bridge without (a) and with foundation structure (b).	61
Fig. 3.9 Horizontal and vertical elastic target spectra (life-safety limit state) considered for Fener bridge.	61
Fig. 3.10 Fragility curves (longitudinal direction). Comparison between 4 analytical models: single pier with fixed end, the entire bridge with fixed end of the piers at bottom, the entire bridge simulating soil-structure interaction by means of translational and rotational springs at the base of the piers and the entire bridge modelling the whole foundation structure.	62
Fig. 3.11 Fragility curves (transversal direction). Comparison between 4 analytical models: single pier with fixed end, the entire bridge with fixed end of the piers at bottom, the entire bridge simulating soil-structure interaction by means of translational and rotational springs at the base of the piers and the entire bridge modelling the whole foundation structure.	63
Fig. 3.12 Fragility curves (longitudinal direction): comparison between three groups of three accelerograms (entire bridge with fixed end of the piers). .	64
Fig. 3.13 Fragility curves (longitudinal direction): comparison between numerical models with different pier height and RISK-UE method (Mongeo et al., 2003).	66
Fig. 3.14 Fragility curves (transversal direction): comparison between numerical models with different pier height and RISK-UE method (Mongeo et al., 2003).	67
Fig. 3.15 Fragility curves (longitudinal direction): comparison between entire bridge without retrofit and retrofitted bridge: models by Pellegrino & Modena (2010) and by National Research Council (2004) are used for modelling the constitutive law of the bridge with confined piers.	69

Fig. 3.16 Fragility curves (transversal direction): comparison between entire bridge without retrofit and retrofitted bridge: models by Pellegrino & Modena (2010) and by National Research Council (2004) are used for modelling the constitutive law of the bridge with confined piers.	70
Fig. 3.17 A27 highway overpass images: view from the highway (a), view of the main span (b), view of a lateral span (c) and view of a RC framed pier (d).	72
Fig. 3.18 Normal (a) and lognormal (b) probabilistic distribution of unconfined concrete maximum stress f_{c0} (C25/30) and reinforcing steel yielding strength f_y (FeB32K), respectively.	73
Fig. 3.19 Numerical model of the A27 highway overpass (15° skew angle): global view (a) and plant view (b).	76
Fig. 3.20 Horizontal and vertical elastic target spectra (life-safety limit state) considered for A27 overpass.	76
Fig. 3.21 Fragility curves (longitudinal direction): comparison between numerical models with different skew angles and RISK-UE method (Mongeo et al., 2003) with 15° skew angle. PL4 analytical fragility curves are overlapped.	77
Fig. 3.22 Fragility curves (transversal direction): comparison between numerical models with different skew angles and RISK-UE method (Mongeo et al., 2003) with 15° skew angle. PL3 and PL4 analytical fragility curves are overlapped.	78
Fig. 3.23 Hazard and Δ -Hazard curves for Fener bridge site (50 years).	82
Fig. 3.24 10% PL2 probability in 50 years: PGA threshold value (red line) beyond which visual inspections can start in case study bridge from Fener bridge (§3.2.1.1).	82
Fig. 3.25 The considered step defect detectability function for visual inspections.	84
Fig. 3.26 Case study bridge from Fener bridge PL2 (longitudinal direction, 1 pier): calculation of fragility curve taking into account inspection uncertainties (red curve).	87
Fig. 3.27 PL4 fragility curves and Δ -Hazard curve for the case study bridge from Fener bridge.	90

LIST OF TABLES

Table 2.1 Typologies of bridges (RISK-UE).....	26
Table 2.2 Possible consequences of earthquake on bridges (HAZUS'99 and RISK-UE).....	26
Table 2.3 Definition of damage states based on ductility base pier section (Choi, 2002) in accordance to HAZUS'99 (RISK-UE) damage states.....	28
Table 3.1 Case study bridge geometrical characteristics.	55
Table 3.2 Characteristics of the 15 considered bridge samples (unconfined concrete) for Fener bridge.	57
Table 3.3 Springs stiffness values for soil-structure interaction.....	58
Table 3.4 Springs stiffness values for soil-pile interaction.	59
Table 3.5 Fragility curves parameters, median and standard deviation, (longitudinal direction) for the 4 numerical models.	62
Table 3.6 Fragility curves parameters, median and standard deviation, (transversal direction) for the 4 numerical models.....	63
Table 3.7 Fragility curves parameters, median and standard deviation, (longitudinal direction) for the three groups of three accelerograms (entire bridge with fixed end of the piers).....	65
Table 3.8 Fragility curves parameters, median and standard deviation, (longitudinal direction) for the 6 numerical models.	66
Table 3.9 Fragility curves parameters, median and standard deviation, (transversal direction) for the 6 numerical models.....	68
Table 3.10 FRP confined concrete ultimate strain (National Research Council, 2004).....	69
Table 3.11 Fragility curves parameters, median and standard deviation, (longitudinal direction) for the 3 numerical models.	70
Table 3.12 Fragility curves parameters, median and standard deviation, (transversal direction) for the 3 numerical models.....	71
Table 3.13 A27 overpass geometrical characteristics.	72
Table 3.14 Characteristics of the 15 considered bridge samples (unconfined concrete) for A27 highway overpass.	74
Table 3.15 Fragility curves parameters, median and standard deviation, (longitudinal direction) for the studied numerical models.....	77
Table 3.16 Fragility curves parameters, median and standard deviation, (transversal direction) for the studied numerical models.....	78

Table 3.17 Damage states considered for piers visual inspections: visual and analytical description, partially from Franchin & Pinto (2009), and their probability to be detected.....85

BIBLIOGRAPHY

- Alessandri S., Giannini R. and Paolacci F., (2011), *A new method for probabilistic aftershock risk evaluation of damaged bridge*, Proceedings of the Conference 3rd ECCOMAS Thematic Conference on Computational Methods in Structural Dynamics and Earthquake Engineering, 25-28 May, Corfu, Greece.
- Applied Technology Council, (1981), *Seismic Design Guidelines For Highway Bridges*, ATC-6, Berkeley, California, USA.
- Bender B. and Perkins D. M., (1987), *Seisrisk III: a computer program for seismic hazard estimation*, U.S. Geological Survey Bulletin, 1772, 48pp.
- Biondini F., Camnasio E. and Palermo A., (2013), *Lifetime seismic performance of concrete bridges exposed to corrosion*, Structure and Infrastructure Engineering, 1-21. DOI:10.1080/15732479.2012.761248.
- Biondini F. and Frangopol D. M., (2011), *Life-cycle of civil engineering systems*, Structure and Infrastructure Engineering, 7, 1-2, 1-2.
- Calvi G. M., Pavese A., Rasulo A. and Bolognini D., (2005), *Experimental and Numerical Studies on the Seismic Response of R.C. Hollow Bridge Piers*, Bulletin of Earthquake Engineering, 3, 3, 267-297.
- Carturan F., Morbin R., Zanini M. A. and Pellegrino C., (2012), *A parametric study on the fragility of typical existing concrete bridges in seismic areas*, Proceedings of the Conference OpenSeesDays, 24th-25th May, Roma, Italy.
- Carturan F., Pellegrino C., Modena C., Rossi R. and Gastaldi M., (2010a), *Optimal resource allocation for seismic retrofitting of bridges in transportation networks*, Proceedings of the Conference IABMAS 2010 - 5th International Conference on Bridge Maintenance, Safety and Management, July 11-15, Philadelphia, USA.
- Carturan F., Pellegrino C., Rossi R., Gastaldi M. and Modena C., (2013), *An integrated procedure for management of bridge networks in seismic areas*, Bulletin of Earthquake Engineering, 11, 2, 543-559.
- Carturan F., Pellegrino C., Zampellini A., Modena C., Rossi R. and Gastaldi M., (2010b), *A procedure for the evaluation of the seismic vulnerability of bridge networks*, Proceedings of the Conference 14th European Conference on Earthquake Engineering, 30th August - 3rd September, Ohrid, Republic of Macedonia.
- CEN Comité Européen de Normalisation, (2004), *Eurocode 2: design of concrete structures – Part 1-1: General rules and rules for buildings*, EN 1992-1-1, Brussels, Belgium.
- Choi E., (2002), *Seismic Analysis and Retrofit of Mid-America Bridges*, Georgia Institute of Technology.
- Choi E. S., DesRoches R. and Nielson B., (2003), *Seismic fragility of typical bridges in moderate seismic zones*, Engineering Structures, 26, 2, 187-199.

- Codermatz R., Nicolich R. and Slejko D., (2003), *Seismic risk assessments and GIS technology: applications to infrastructures in the Friuli-Venezia Giulia region (NE Italy)*, Earthquake Engineering & Structural Dynamics, 32, 11, 1677-1690.
- Cornell C. A., (1968), *Engineering seismic risk analysis*, Bulletin of the Seismological Society of America, 58, 5, 1583-1606.
- Cornell C. A., (2004), *Hazard analysis, ground motions and probabilistic assessments for PBSD*, Proceedings of the Conference International Workshop on Performance-Based Design, Bled, Slovenia.
- Cornell C. A., Jalayer F., Hamburger R. and Foutch D., (2002), *Probabilistic Basis for 2000 SAC Federal Emergency Management Agency Steel Moment Frame Guidelines*, Journal of Structural Engineering, 128, 4, 526-533.
- Cornell C. A. and Krawinkler H., (2000), *Progress and Challenges in Seismic Performance Assessment*, Pacific Earthquake Engineering Research Center (PEER).
- Cosenza E. and Manfredi G., (2000), *Damage indices and damage measures*, Progress in Structural Engineering and Materials, 2, 1, 50-59.
- Ellingwood B. R., (2009), *Role of modeling uncertainties in assessing vulnerability and risk to civil infrastructure from rare events*, 10th International Conference on Structural Safety and Reliability, ICOSSAR, 13-17 September, Osaka, Japan.
- Ellingwood B. R. and Kinali K., (2009), *Quantifying and communicating uncertainty in seismic risk assessment*, Structural Safety, 31, 2, 179-187.
- Elwood K. J., (2002), *Shake Table Tests and Analytical Studies on the Gravity Load Collapse of Reinforced Concrete Frames*, Ph. D. thesis, University of California at Berkeley, USA.
- Federal Emergency Management Agency, (2001), *Direct Physical Damage to Lifelines-Transportation Systems*, HAZUS 99.
- fédération internationale du béton, (2001), *Externally bonded FRP reinforcement for RC structures*, Bulletin No.14, Lausanne, Switzerland.
- FEMA (Federal Emergency Management Agency), (2004), *Hazus®-MH 2.0 Technical Manual*, Washington, DC.
- Franchin P., Lupoi A. and Pinto P. E., (2006), *On the role of road networks in reducing human losses after earthquakes*, Journal of Earthquake Engineering, 10, 2, 195-206.
- Franchin P. and Pinto P. E., (2009), *Allowing Traffic Over Mainshock-Damaged Bridges*, Journal of Earthquake Engineering, 13, 5, 585-599.
- Gasparini D. A. and Vanmarcke E. H., (1976), *Simulated earthquake motions compatible with prescribed response spectra*, Massachusetts Institute Technology, R76-4420 G32 1976.
- Grendene M., (2006), *Simplified Approach to Expected Seismic Damage for Existing Bridges*, Ph.D. thesis, University of Trento, Trento, Italy, p.227.
- Harajli M. H., Hantouche E. and Soudki K., (2006), *Stress-strain model for fiber-reinforced polymer jacketed concrete columns*, Aci Structural Journal, 103, 5, 672-682.

- Hwang H., Jernigan J. B. and Lin Y. W., (2000), *Evaluation of Seismic Damage to Memphis Bridges and Highway Systems*, Journal of Bridge Engineering, 5, 4, 322-330.
- Iervolino I., Galasso C. and Cosenza E., (2010), *REXEL: computer aided record selection for code-based seismic structural analysis*, Bulletin of Earthquake Engineering, 8, 2, 339-362.
- Italian Ministry of Infrastructures, (2008), *Norme Tecniche per le Costruzioni*, DM 2008-1-14, Rome, Italy.
- Jerome S. and O'Connor P. E., (2010), *Post-Earthquake Bridge Inspection Guidelines*, MCEER/University at Buffalo, C-06-14.
- Karim K. R. and Yamazaki F., (2001), *Effect of earthquake ground motions on fragility curves of highway bridge piers based on numerical simulation*, Earthquake Engineering & Structural Dynamics, 30, 12, 1839-1856.
- Karim K. R. and Yamazaki F., (2003), *A simplified method of constructing fragility curves for highway bridges*, Earthquake Engineering & Structural Dynamics, 32, 10, 1603-1626.
- Kent D. C. and Park R., (1971), *Flexural Members with Confined Concrete*, Journal of Structural Division, 97, 7, 1969-1990.
- Kim S. H. and Shinozuka M., (2004), *Development of fragility curves of bridges retrofitted by column jacketing*, Probabilistic Engineering Mechanics, 19, 1-2, 105-112.
- Kiremidjan A., Moore J., Fan Y. Y., Yazla-li O., Basoz N. and William M., (2007), *Assessment of Transportation Network Systems*, Journal of Earthquake Engineering, 11, 371-382.
- Kowalsky M. J. and Priestley M. J. N., (2000), *Improved analytical model for shear strength of circular reinforced concrete columns in seismic regions*, Aci Structural Journal, 97, 3, 388-396.
- Li Q., (2006), *Mathematical Formulation of Tools for Assessment of Fragility and Vulnerability of Damaged Buildings*, Ph.D. thesis, Georgia Institute of Technology, Atlanta, Georgia, USA, p.191.
- Lupoi G., Franchin P., Lupoi A. and Pinto P. E., (2006), *Seismic fragility analysis of structural systems*, Journal of Engineering Mechanics-Asce, 132, 4, 385-395.
- Mackie K. R. and Stojadinović B., (2006), *Post-earthquake functionality of highway overpass bridges*, Earthquake Engineering & Structural Dynamics, 35, 1, 77-93.
- McKenna F., Fenves G. and Scott M. H., (2009), *Open System for Earthquake Engineering Simulation*, <http://opensees.berkeley.edu>, Pacific Earthquake Engineering Reaserach Center, University of California, Berkeley, California.
- Melchers R. E., (1999), *Structural reliability analysis and prediction*, John Wiley.
- Miranda P. A., Calvi G. M., Pinho R. and Priestley M. J. N., (2005), *Displacement-Based Assessment of RC Columns with Limited Shear Resistance*, IUSS Press, Pavia.
- Mirza S. A. and MacGregor J. G., (1979), *Variability of Mechanical Properties of Reinforcing Bars*, Journal of the Structural Division, 105, 5, 921-937.

- Mongeo O., Alexoudi M., Argyroudou S., Martin C., Pitilakis K. and POLIMI, (2003), *An advanced approach to earthquake risk scenarios with applications to different European towns. Vulnerability assessment of lifelines and essential facilities (WP06): basic methodological handbook*, 71.
- Monti G. and Nisticò N., (2002), *Simple Probability-Based Assessment of Bridges under Scenario Earthquakes*, Journal of Bridge Engineering, 7, 2, 104-114.
- Morbin R., Casadei E., Pellegrino C. and Modena C., (2012), *Effect of FRP retrofit interventions on seismic vulnerability of existing bridges*, Proceedings of the Conference IABMAS 2012 - 6th International Conference on Bridge Maintenance, Safety and Management, 8th-12th July, Stresa, Lake Maggiore, Italy, 1228-1234.
- Morbin R., Pellegrino C., Grendene M. and Modena C., (2010), *Strategies for seismic vulnerability evaluation of common RC bridges typologies*, Proceedings of the Conference 14th European Conference on Earthquake Engineering, 30th August - 3rd September, Ohrid, Republic of Macedonia.
- Mori Y. and Ellingwood B., (1994), *Maintaining Reliability of Concrete Structures. I: Role of Inspection/Repair*, Journal of Structural Engineering, 120, 3, 824-845.
- National Research Council, (2004), *Guide for the Design and Construction of Externally Bonded FRP Systems for Strengthening Existing Structures*, CNR-DT 200, Roma, Italy.
- Nielson B. G. and DesRoches R., (2007), *Analytical seismic fragility curves for typical bridges in the central and southeastern United States*, Earthquake Spectra, 23, 3, 615-633.
- Padgett J. E. and DesRoches R., (2008), *Methodology for the development of analytical fragility curves for retrofitted bridges*, Earthquake Engineering & Structural Dynamics, 37, 8, 1157-1174.
- Pan Y., Agrawal A. K., Ghosn M. and Alampalli S., (2010), *Seismic Fragility of Multispan Simply Supported Steel Highway Bridges in New York State. I: Bridge Modeling, Parametric Analysis, and Retrofit Design*, Journal of Bridge Engineering, 15, 5, 448-461.
- Park R., Priestley M. J. N. and Gill W. G., (1982), *Ductility of Square-Confined Concrete Columns*, Journal of Structural Division, 108, 4, 929-950.
- Pellegrino C. and Modena C., (2010), *Analytical Model for FRP Confinement of Concrete Columns with and without Internal Steel Reinforcement*, Journal of Composites for Construction, 14, 6, 693-705.
- Priestley M. J. N., Seible F. and Calvi G. M., (1996a), *Seismic design and retrofit of bridges*, John Wiley & Sons, New York.
- Priestley M. J. N., Verma R. and Xiao Y., (1996b), *Seismic shear strength of reinforced concrete columns - Closure*, Journal of Structural Engineering-Asce, 122, 4, 464-467.
- Priestley M. J. N., Verma R. and Xiao Y., (1994), *Seismic Shear-Strength of Reinforced-Concrete Columns*, Journal of Structural Engineering-Asce, 120, 8, 2310-2327.

- Ranf R. T., Eberhard M. O. and Malone S., (2007), *Post-earthquake Prioritization of Bridge Inspections*, Earthquake Spectra, 23, 1, 131-146.
- Seville E. and Metcalfe J., (2005), *Developing a hazard risk assessment framework for the New Zealand State Highway Network*, University of Canterbury, NZ, Research Report 276.
- Sezen H., (2002), *Seismic Behaviour and Modelling of Reinforced Concrete Building Columns*, Ph. D. thesis, University of California at Berkeley, USA.
- Sgaravato M., Banerjee S. and Shinozuka M., (2008), *Seismic risk assessment of highway transportation network and cost-benefit analysis for bridge retrofitting*, Proceedings of the Conference 14th World Conference on Earthquake Engineering, October 12-17, Beijing, China.
- Shinozuka M., Feng M. Q., Kim H. K. and Kim S. H., (2000a), *Nonlinear static procedure for fragility curve development*, Journal of Engineering Mechanics-Asce, 126, 12, 1287-1295.
- Shinozuka M., Feng M. Q., Lee J. and Naganuma T., (2000b), *Statistical analysis of fragility curves*, Journal of Engineering Mechanics-Asce, 126, 12, 1224-1231.
- Shinozuka M., Zhou Y., Banerjee S. and Murachi Y., (2006), *Cost-effectiveness of seismic bridge retrofit*, Proceedings of the Conference 3rd International Conference on Bridge Maintenance, Safety and Management, July, 16-19, Porto, Portugal.
- Shiraki N., Shinozuka M., Moore J. E., Chang S., Kameda H. and Tanaka S., (2007), *System risk curves: probabilistic performance scenarios for highway networks subjected to earthquake damage*, Journal of Infrastructure Systems, 13, 43-54.
- Song J. and Ellingwood B., (1999), *Seismic Reliability of Special Moment Steel Frames with Welded Connections: II*, Journal of Structural Engineering, 125, 4, 372-384.
- Tastani S. P., Pantazopoulou S. J., Zdoumba D., Plakantaras V. and Akritidis E., (2006), *Limitations of FRP jacketing in confining old-type reinforced concrete members in axial compression*, Journal of Composites for Construction, 10, 1, 13-25.
- Teng J. G., Chen J. F., Smith S. T. and Lam L., (2002), *FRP Strengthened RC Structures*, John Wiley and Sons, Chichester, UK.
- Terzic V. and Stojadinović B., (2010), *Post-Earthquake Traffic Capacity of Modern Bridges in California*, Pacific Earthquake Engineering Research Center (PEER), 2010/ 103.
- Tinazzi D., Pellegrino C., Cadelli G., Barbato M., Modena C. and Gottardo R., (2003), *An experimental study of RC columns confined with FRP sheets*, Proceedings of the Conference Structural Faults & Repair, 10th International Conference, 1-3 July, London, UK.
- Vanmarcke E. H., (1976), *Structural response to earthquakes*, in Seismic risk and engineering decisions, Elsevier Scientific Pub. Co.: distributions for the United States and Canada, Elsevier/North Holland, p. 287-337.
- Viggiani C., (1999), *Fondazioni*, Hevelius.

- VV.AA., Italian Bridge Interactive Database Project - I.Br.I.D. Project, (2006-2012), Dept. of Civil, Environmental and Architectural Engineering - University of Padova, <http://librid.dic.unipd.it/index.php?&page=home>.
- VV.AA., (1999), *Research Progress and Accomplishments (1997-1999): A Selection of Papers Chronicling Technical Achievements of the Multidisciplinary Center of Earthquake Engineering Research*, Red Jacket Quadrangle, Buffalo, New York 14261, New York.
- Wang L. M. and Wu Y. F., (2008), *Effect of corner radius on the performance of CFRP-confined square concrete columns: Test*, Engineering Structures, 30, 2, 493-505.
- Werner S. D., Cho S., Taylor C. E. and Lavoie J. P., (2006), *Use of Seismic Risk Analysis of Roadway Systems to Facilitate Performance-Based Engineering and Risk-Reduction Decision Making*, <http://www.pwri.go.jp/eng/ujnr/tc/g/pdf/23/23-4-1werner.pdf>.
- Yeo G. L. and Cornell C. A., (2005), *Stochastic Characterization and Decision Bases under Time-Dependent Aftershock Risk in Performance-Based Earthquake Engineering*, Pacific Earthquake Engineering Research Center (PEER), 2005/13.
- Zanini M. A., Pellegrino C., Morbin R. and Modena C., (2013), *Seismic vulnerability of bridges in transport networks subjected to environmental deterioration*, Bulletin of Earthquake Engineering, 11, 2, 561-579.
- Zhou Y. W., Banerjee S. and Shinozuka M., (2010), *Socio-economic effect of seismic retrofit of bridges for highway transportation networks: a pilot study*, Structure and Infrastructure Engineering, 6, 1-2, 145-157.